สำนักหอสมุดกลาง พระจอมเกล้าลาดกระบัง

A STUDY OF TARGET AND EQUALIZER DESIGN FOR PERPENDICULAR HEAT-ASSISTED MAGNETIC RECORDING SYSTEMS


E076522

PANATDA TUEKU

เลขหมู่.....
เลขทะเบียน.....76522
วัน,เดือน,ปี.....26 ส.ค. 2557

b.....
i.....

A THESIS SUBMITTED IN PARTIAL FULFILLMENT

OF THE REQUIREMENT FOR THE DEGREE OF

MASTER OF ENGINEERING IN DATA STORAGE TECHNOLOGY AND INNOVATION

(INTERNATIONAL PROGRAM)

INTERNATIONAL COLLEGE

KING MONGKUT'S INSTITUTE OF TECHNOLOGY LADKRABANG

2013

KMITL-2013-IC-M-005-016

This material is reserved for educational use only, not allowed for commercial use.
Forbidden to modify the content, and cite the document when use.

COPYRIGHT 2013

INTERNATIONAL COLLEGE

COLLEGE OF DATA STORAGE TECHNOLOGY AND INNOVATION

KING MONGKUT'S INSTITUTE OF TECHNOLOGY LADKRABANG

This material is reserved for educational use only, not allowed for commercial use.

Forbidden to modify the content, and cite the document when use.

Thesis	A Study of Target and Equalizer Design for Perpendicular Heat-Assisted Magnetic Recording Systems
Student	Panatda Tueku
Student ID	52600622
Degree	Master of Engineering
Program	Data Storage Technology and Innovation
Year	2013
Thesis Advisor	Assoc. Prof. Dr. Pornchai Supnithi

ABSTRACT

The storage capacity of hard disk drives has increased tremendously over the last decade. Heat-Assisted Magnetic Recording (HAMR) is one of the leading technologies identified to enable areal density beyond 1 Tb/in^2 of magnetic recording systems. A key challenge to HAMR design is accuracy of positioning, timing of the firing laser, power of the laser, thermo-magnetic head, head-disk interface and cooling system. In this thesis, we study the effect of HAMR parameters on transition center and transition width. The HAMR is modeled using Thermal Williams-Comstock (TWC) and microtrack model. Furthermore, the target and equalizer are designed by the minimum mean square error (MMSE). We are interested in 4 types of target constraints. There are the monic (h_0 = 1) constraint, h_1 = 1 constraint, the unit energy constraint and the fixed target constraint (PR2). From the simulation results, the frequency responses of GPR targets of the HAMR systems at 4 Tb/in^2, 5 Tb/in^2 (reduced track width) and 5 Tb/in^2 (reduced bit period) are similar to the frequency response of longitudinal magnetic recording (LMR) [and provide the lower MMSE than PR targets. Although the lowest MMSE of all systems is from the unit energy constraint, the monic constraint gives the lowest bit error rate (BER). Therefore, the monic constraint outperforms the other constraints.

Index Terms – Heat-Assisted Magnetic Recording, Thermal Williams-Comstock equation, Transition Parameters, Microtrack model, Equalizer.

This material is reserved for educational use only, not allowed for commercial use.

Forbidden to modify the content, and cite the document when use.

ACKNOWLEDGEMENTS

I would like to extend my sincere gratitude to my advisor at College of Data Storage Technology and Innovation, King Mongkut's Institute of Technology Ladkrabang: Assoc. Prof. Dr. Pornchai Supnithi for this research work. This work also was supported in part by Communication, Signal processing and Storage Research Group (CSSRG) Laboratory, Faculty of Engineering, King Mongkut's Institute of Technology Ladkrabang. Special mention goes to Mr. Rati Wongsathan, and Ms. Atitaya Sirirungsakulwong who have provided invaluable support and guidance during my Master study.

Also, I would like to acknowledge Western Digital (Thailand) Co., Ltd. for granting the scholarship at the International College, King Mongkut's Institute of Technology Ladkrabang. Appreciation goes to my supervisor in the Test Equipment Engineering team at Western Digital (Thailand) for supporting my Masters study and also thank you to my colleagues for the valuable advises and comments.

I am fortunate enough to have my parents and my sister who have believed in me even when I myself did not. They always understand, give motivation and support me throughout my life.

Panatda Tueku

This material is reserved for educational use only, not allowed for commercial use.
Forbidden to modify the content, and cite the document when use.

CONTENTS

	Page
ABSTRACT	I
ACKNOWLEDGEMENTS	II
CONTENTS	III
LIST OF ABBREVIATIONS	VI
LIST OF FIGURES	VII
LIST OF TABLES	X
CHAPTER 1 INTRODUCTION	1
1.1 Statement and Significance of the Problems	3
1.2 Objectives	3
1.3 Expectation	4
1.4 Conceptual framework	4
1.5 Hypothesis	4
1.6 Thesis Outline	4
CHAPTER 2 PERPENDICULAR HEAT-ASSIESED MAGNETIC RECORDING	6
2.1 Superparamagnetic limit	6
2.2 Heat-assisted magnetic recording (HAMR)	7
2.3 The channel model of perpendicular Heat-assisted magnetic recording..	8
2.3.1 Williams-Comstock (WC) model	9
2.3.2 Thermal Williams-Comstock (TWC) Model	11
2.3.3 Transition center (*x0*) and transition parameter (*a*)	15
2.3.4 Microtrack model	17
CHAPTER 3 TARGET AND EQUALIZER DESIGN	18
3.1 The conventional magnetic recording model	18
3.2 The channel model for Heat-assisted magnetic recording (HAMR)	21
3.3 Target and Equalizer design	22
3.4 Viterbi detector	25

This material is reserved for educational use only, not allowed for commercial use.

Forbidden to modify the content, and cite the document when use.

CONTENTS (CONT.)

Page

3.4.1 Finite State Machine (FSM) 26
3.4.2 Trellis diagram 27
3.4.3 Viterbi algorithm (VA) 28

CHAPTER 4 SIMULATION AND RESULTS 30
4.1 The temperature profile 30
4.2 The magnetization field 32
4.3 The Karlqvist head field 32
4.4 The Coercivity field 34
4.5 The results of perpendicular HAMR simulation at the areal density of 4 Tb/in^2 34
4.6 The results of perpendicular HAMR simulation at the areal density of 5 Tb/in^2 40
4.6.1 The results of perpendicular HAMR simulation at the areal density of 5 Tb/in^2 (reduced track width) 40
4.6.2 The results of perpendicular HAMR simulation at 5 Tb/in^2 (reduced bit period) 46
4.7 The results and performance of target shaping design of the HAMR system at 4 Tb/in^2 48
4.8 The results and performance of target shaping design of the HAMR system at 5 Tb/in^2 52
4.8.1 The results and performance of target shaping design of the HAMR system at 5 Tb/in^2 (reduced track width) 52
4.8.2 The results and performance of target shaping design of the HAMR system at 5 Tb/in^2 (reduced bit period) 56

CHAPTER 5 CONCLUSION AND SUGGESTION FOR FUTURE WORK 61
5.1 Conclusion 61
5.2 The suggestion for further work 62

This material is reserved for educational use only, not allowed for commercial use.

Forbidden to modify the content, and cite the document when use.

CONTENTS (CONT.)

	Page
REFERENCE	63
APPENDICES	65

This material is reserved for educational use only, not allowed for commercial use.
Forbidden to modify the content, and cite the document when use.

LIST OF ABBREVIATIONS

AWGN : Additive White Gaussian Noise

BER : Bit Error Rate

ECC : Error Correction Code

GPR : Generalized Partial Response

HAMR : Heat-Assisted Magnetic Recording

ISI : Inter-Symbol Interference

ML : Maximum Likelihood

MLSE : Maximum Likelihood Sequence Equalization

MMSE : Minimum Mean Square Error

MSE : Mean Square Error

PR : Partial Response

PRML : Partial Response Maximum Likelihood

SNR : Signal-to-Noise Ratio

Tb : Terabit

TWC : Thermal Williams-Comstock

VD : Viterbi Detector

WC : Williams-Comstock

This material is reserved for educational use only, not allowed for commercial use.
Forbidden to modify the content, and cite the document when use.

LIST OF FIGURES

Figure Page

1.1 The areal density research and development targets..... 1

1.2 Future technology options for HDD storage..... 2

2.1 The write-ability trilemma..... 7

2.2 A schematic diagram of the HAMR write process..... 8

2.3 Idealized magnetization versus magnetic field hysteresis loop (MH loop) of the medium before and after heating..... 10

2.4 Head pole and field of set up for longitudinal and perpendicular recording systems..... 13

2.5 Transition center (x_0) and transition parameter (a) of perpendicular recording system..... 13

2.6 Microtrack modeling of HAMR channel..... 16

3.1 Magnetic recording system model..... 19

3.2 The conventional read channel model..... 19

3.3 Transition responses for perpendicular channel with various NDs..... 21

3.4 The HAMR system with target-shaping equalization..... 21

3.5 Viterbi detection in the channel model..... 26

3.6 Finite state machine (FSM) diagram of PR1, H(D) = 1+D..... 27

3.7 Block diagram and trellis diagram of the 1-D PR1 channel..... 28

4.1 Temperature profile using σ_t = 16.2 nm and T_{peak} = 330 °C..... 31

4.2 The effect of laser position on the temperature profile in the along-track position..... 31

4.3 The effect of laser position on the temperature profile in the cross-track position..... 32

4.4 The effect of peak temperature and laser position on the magnetization field..... 33

4.5 Karlqvist head fields of longitudinal HAMR system 33

4.6 Karlqvist head fields of perpendicular HAMR system 33

4.7 The coercivity field with various laser spot positions 34

4.8 Transition center and parameter with various H_c functions at the areal 37

This material is reserved for educational use only, not allowed for commercial use.
Forbidden to modify the content, and cite the document when use.

LIST OF FIGURES (CONT.)

Figure | Page

density of 4 Tb/in^2 (M_r=-1000T+1.8x10^6) .....

4.9 Transition center and parameter with various M_r functions at the areal density of 4 Tb/in^2 (H_c = -3100T+2.4x10^6) 37

4.10 Transition center and parameter with various H_c and M_r functions at the areal density of 4 Tb/in^2 38

4.11 Transition center and parameter with various head field at the areal density of 4 Tb/in^2 38

4.12 Transition center and parameter with various peak temperatures at the areal density of 4 Tb/in^2 39

4.13 Transition response and bit response at the areal density of 4 Tb/in^2 39

4.14 Playback signal at the areal density of 4 Tb/in^2 40

4.15 Transition center and parameter with various H_c functions at the areal density of 5 Tb/in^2 (reduced track width) with M_r=-1000T+1.8x10^6 43

4.16 Transition center and parameter with various M_r functions the areal density of 5 Tb/in^2 (reduced track width) with H_c = -2900T+2.4x10^6 43

4.17 Transition center and parameter with various H_c and M_r functions at the areal density of 5 Tb/in^2 (reduced track width) 44

4.18 Transition center and parameter with various head field at the areal density of 5 Tb/in^2 (reduced track width) 44

4.19 Transition center and parameter with various peak temperatures at the areal density of 5 Tb/in^2 (reduced track width) 45

4.20 Transition response and bit response of HAMR at the areal density of 5 Tb/in^2 (reduced track width) 45

4.21 Playback signal at the areal density of 5 Tb/in^2 (reduced track width) 46

4.22 Transition response and bit response of HAMR at the areal density of 5 Tb/in^2 (reduced bit period) 47

4.23 Playback signal at the areal density of 5 Tb/in^2 (reduced bit period) 47

4.24 MMSE of fixed-target constraint with various equalizer taps of the HAMR system at 4 Tb/in^2 49

This material is reserved for educational use only, not allowed for commercial use.
Forbidden to modify the content, and cite the document when use.

LIST OF FIGURES (CONT.)

Figure Page

4.25 Frequency responses of PR targets of the HAMR system at 4 Tb/in^2 49

4.26 MMSE of various targets constraint using 3 target taps with 11-taps equalizer of the HAMR system at 4 Tb/in^2 50

4.27 Frequency responses of GPR targets versus fixed-target (PR2) of the HAMR system at 4 Tb/in^2 50

4.28 MMSE of unit energy constraint equalizers with various target taps of the HAMR system at 4 Tb/in^2 51

4.29 Bit error rates (BER) of the HAMR system at 4 Tb/in^2 52

4.30 MMSE of fixed-target constraint with various equalizer taps of the HAMR system at 5 Tb/in^2 (reduced track width) 53

4.31 MMSE of various targets constraint using 3 target taps with 11-taps equalizer of the HAMR system at 5 Tb/in^2 (reduced track width) 54

4.32 Frequency responses of GPR targets versus fixed-target (PR2) of the HAMR system at 5 Tb/in^2 (reduced track width) 54

4.33 MMSE of unit energy constraint equalizers with various target taps of the HAMR system at 5 Tb/in^2 (reduced track width) 55

4.34 Bit error rates (BER) of the HAMR system at 5 Tb/in^2 (reduced track width). 56

4.35 MMSE of fixed-target constraint with various equalizer taps of the HAMR system at 5 Tb/in^2 (reduced bit period) 57

4.36 MMSE of various targets constraint using 3 target taps with 11-taps equalizer of the HAMR system at 5 Tb/in^2 (reduced bit period) 57

4.37 Frequency responses of GPR targets and fixed-target (PR2) of the HAMR system at 5 Tb/in^2 (reduced bit period) 58

4.38 MMSE of unit energy constraint equalizers with various target taps of the HAMR system at 5Tb/in^2 (reduced bit period) 58

4.39 Bit error rates (BER) of the HAMR system at 5 Tb/in^2 (reduced bit period)... 59

This material is reserved for educational use only, not allowed for commercial use.
Forbidden to modify the content, and cite the document when use.

LIST OF TABLES

Table Page

3.1 The relationship of input and output sequence in 1+D PR1 channel..... 27

4.1 HAMR System parameters with the areal density of 4 Tb/in^2 36

4.2 HAMR System parameters with the areal density of 5 Tb/in^2 (reduced track width) 42

4.3 The target coefficients and MMSE values of fixed target constraint at 11-tap equalizer of the HAMR system at 4 Tb/in^2..... 49

4.4 The target coefficients and MMSE values of various targets constraint using 3 target taps with 11-tap equalizer of the HAMR system at 4 Tb/in^2..... 50

4.5 The coefficients and MMSE values of unit-energy constraint equalizers with various target tabs of the HAMR system at 4 Tb/in^2..... 51

4.6 The target coefficients and MMSE values of fixed target constraint at 11-tap equalizer of the HAMR system at 5 Tb/in^2 (reduced track width) 53

4.7 The target coefficients and MMSE values of various targets constraint using 3 target taps with 11-tap equalizer of the HAMR system at 5 Tb/in^2 (reduced track width) 54

4.8 The coefficients and MMSE values of unit-energy constraint of 11-tap equalizers with various target taps of the HAMR system at 5 Tb/in^2 (reduced track width) 55

4.9 The target coefficients and MMSE values of fixed target constraint at 11-tap equalizer of the HAMR system at 5 Tb/in^2 (reduced bit period) 57

4.10 The target coefficients and MMSE values of various targets constraint using 3 target taps with 11-tap equalizer of the HAMR system at 5 Tb/in^2 (reduced bit period) 58

4.11 The coefficients and MMSE values of unit-energy constraint of 11-tap equalizers with various target taps of the HAMR system at 5 Tb/in^2 (reduced bit period) 59

This material is reserved for educational use only, not allowed for commercial use.
Forbidden to modify the content, and cite the document when use.

CHAPTER 1

INTRODUCTION

The proliferation of digital content creation and consumption brings an increasing demand for data storage devices, such as the hard disk drive (HDD). This demand drives require increasing storage capacity, which in turns drives increasing growth in areal density (AD).

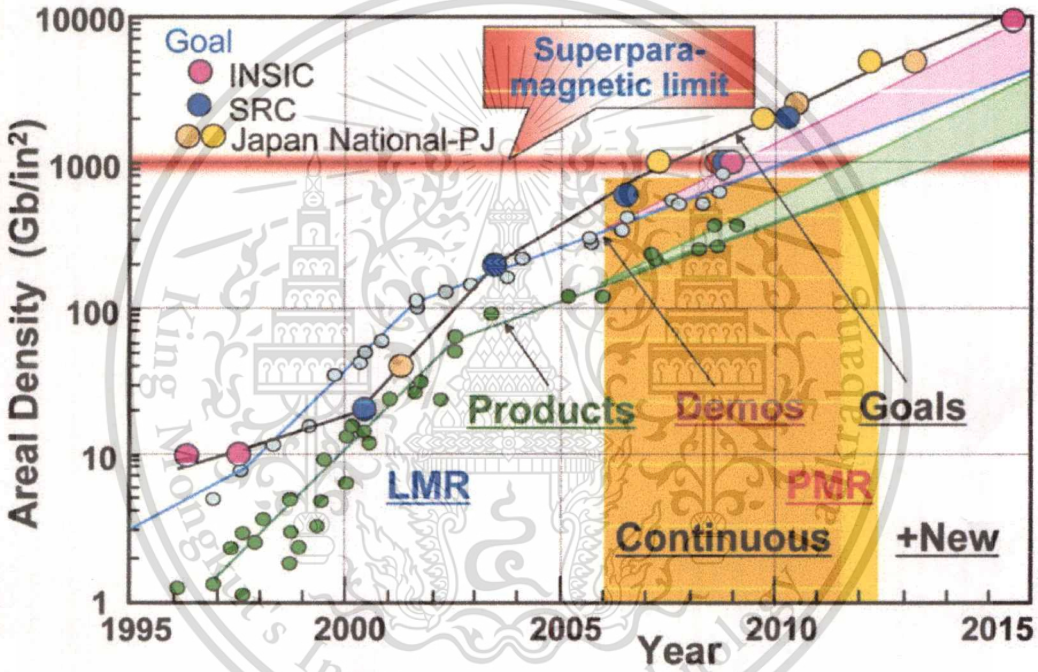


Figure 1.1 The areal density research and development targets [2].

The AD is defined as the number of bits stored in a bit area of medium and it is determined by the average size of the grains and the number of grains that is used to store 1 bit of information. The AD growth of research targets versus recent studies and HDD products reveals in Figure 1.1. The HDD industry is expected to demonstrate and manufacture the 10 Tb/in^2 technology and products by 2015 for the Information Storage Industry Consortium (INSIC). Heat-assisted magnetic recording (HAMR) is one of the four enabling technologies which surpass the critical point of storage density limit known as the superparamagnetic limit at 1 Tb/in^2 AD as shown in Figure 1.2 [2].

This material is reserved for educational use only, not allowed for commercial use.
Forbidden to modify the content, and cite the document when use.

To increase the AD, the magnetic grain size must be reduced and to maintain the right levels of signal to noise ratio (SNR), the number of grains per bit must be constant. However, small grains will face thermal instability problem. To remedy this issue, media need to have high coercivity (H_c) which means anisotropy (K_u) is high and, therefore, it is difficult to write data bits because the current write field limitation by CoFe material with 2.4 Tesla in the late 1990's and no material seem to increase the write field further.

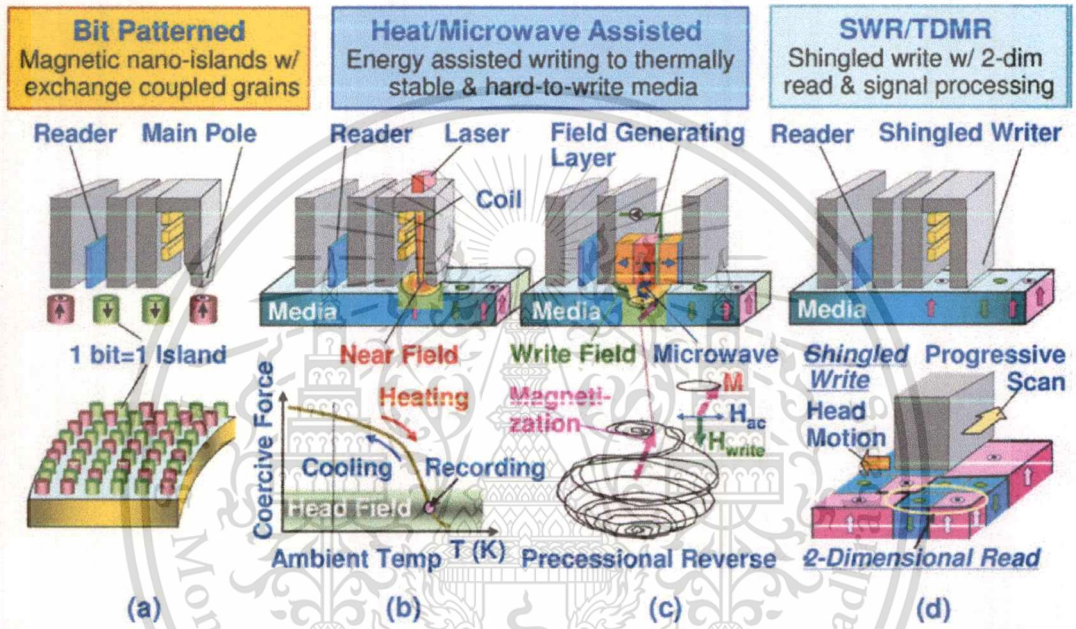


Figure 1.2 Future technology options for HDD storage [2].

New write mechanism has been researched by many researchers around the world. It is able to utilize higher anisotropy to produce smaller grain sizes and to secure a signal to noise ratio (SNR) and bit error rate (BER). HAMR can overcome the write field limitation by temporarily reducing H_c during the write process by heating the medium. That means K_u is also reduced and the energy barrier to write on the medium is also decreased. The medium is then rapidly cooled down to the room temperature after magnetization completed, where thermal stability is acceptable.

HAMR system has many thermal issues compared to the conventional magnetic recording. Therefore, each work step and the whole system need to be investigated and clarified, as well as improving the stability and reliability of the system against thermal issues. The HAMR channel model has been recently developed and the thermal Williams-Comstock (TWC) model has been used to predict the limitation.

This material is reserved for educational use only, not allowed for commercial use.
Forbidden to modify the content, and cite the document when use.

The read process of the conventional read channel models employed in current magnetic recording systems has been used to produce the HAMR playback signals.

1.1 Statement and significance of the problem

HAMR system has many thermal issues compared to the conventional magnetic recording. The key challenge to HAMR design is the accuracy of positioning, timing of the firing laser, power of the laser, thermo-magnetic head, head-disk interface and cooling system. Each work step and the whole system need to be investigated and clarified.

The William-Comstock (WC) model is a well-known model to predict the transition width in longitudinal magnetic recording, as in [4] and [13]. Even though the WC model does not provide the accuracy result at the level of the micromagnetic model, it provides a simple and fast analysis for initial read channel design and simulations. This is achieved by neglecting the fine details and make reasonable approximations that lead to analytic expressions while still capturing the relevant physics by the model. As the WC model does not account for the effects of heating in the HAMR system, in 2004, it was extended by incorporating thermal gradients of coercivity H_c and magnetization M for a longitudinal HAMR system and is known as the Thermal Williams–Comstock (TWC) model, as in [4]. In HAMR, the temperature profile changes in both along-track and cross track direction, hence, the microtrack model is used for 2D process of heating and magnetization of a medium to solve the problem of determining the transition characteristics.

In this thesis, the perpendicular HAMR systems is studied using the TWC model, transition parameters and the microtrack modeling to determine the transition characteristics of both large and non-large spot laser. Furthermore, the target and equalizer are designed by the minimum-mean squared error (MMSE) method in the performance of HAMR system.

1.2 Objectives

The objectives of this study are

1.2.1 to study the channel model of the conventional magnetic recording

1.2.2 to study the system of the Heat-Assisted Magnetic Recording (HAMR)

This material is reserved for educational use only, not allowed for commercial use.
Forbidden to modify the content, and cite the document when use.

1.2.3 to study the channel model and system behavior of Heat-Assisted Magnetic Recording (HAMR)

1.2.4 to design the target and equalizer by using the minimum-mean squared error (MMSE) method and evaluate the performance of target shaping design .

1.3 Expectation

This study is expected to improve the system performance in the heat-assisted magnetic recording (HAMR) channels. Understanding of the HAMR system behavior, using the proper parameters and model can give the optimal results from the HAMR channel model. Moreover, the design of target and equalizer by using the minimum-mean squared error (MMSE) method offers the good system performance.

1.4 Conceptual framework

In this thesis, we will study the principles of perpendicular HAMR systems using the Thermal Williams-Comstock (TWC) model, transition parameters and the microtrack modeling to determine the transition characteristics of both large and non-large spot laser. Furthermore, we will design the target and equalizer by the minimum-mean squared error (MMSE) method and present the system performance.

1.5 Hypothesis

A key challenge to HAMR designing is accuracy of positioning, timing of the firing laser, power of the laser, thermo-magnetic head, head-disk interface and cooling system. The study of the effect of HAMR parameters on transition center and transition width by using Thermal Williams-Comstock (TWC) and microtrack model with the proper system parameters should present the performance of HAMR system. The target and equalizer which are designed by the minimum mean square error (MMSE) should present the optimal system performance.

1.6 Thesis outline

The organization of this thesis is as follows:

This material is reserved for educational use only, not allowed for commercial use.
Forbidden to modify the content, and cite the document when use.

Chapter 2 the superparamagnetism is explained. Heat-assisted magnetic recording (HAMR) technology which surpasses the critical point of storage density limit at 1 Tb/in^2 by using laser attached to the writer is then introduced. After that we will give some background of the HAMR channel modeling which has been researched. Finally, the read channel for perpendicular Heat-assisted magnetic recording (HAMR) will be discussed in the last section.

Chapter 3 briefly explains the conventional magnetic recording model and after that the read channel for HAMR will be discussed. We will describe the design of the target and equalizer by the minimum-mean squared error (MMSE) method. In the last section, we will also briefly explain the Viterbi Detector (VD).

Chapter 4 presents the simulation results. The results and discussions about the temperature profile, the Karlqvist head field, the magnetization field, the coercivity field, the results of HAMR simulation with the areal density of 4 Tb/in^2, 5 Tb/in^2 (reduced track width) 5 Tb/in^2 (reduced bit period). The results and performance of target shaping design will be presented in this chapter.

Chapter 5 gives the conclusion of the HAMR systems simulation and the suggestion for the future work.

This material is reserved for educational use only, not allowed for commercial use.
Forbidden to modify the content, and cite the document when use.

CHAPTER2

PERPENDICULAR

HEAT-ASSISTED MAGNETIC RECORDING

In this chapter, the superparamagnetism is explained in Section 2.1. Heat-assisted magnetic recording (HAMR) technology which surpasses the critical point of storage density limit at 1 Tb/in^2 by using laser attached to the writer is introduced in Section 2.2. Finally, we will provide some background of the channel model of perpendicular heat-assisted magnetic recording which has been researched in Section 2.3. The Williams-Comstock (WC) Model, the thermal Williams-Comstock (TWC) Model, transition center (x_0), transition Parameter (a) and the Microtrack model will be explained in this section.

2.1 The superparamagnetic limit

The areal density (AD) is defined as the number of bits stored in a bit area of medium and it is determined by the average size of the grains and the number of grains that is used to store 1 bit of information. To increase the AD, the magnetic grain size must be reduced and to maintain the right levels of proportional signal to noise ratio (SNR), the number of grains per bit must be constant. However, scaling the bit size means reducing the grain size. Scaling bit size is no longer applicable because small grains will face thermal instability problem as there is a limit that is known as the superparamagnetic limit.

The superparamagnetic limit is the event which magnetic material may show a behavior similar to paramagnetism even at below the Curie temperature (T_c). The super-paramagnetic trilemma is related to grain size, media anisotropy and write-ability shown in Figure 2.1. The material's internal thermal energy can flip the direction of magnetization at the room temperature. Grain magnetization flipping is thermal activation process governed by the Neel-Arrhenius law giving a time constant

$$\tau^{-1} = f_0 \exp(-\frac{K_u V}{k_B T}) \tag{2.1}$$

This material is reserved for educational use only, not allowed for commercial use.
Forbidden to modify the content, and cite the document when use.

where K_u is the anisotropy constant, V denotes the grain volume, k_B is Boltzman constant, T stands for the ambient or room temperature and f_0 is the attempt frequency determined by intrinsic magnetic properties and is in the order of 10^9-10^{12} hertz.

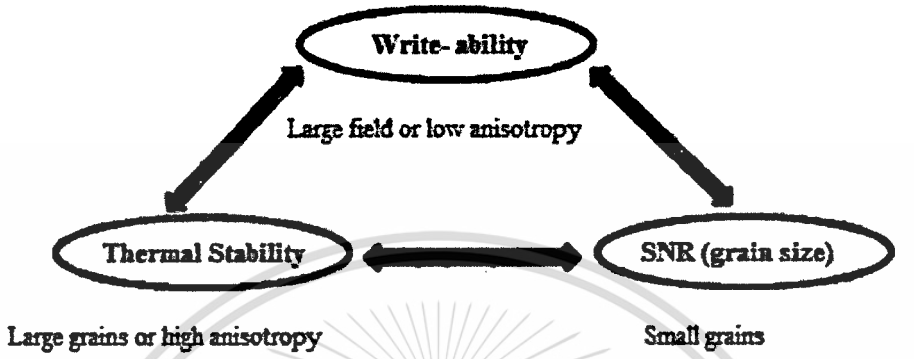


Figure 2.1 The write-ability trilemma: the available field from writer has to trade off against the thermal stability (large grains or high anisotropy) and the media SNR (small grains) [1].

In order to ensure the long storage stability, high anisotropy material is needed to have a high stability factor K_uV / k_BT such as 60 [3], [15]. To maintain the media SNR, smaller grains are needed causing K_u in media to be increased. On the other hand, it is difficult to write on high K_u grains because the strength of the writing field is limited by the material and design of write heads. The current write field limitation by CoFe material have been 2.4 Teslas since the late 1990's and no material can increase the write field further [1], [15].

2.2 Heat-assisted magnetic recording (HAMR)

HAMR is one of the four enabling technologies which surpass the critical point of storage density limit known as the super-paramagnetic limit at 1 Tb/in^2 AD, as in [1]-[3]. HAMR is able to utilize higher anisotropy to produce smaller grain sizes and to secure a high signal to noise ratio (SNR) and low bit error rates (BER). HAMR chooses the high coercivity H_c media, indicating high anisotropy K_u such as iron platinum alloy while writing by a tiny focused laser at the location of transition to remedy the super-paramagnetic limit. This briefly reduces the high H_c which means K_u is also reduced and the energy barrier to write on the medium is also decreased to below

This material is reserved for educational use only, not allowed for commercial use.
Forbidden to modify the content, and cite the document when use.

the available applied field H_a for the magnetization process to take place. The medium is then rapidly cooled down after magnetization to the room temperature after magnetization is completed, where thermal stability is acceptable [3], [8]. A schematic diagram of the HAMR write process is presented in Figure 2.2.

The HAMR system face many thermal issues compared to the conventional magnetic recording. Hence, each work step and the whole system need to be studied and clarified, as well as improving the stability and reliability of the system against thermal issues. The HAMR channel model has recently been investigated and the read process of the conventional read channel models employed in the current magnetic recording systems has been used to produce the HAMR playback signals [4]-[11].

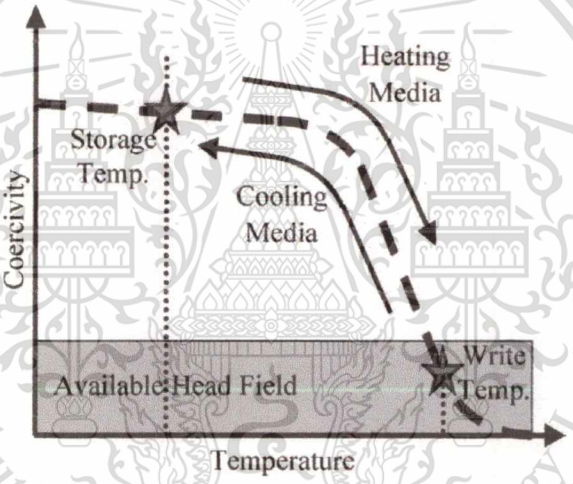


Figure 2.2 A schematic diagram of the HAMR write process [8].

2.3 The channel model of perpendicular heat-assisted magnetic recording (HAMR)

In this section, we present the literature review of the channel model of the HAMR which has been developed previously. The initial work in the channel modeling of the HAMR is from [4] where the microtrack model is used to capture the effects of transition curvatures. The thermal William-Comstock transition parameter is used in the microtrack model. The results from the model are compared to the experimental data which taken from a dual-side spin stand and found that it can be sufficiently predicted and explained by the model. Under optimal alignment and with the optimal write current and laser power, the pulse width at half maximum of

This material is reserved for educational use only, not allowed for commercial use.
Forbidden to modify the content, and cite the document when use.

amplitude PW_{50} is small [4]. The temperature profile on the system behavior from the read-channel system design in [5] is investigated and found that the large HAMR spot approximation presents a good approximation if its underlying assumptions are matched [5]. In [6], the effects of laser spot position on the system response are determined and found that the tribit errors are found in the presence of electronic noise. It is found that the higher peak temperature which the laser spot is aligned close to the write head gap center leads to small PW_{50} [7].

In the review of spot approximation and the relationship between the remanent magnetization M_r and coercivity H_c with temperature (T), the summary is as follows. The works in [4] and [5] show the longitudinal HAMR with large spot approximation is used to simplify the equation, but it is only valid if the assumptions are fulfilled. Large spot approximation is also used for the perpendicular HAMR, as in [6]. References [7] and [9] show the perpendicular channels with non-large spot approximation are used to simulate the channel model. A linear relationship for M_r and H_c with T is assumed to be used in [4]-[7] and [9] but as in [10], the non-linear relationship for M_r and H_c with temperature T is assumed instead.

2.3.1 Williams-Comstock (WC) model

In 1971, Mason Williams and Larry Comstock developed the William-Comstock (WC) model to predict the transition width in longitudinal magnetic recording, as in [13]. They provide a simple analysis of the write process. Even though WC model does not provide the accuracy result comparable to the micromagnetic model, it provides a simpler and faster analysis for initial channel design and simulations. This is achieved by neglecting the fine details and made reasonable approximations that lead to analytic expressions while still capturing the relevant physics by the model. The WC model is a well-known approximate analytical model which describes the transition characteristics in a conventional magnetic recording system. In the model, the "zigzag" nature of magnetic transition is ignored and the shape of magnetic transition is presumed to be described by the arctangent function. The transition center x_0 and the transition parameter a are the two main parameters which can be derived from this model.

This material is reserved for educational use only, not allowed for commercial use.
Forbidden to modify the content, and cite the document when use.

The relationship between the applied field H_a and the resultant magnetization M in the medium is given by the hysteresis loop of the medium and can be written as $M=F_{loop}(H_a)$, where F_{loop} represents the hysteresis loop as shown in Figure 2.3. The applied magnetic field H_a during the transition formation can be described by the contribution from the head field H_h and the demagnetization field H_d from the recorded transition, i.e.,

$$H_a(x) = H_h(x) + H_d(x) \tag{2.2}$$

In the down track direction (x-direction), $M(x)$ can be determined by solving

$$M(x) = M\left[H_a(x)\right] = M\left[H_h(x) + H_d(x)\right] \tag{2.3}$$

where H_d is dependent on M, and (2.3) can only be solved by iteration method.

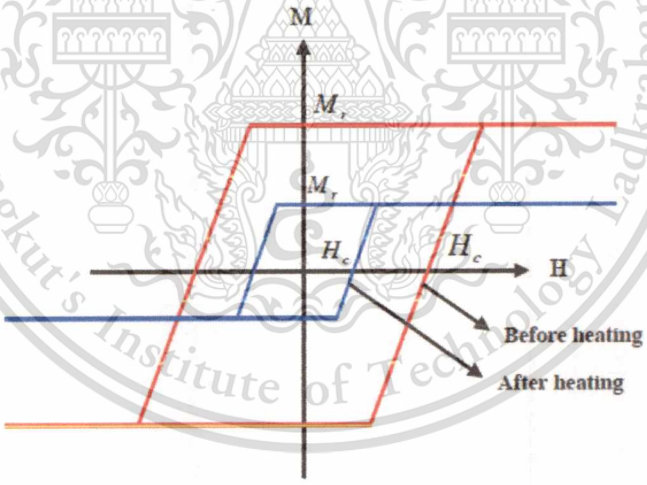


Figure 2.3 Idealized magnetization versus magnetic field hysteresis loop (MH loop) of the medium before and after heating [3].

Williams and Comstock noted it is possible to solve the derivative of (2.3) by evaluating at the x_0 where H_a at x_0 is equal to the coercivity H_c. The WC slope equation can be derived from

This material is reserved for educational use only, not allowed for commercial use.
Forbidden to modify the content, and cite the document when use.

$$\left.\frac{dM(x)}{dx}\right|_{x_0} = \left.\frac{dM(H)}{dH_a}\right|_{H_r} \left.\frac{dH_a(x)}{dx}\right|_{x_0} = \left.\frac{dM(H)}{dH_a}\right|_{H_c} \left[\left.\frac{dH_h(x)}{dx}\right|_{x_0} + \left.\frac{dH_d(x)}{dx}\right|_{x_0}\right] \quad (2.4)$$

The magnetization transition during recording can be described by the arctangent function, both the magnetization gradient dM/dx and demagnetization field gradient dH_d/dx can be expressed analytically in terms of only one unknown quantity, namely, the transition parameter a. Furthermore, the head field gradient dH_h/dx and magnetization gradient with applied field $dM(H)/dH_a$ can be evaluated from the analytic Karlqvist head field expressions and the M–H loop for the medium. These assumptions allow (2.4) to be solved analytically, giving an expression for a containing all the relevant factors in the write process.

2.3.2 Thermal Williams-Comstock (TWC) model

The function $F_{loop}(H_a)$ in the WC model does not account for the effects of heating in the HAMR system. In 2004, WC model was extended by incorporating thermal gradients of H_c and M_r for a longitudinal HAMR system and is known as the Thermal Williams–Comstock (TWC) model, as in [4]. The effective field h is introduced to account for heating behavior, i.e.,

$$h(x) = \frac{H_a(x)}{H_c(T(x))}. \quad (2.5)$$

The dependence of M on the temperature captured by h is substituted into $M=F_{loop}(h)$. Evaluating the derivative of $M(x)$ at x_0, where the applied field is equal to coercivity $H_a=H_c$, we obtain

$$\left.\frac{dM(x)}{dx}\right|_{x_0} = \left.\frac{dM(h)}{dh}\right|_{H_c} \left.\frac{dh(x)}{dx}\right|_{x_0} \quad (2.6)$$

The derivative at the H_c is simply the linear slope and S^* is coercivity squareness factor.

This material is reserved for educational use only, not allowed for commercial use.
Forbidden to modify the content, and cite the document when use.

$$\left.\frac{dM(x)}{dx}\right|_{H_c(T(x_0))} = \frac{M_r(T(x_0))}{(1-S^*(T(x_0)))} = \left.\frac{H_c(T(x_0))dM(H)}{dH_a}\right|_{H_c(T(x_0))} \tag{2.7}$$

The thermal Williams-Comstock slope equation can then be derived from (2.4) giving

$$\left.\frac{dM(x)}{dx}\right|_{x_0} = \left.\frac{dM(H)}{dH_a(T(x_0))}\right|_{H_c(T(x_0))} \times \left[\left.\frac{dH_h(x)}{dx}\right|_{x_0} + \left.\frac{dH_d(x)}{dx}\right|_{x_0} - \left.\frac{dH_c(T(x_0))}{dT}\right|_{T(x_0)} \left.\frac{dT}{dx}\right|_{x_0}\right]. \tag{2.8}$$

Since dM/dx and dH_d/dx depend on a, a can be solved by using (2.5). To obtain dM/dx, it is assumed that the transition during recording can be described by the arctangent function from which dM/dx can be derived from

$$M(x) = \frac{2M_r(T(x))}{\pi} \tan^{-1}\frac{x-x_0}{a}, \tag{2.9}$$

and dM/dx at x_0 can be solved by differentiating (2.9), i.e.,

$$\left.\frac{dM(x)}{dx}\right|_{x_0} = \frac{2M_r(T(x_0))}{\pi a} \tag{2.10}$$

The term $dM(h)/dh$ from (2.6) at x_0 can be solved as the slope of hysteresis loop is always positive at either transition is made from positive or negative H_c, therefore,

$$\left.\frac{dM(h)}{dh}\right|_{H_c(T(x_0))} = \left|\frac{1}{H_c(T(x_0))} \times \frac{M_r(T(x_r))}{1-S^*}\right| \tag{2.11}$$

As we are using perpendicular recording in that the field of head magnetizes the medium in the vertical direction, the head pole and field setup are illustrated in Figure 2.4.

The term dH_h/dx of perpendicular recording at x_0 can be solved by using the symmetry of the longitudinal Karlqvist head field component. An image of the pole head can be considered to be placed below the medium. The perpendicular setup as in Figure 2.4 (b) is similar to longitudinal setup in Figure 2.4 (a) when it is turned sideways [7], [12]. The perpendicular head field can be derived by facilitating to turned sideways of the longitudinal system as

This material is reserved for educational use only, not allowed for commercial use.
Forbidden to modify the content, and cite the document when use.

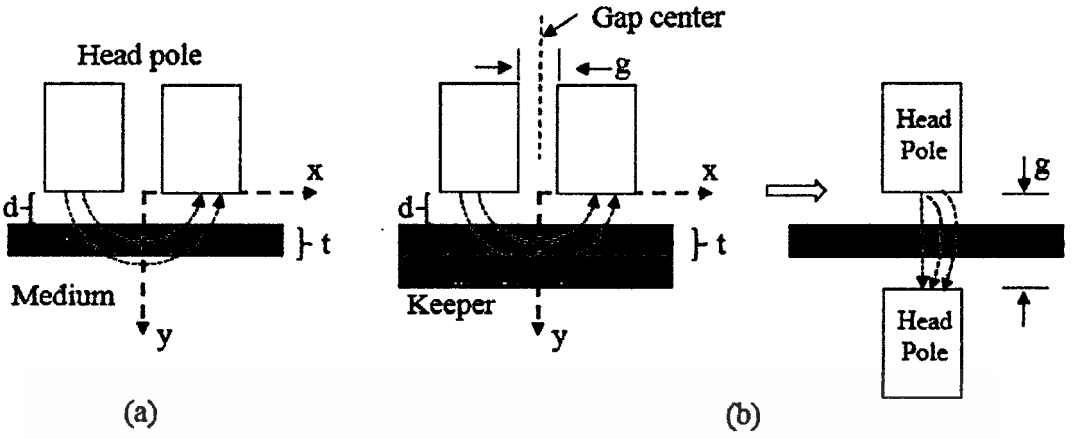


Figure 2.4 Head pole and field set up for (a) longitudinal and (b) perpendicular recording systems [9].

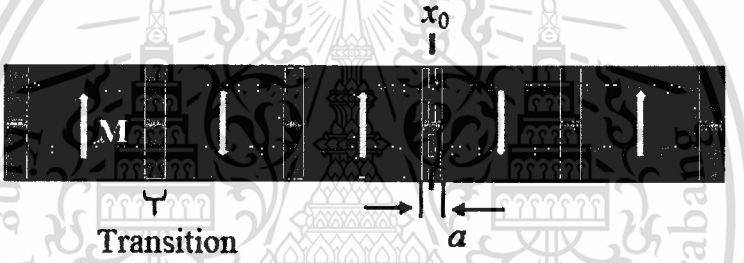


Figure 2.5 Transition center (x_0) and transition parameter (a) of perpendicular recording system.

$$H_h = \frac{H_0}{\pi}\left[\tan^{-1}\left(\frac{y+g/2}{x}\right) - \tan^{-1}\left(\frac{y-g/2}{x}\right)\right] \tag{2.12}$$

and

$$\left.\frac{H_h(x)}{dx}\right|_{x_0} = -\frac{gH_0}{\pi\left(x^2+(g/2)^2\right)} \tag{2.13}$$

where H_0 is the deep gap field, g is the gap width between pole head and its image ($g = 2d+2t$), t is the medium thickness and the field is evaluated at the center of medium ($y = t/2$). The parameter H_d for perpendicular recording is obtained by convolving the unit step response at the original and the magnetization gradient, i.e.,

This material is reserved for educational use only, not allowed for commercial use.
Forbidden to modify the content, and cite the document when use.

$$H_{d,perp} = -\frac{\partial M(x)}{\partial x} * H_y^{step} = -\frac{\partial M(x)}{\partial x} * \frac{1}{\pi}\tan^{-1}\left(\frac{2x}{t}\right) \tag{2.14}$$

$$H_d = -\frac{2}{\pi}\int_{-\infty}^{\infty}\left[\frac{M_r(T(x'))a}{a^2+(x_0-x')^2} + \tan^{-1}\left(\frac{x'-x_0}{a}\right)\frac{dM_r\left(T\left(x'\right)\right)}{dx'}\right]\times\tan^{-1}\left(\frac{2(x-x')}{t}\right)dx' \tag{2.15}$$

and

$$\begin{aligned}\frac{dH_d(x)}{dx} = &-\frac{4}{\pi^2}\int_{-\infty}^{\infty}\frac{M_r(T(x'))a}{a^2+(x'-x_0)^2}\frac{t}{t^2+4(x-x')^2}dx' + \\ &\frac{4}{\pi^2}\int_{-\infty}^{\infty}\tan^{-1}\left(\frac{x'-x_0}{a}\right)\frac{dM_r(T(x'))}{dT}\bigg|_{T(x')}\frac{dT(x')}{dx'}\frac{t}{t^2+4(x-x')^2}\end{aligned} \tag{2.16}$$

Here, H_c and M_r are linearly temperature-dependent (T),i.e,

$$H_c = -H_{c0}T(x,y) + H_{c,const} \tag{2.17}$$

and

$$M_r = -M_{r0}T(x,y) + M_{r,const} \tag{2.18}$$

where H_{c0} and M_{r0} are the temperature sensitivities of H_c and M_r, $H_{c,const}$ and $M_{r,const}$ are H_c and M_r at 0 Kelvin (K). So dH_c/dT is $-H_{c0}$ and dM_r/dT is $-M_{r0}$. A two-dimensional (2D) Gaussian thermal profile is given as

$$T(x,z) = T_{peak}\exp\left(-\frac{(x-c_0)^2}{2\sigma_t^2}\right)\exp\left(-\frac{z^2}{2\sigma_t^2}\right) + 300 \quad (\mathrm{K}) \tag{2.19}$$

where T_{peak} is the peak temperature in the medium above room temperature in degree Celsius, c_0 is the laser spot position, x is defined to the position in down-track direction and z is defined to the position in cross-track direction. Differentiating (2.19), we have

$$\frac{T(x,z)}{dx} = T_{peak}\left(-\frac{(x-c_0)}{\sigma_t^2}\right)\exp\left(-\frac{(x-c_0)^2}{2\sigma_t^2}\right)\exp\left(-\frac{z^2}{2\sigma_t^2}\right) \tag{2.20}$$

This material is reserved for educational use only, not allowed for commercial use.
Forbidden to modify the content, and cite the document when use.

2.3.3 Transition center (x_0) and transition parameter (a)

The position of transition center x_0 is defined as the point where the medium reverses its direction of magnetization and transition parameter a is measured and related to the width of the magnetization transition. The transition parameter is related to the magnetization width. If transition is big, the transition is wide. Achieving the narrowest possible transition (smallest a) allows placing recording bits close together and, hence, results in high linear density. The position x_0 of perpendicular HAMR with large spot and linear relationship for H_c and M_r can be calculated, as in [9],

$$x_0 = \frac{g + \sqrt{g^2 - a\tan^2\left(\pi \frac{H_c\left(T(x_0)\right)}{H_0}\right)\left(y^2 - (g/2)^2\right)}}{2\tan\left(\pi\left(\frac{H_c\left(T(x_0)\right)}{H_0}\right)\right)} \tag{2.21}$$

and a can be also calculated from

$$a = -\frac{\gamma}{2} + \frac{1}{2}\sqrt{\gamma^2 + \left.\frac{4H_c\left(1-S^*\right)t}{\Delta\pi}\right|_{x_0}} \tag{2.22}$$

where

$$\Delta \equiv \frac{H_g g}{\pi\left(x_0^2 + (g/2)^2\right)} - \left.\frac{dH_0}{dT}\frac{dT}{dx}\right|_{x_0}$$

and

$$\gamma \equiv \frac{2M_r}{\Delta\pi} - \frac{t}{2} + \frac{2H_c(1-S^*)}{\Delta\pi},$$

This material is reserved for educational use only, not allowed for commercial use.
Forbidden to modify the content, and cite the document when use.

For non-large spot HAMR, x_0 can be solved by

$$x_{0,j+1} = \frac{g + \sqrt{g^2 - 4\tan^2\left(\pi \frac{H_c(T(x_0)) + H_d(x_0, j, a_k)}{H_0}\right)\left(y^2 - (g/2)^2\right)}}{2\tan^2\left(\pi \frac{H_c(T(x_0)) + H_d(x_0, j, a_k)}{H_0}\right)} \tag{2.23}$$

and a can be solved by

$$a_{k+1} = \frac{-\beta + \sqrt{\beta^2 + 4\pi(\alpha+\delta)H_C(1-S^*)t}}{2\pi(\alpha+\delta)} \tag{2.24}$$

where

$$\alpha = \frac{H_g g}{\pi\left(x_{0,j+1}^2 + (g/2)^2\right)}, \delta = \frac{dH_d\left(a_k, x_{0,j+1}\right)}{dx} - \frac{dH_c}{dx},$$

and

$$\beta = -\frac{\pi\alpha t}{2} + 2M_r - \frac{\pi t}{2}\left(\frac{dH_d\left(a_k, x_{0,j+1}\right)}{dx} - \frac{dH_c}{dx}\right) + 2H_c(1-S^*)$$

where j is the iteration of x_0 and k is the iteration of a

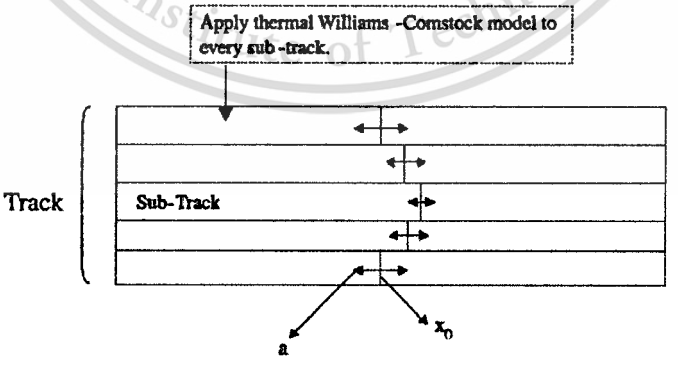


Figure 2.6 Microtrack modeling of HAMR channel [7].

This material is reserved for educational use only, not allowed for commercial use.
Forbidden to modify the content, and cite the document when use.

2.3.4 Microtrack model

The microtrack model, which is illustrated in Figure 2.5, is used for 2D process of the heating and magnetization of a medium to determine the transition characteristics in HAMR by dividing recorded track into *N* individual sub-tracks of equal width with different transition parameters. The TWC equation is then applied to determine x_0 and a on each individual sub-track, as in [4]-[9]. The playback voltage (V) of perpendicular recording is given from [12]

$$V(x,a_i,x_{0,i}) = -CM_r t \ln\left(\frac{\left(g_r/2-(x-x_{0,i})\right)^2+\left(d+a_i+t/2\right)^2}{\left(g_r/2+(x-x_{0,i})\right)^2+\left(d+a_i+t/2\right)^2}\right) \tag{2.25}$$

where C is a system specific constant, g_r is the read head gap, and d is the head-medium spacing, i is the i^{th} of microtrack and t is defined to media thickness.

The overall transition response $p(x)$ can be obtained by weighting the transition response $p_i(x)$ of each sub-track to obtain

$$p_i(x) = \exp\left(-\frac{\left(\frac{N+1}{2}\Delta z+i\Delta z\right)^2}{2\sigma_r^2}\right)\cdot V(x,a_i,x_{0,i}) \tag{2.26}$$

and

$$p(x) = \frac{1}{N}\sum_{i=1}^{N} p_i(x) \tag{2.27}$$

where a_i and x_{0i} are the transition parameter and transition center of the i^{th} microtrack, $I \in \{1, ..., N\}$, Δz stands for the width of each sub-track and σ_r is defined as the sigma of reader sensitivity function. The bit response $h(x)$ is then

$$h(x) = 0.5\{p(x)-p(x-T_x)\} \tag{2.28}$$

where T_x denotes the along-track bit period.

This material is reserved for educational use only, not allowed for commercial use.
76522
Forbidden to modify the content, and cite the document when use.

CHAPTER 3

TARGET AND EQUALIZER DESIGN

In this Section, we explain the conventional magnetic recording model in Section 3.1 and after that the read channel for the HAMR system is discussed in Section 3.2. Afterward, we will describe the design of the target and equalizer by the minimum-mean squared error (MMSE) method in Section 3.3. Finally, the Viterbi detector will also be explained in Section 3.4.

3.1 The conventional magnetic recording model

The conventional magnetic recording system is shown in Figure. 3.1. The magnetic recording system consists of the playback signal generator, the low-pass filter (LPF) which is used to remove out-of-band noise, the FIR equalizer that is used to reduce the effect of intersymbol interference (ISI) and the Viterbi detector (VD). In the write process, the binary bits are first encoded by the error correction code (ECC) encoder. Currently, most hard disk drives employ low-density parity-check codes code as ECC. The encoded data are then further encoded by the modulation encoder to ensure the minimum and maximum run length of 0's in the data sequence. The commonly used code is the run length limited (RLL) code. The output data bits from the modulation encoder are sent to the modulator for converting the data bits to the write current waveform and then to the write head for writing the data on the media. For the read process, the read head senses the magnetic transition from the media. When it moves to the magnetic transition zone, it reads out the voltage waveform, called playback signal. The playback signal is then sent for processing in the read channel circuits consisting of LPF, analog-to-digital (A/D) converter for sampling data, FIR equalizer and VD. The combination of partial response (PR) target and VD is often termed "PRML". The output data are decoded by the modulation decoder and the ECC decoder, respectively, to produce the estimate of message bits [14], [16], [18], [19].

This material is reserved for educational use only, not allowed for commercial use.
Forbidden to modify the content, and cite the document when use.

Figure 3.2 depicts the block diagram of the conventional read channel model. The sequential binary input data $a_k \in \{-1, 1\}$ with bit period T being sent to ideal differentiator *(1-D)/2*, where D is delay. This changes data to $b_k \in \{-1, 0, 1\}$, where $b_k = \pm 1$ is a positive transition or negative transition and $b_k = 0$ represents no transition change.

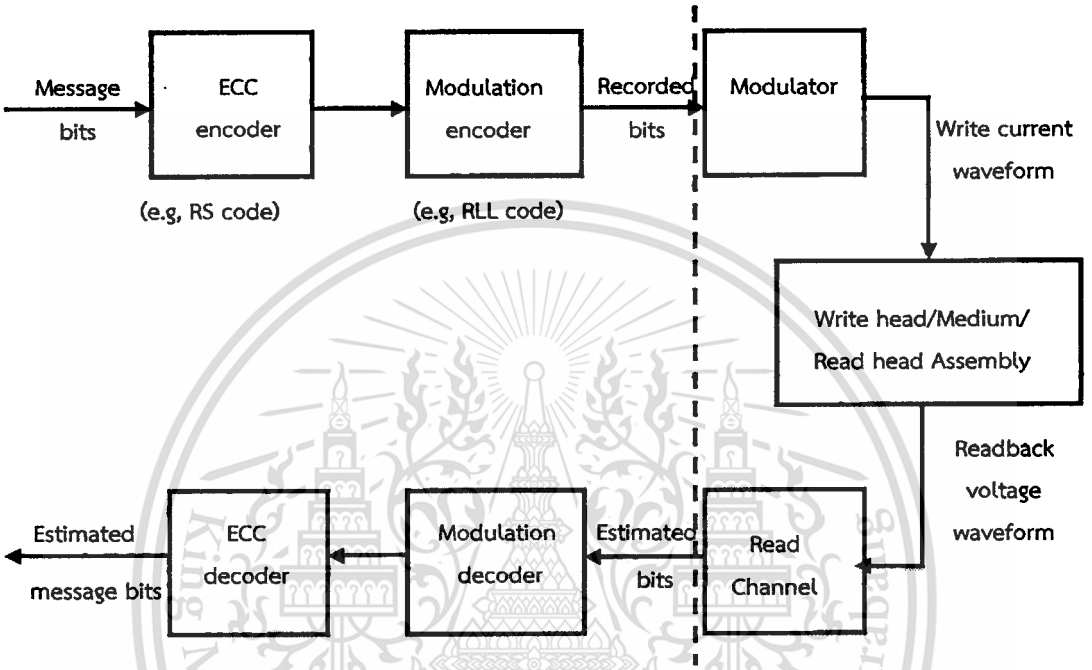


Figure 3.1 Magnetic recording system model [14].

The signal b_k will be sent through the recording channel with isolated response *g(t)* to generate the playback signal *b(t)*, then the noise *n(t)* corrupts the read-back signal *p(t)*. The *p(t)* is then filtered by a the low-pass filter to remove out-of-band noise. Consequently, the resulting signal is sampled by the A/D converter [14].

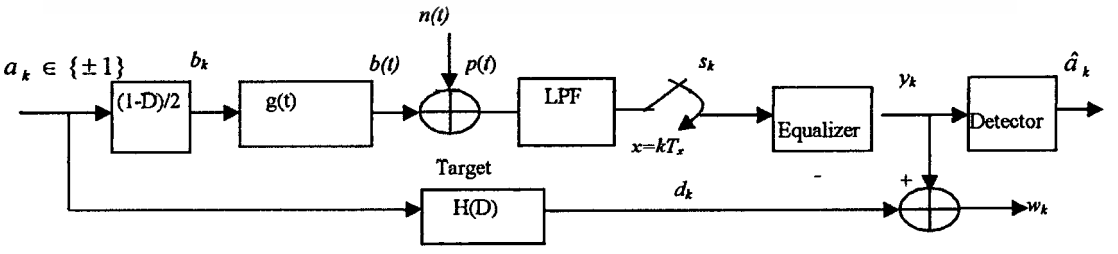


Figure 3.2 The conventional read channel model [18].

This material is reserved for educational use only, not allowed for commercial use.
Forbidden to modify the content, and cite the document when use.

For longitudinal channel, *g(t)* is defined as

$$g(t)=\frac{1}{1+\left(\frac{2t}{PW_{50}}\right)^2} \tag{3.1}$$

where PW_{50} is the pulse width of *g(t)* at half of the maximum amplitude. The transition response g(t) for the perpendicular channel is defined as

$$g(t)=erf\left(\frac{2t\sqrt{\ln 2}}{PW_{50}}\right) \tag{3.2}$$

where PW_{50} is the pulse width of differential of *g(t)* or *g'(t)* at half of the maximum amplitude. An error function is defined as

$$erf(x)=\frac{1}{\sqrt{x}}\int_0^x e^{-t^2}dt \tag{3.3}$$

The playback signal which is corrupted by AWGN noise can be written as

$$p(t)=\sum_{k=-\infty}^{\infty} b_k \cdot g(t-kT)+n_k \tag{3.4}$$

The sampled data s_k are put in FIR equalizer to equalize the signal into partial response (PR) target, and then sent to VD to find the possible input data.

The classical metric of data storage products is the areal density (AD). AD can be calculated by

$$Areal\ Density\left[bits/inch^2\right]=\frac{1\,bit}{T[inch]\times TW[inch]} \tag{3.5}$$

where *T* is bit period and *TW* is track width respectively, of the specific area of interest to be magnetized to store 1 bit of information. The unit of *T* and *TW* are inch. The recording linear density or normalized density (*ND*) is can be obtained by

This material is reserved for educational use only, not allowed for commercial use.
Forbidden to modify the content, and cite the document when use.

$$ND = \frac{PW_{50}}{T} \tag{3.6}$$

which indicates how many bits are recorded in the interval PW_{50}. If T is fixed, increasing of *ND* or *PW50* means the HDD have the higher capacity.

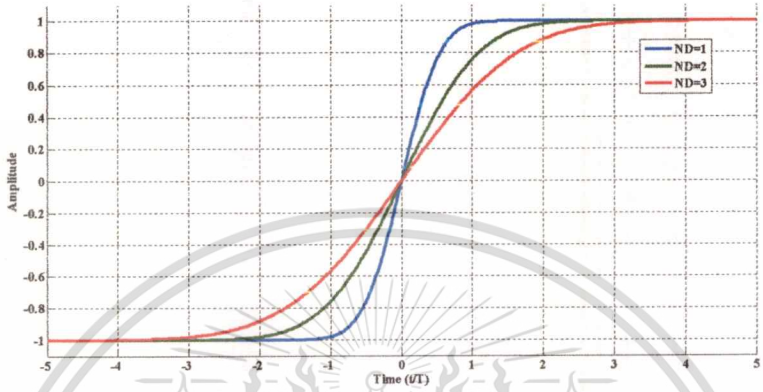


Figure 3.3 Transition responses for perpendicular channel with various *ND*s.

Figure 3.3 shows the transition response of perpendicular channel when *ND* is 1, 2 and 3 respectively. The transition pulses span many symbol interval as *ND* increases. The ISI becomes more severe as *ND* increases because there is a high possibility of overlapping between the output from transitions.

3.2 The channel model for heat-assisted magnetic recording (HAMR)

The read process of the conventional read channel models employed in current magnetic recording systems has been used to produce the HAMR playback signals, as in [4]-[11].

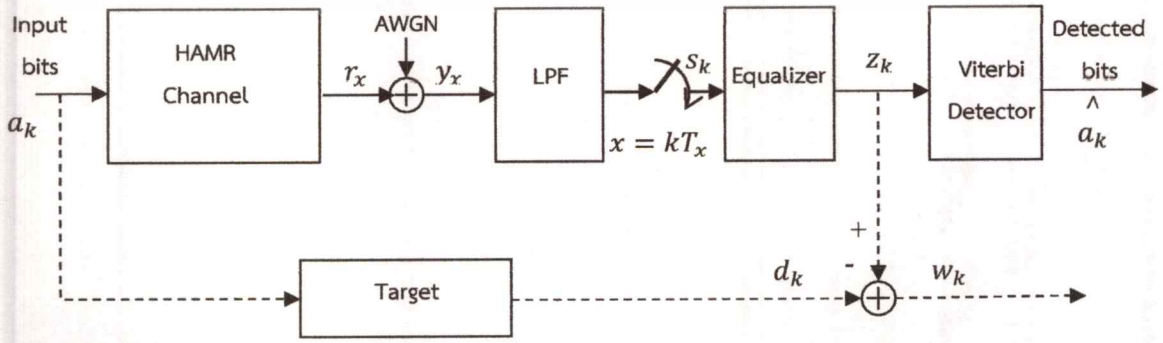


Figure 3.4 The HAMR system with target-shaping equalization.

This material is reserved for educational use only, not allowed for commercial use.
Forbidden to modify the content, and cite the document when use.

For this section, we investigate the read channel performance of HAMR by using the conventional PRML system. In this work, we assume that the HAMR medium is ideal which has no jitter noise in the position of transition. There is only the AWGN corruption and included to the playback signal. The channel which is used in this simulation is shown in Figure 3.4. The random binary input sequences $a_k \in \{\pm 1\}$ with bit period T_x is put to the HAMR channel. The playback signal r_x is obtained and corrupted by the additive white Gaussian noise (AWGN). In this simulation, the signal-to-noise ratio *SNR* is defined as $SNR = 10\log(1/\sigma^2)$, where σ^2 is the variance of AWGN.

$$r(x) = \sum_{k=-\infty}^{\infty} b_k \left(\frac{1}{N}\sum_{i=1}^{N} p_i(x - kT_x)\right) + n(x) \tag{3.7}$$

The playback signal with AWGN y_x will be passed to low pass filter (LPF) to remove out-of-band noise, sampled and then put in equalizer (FD) to equalize the signal in order to facilitate the application of Viterbi detector (VD). Finally, the equalized output bits z_k are detected by VD.

3.3 Target and equalizer design

In this study, we design the targets H(D) and the equalizers F(D) by using the minimum-mean squared error (MMSE) method to minimize the mean-squared error (MSE) between the desired outputs and the equalizer outputs, as in [11], [14], [23]. Using the channel model in Figure 3.4, the desired output *H(D)* and equalizer output *F(D)* can be written in the *D* domain of the mathematical form

$$H(D) = \sum_{k=0}^{L-1} h_k D^k \tag{3.8}$$

and

$$F(D) = \sum_{k=-K}^{K} f_k D^k \tag{3.9}$$

This material is reserved for educational use only, not allowed for commercial use.
Forbidden to modify the content, and cite the document when use.

where h_k stands for the coefficients of $H(D)$, f_k is the coefficients of $F(D)$, L is the target length and K represents the equalizer tap where the length is N $(N=2K+1)$. The target and equalizer output are expressed as

$$d_k = a_k * h_k \tag{3.10}$$

and

$$z_k = s_k * f_k \tag{3.11}$$

where * is the convolution operator

The target $H(D)$ and its corresponding equalizer $F(D)$ can be obtained based on the MMSE method. The MSE between the desired outputs and the equalizer outputs is given by

$$E\{w_k^2\} = E\left[(z_k - d_k)^2\right] \tag{3.12}$$

where w_k is the difference between output of equalizer, z_k and the desired output, d_k of designed target. The equation (3.12) can be written in a matrix form as

$$\varepsilon^2 = E\{w_k^2\} = \mathbf{F}^T\mathbf{R}\mathbf{F} + \mathbf{H}^T\mathbf{A}\mathbf{H} - 2\mathbf{F}^T\mathbf{P}\mathbf{H} \tag{3.13}$$

where $E\{.\}$ is the expectation operator, $\mathbf{H} = [h_0 \;\; h_1 \;\; h_2 \ldots h_{L-1}]^T$ represents the L–tap GPR target and $\mathbf{F}=[f_{-K}, f_{-K+1}, \ldots f_0 \ldots f_K]^T$ represents the K-tap equalizer which the length of the equalizer is N (N = $2K$+1). The center tap is at K=0. The matrix $\mathbf{A}$ is an LxL autocorrelation matrix of a_k, R is an MxM autocorrelation matrix of sequence s_k, and $\mathbf{P}$ is an MxL cross-correlation matrix sequence of a_k and s_k. During the minimization process, the specified constraint must be used to avoid the trivial solution of $\mathbf{F} = 0$ and $\mathbf{H} = 0$.

This material is reserved for educational use only, not allowed for commercial use.
Forbidden to modify the content, and cite the document when use.

Firstly, by minimizing (3.13) subject to the monic constraint. In the monic constraint, the first coefficient of target is equal to be 1 (h_0=1). The matrix form of this constraint is $\mathbf{I}^T\mathbf{H}$=1. The minimum MSE is

$$\varepsilon^2 = \mathbf{F}^T\mathbf{R}\mathbf{F} + \mathbf{H}^T\mathbf{A}\mathbf{H} - 2\mathbf{F}^T\mathbf{P}\mathbf{H} - 2\lambda\left(\mathbf{I}^T\mathbf{H} - 1\right) \tag{3.14}$$

Step of target and equalizer design of monic constrant are;

(i) define the number of target's tap *L* and equalizer's tab *N* to create vector F and H

(ii) compute matrix R, A and P

(iii) create vector I = [1, 0, 0, ...,0]^T which have the size *L*x1

(iv) compute the Lagrange multiplier

$$\lambda = \frac{1}{\mathbf{I}^T\left(\mathbf{A} - \mathbf{P}^T\mathbf{R}^{-1}\mathbf{P}\right)^{-1}\mathbf{I}} \tag{3.15}$$

(v) compute the target

$$\mathbf{H} = \lambda\left(\mathbf{A} - \mathbf{P}^T\mathbf{R}^{-1}\mathbf{P}\right)^{-1}\mathbf{I} \tag{3.16}$$

(vi) compute the equalizer

$$\mathbf{F} = \mathbf{R}^{-1}\mathbf{P}\mathbf{H} \tag{3.17}$$

where λ is the Lagrange multiplier and *I* is an *L*-element column vector of the first element is 1 and the rest is 0.

Secondly, we subject to the h_1=1 constraint. For this constraint, we fix the second coefficient to be 1, the first and the rest elements can be any values. Here, the column vector J is introduced. J is an *L*x1-element column vector which the second element is defined to 1 and the other elements are 0, J = [0, 1, 0, ...,0]^T. The solutions are identical to the monic constraint solution except that I is replaced by J. The h_1=1 constraint in the matrix form can be expressed as $\mathbf{J}^T\mathbf{H}$ = 1.

This material is reserved for educational use only, not allowed for commercial use.
Forbidden to modify the content, and cite the document when use.

Thirdly, the energy $H^TH=1$ is fixed to minimize ε^2 by always maintaining $H^TH = 1$ called the unit energy constraint.

$$\varepsilon^2 = \mathbf{F}^T\mathbf{R}\mathbf{F} + \mathbf{H}^T\mathbf{A}\mathbf{H} - 2\mathbf{F}^T\mathbf{P}\mathbf{H} - 2\lambda\left(\mathbf{H}^T\mathbf{H} - 1\right) \tag{3.18}$$

In this process, the MMSE can be the lowest value by differentiating (3.18) compared to **F**, **H** and λ, then set all derivatives to be 0, the target and equalizer can be computed from

$$(\mathbf{A} - \mathbf{P}^T\mathbf{R}^{-1}\mathbf{P})\mathbf{H} = \lambda\mathbf{H} \tag{3.19}$$

It is identical to eigenvalue problem where λ is the MMSE.

For the final constraint we use is the fixed target constraint according to PR form. The target function **H** is fixed. The equalizer **F** which is proper to the fixed target can be computed from $\mathbf{F} = \mathbf{R}^{-1}\mathbf{P}\mathbf{H}$ in (3.17) by ensuring the MMSE in (3.13)

3.4 Viterbi detector

The Viterbi detector (VD) is the sequence detection which works based on Viterbi Algorithm (VA) for decoding the input sequence encoded by convolution code. The VD is one of the famous maximum likelihood sequence detector (MLSD) which is an effective method to mitigate the effect of ISI, improving the system performance. VD is widely used in the digital communication problem and also used in the signal processing of magnetic recording system. The VA minimizes the error probability by comparing the likelihoods of a set of possible state transitions that can occur. The VA is viewed as the solution of maximum likelihood (ML) estimation of the transmitted data sequence that is corrupted by the additive white Gaussian noise (AWGN). The combination of VD with equalizer in data storage channels is used to mitigate the ISI effects that resulted in the commercial products. The equalizer is used to reduce the effect of ISI. Then, the equalized output is sent to VD for decoding. The complexity of VD is based on ISI. More ISI presents more complexity of

This material is reserved for educational use only, not allowed for commercial use.
Forbidden to modify the content, and cite the document when use.

VD. VD works through a trellis diagram that constructs from the finite state machine (FSM) [14], [21], [22]. The figure 3.5 shows Viterbi detection in the channel model.

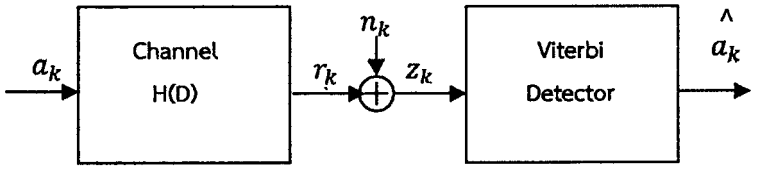


Figure 3.5 Viterbi detection in the channel model.

3.4.1 The finite state machine (FSM)

The trellis in this case represents a graph of a finite set of states from a FSM. Each node in this graph represents a state and each edge a possible transitions between two states at consecutive discrete time intervals. The FSM here is commonly used in digital electronics and is often referred to in the literature as a Markov process which the next state depends on the current state as shown in Figure 3.6. The Markov process is a probability of the state a_{k+1} at time $k+1$ which depends on the state a_k at time k, $(a_{k+1}|a_k)$. The sequence output z_k can be assumed that depends on a_k as

$$p(z|a) = \prod_k p(z_k|a_k) \tag{3.20}$$

where *P(.)* id denotes to the probability and *p(.)* is probability density function (PDF). There are many states and transitions in the Markov process, which the VA is a solution to find transition sequence, where *p(z|a)* is the maximum.

The detected maximum probability sequence is based on the trellis diagram which is created from channel *H(D)* to apply to the VA in convolution code.

$$z_k = \sum_{i=0}^{v} a_i h_{k-1} + n_k \tag{3.21}$$

where a_k is the k-th transmitted symbol from an alphabet set A, h_k is the target response, n_k is AWGN, r_k is the k-th channel output, v is the channel memory and L is the length of input sequence

This material is reserved for educational use only, not allowed for commercial use.
Forbidden to modify the content, and cite the document when use.

The FSM is used to explain the relationship between the input and output sequences. Figure 3.6 illustrates PR1 finite state machine model where a_k is the input bit and D is stands for delay operator. $a_k \in \{-1,1\}$ is sent to a PR1 channel and hence, the possible values of output of PR1 target is $z_k \in \{-2,0,2\}$ as shown in Table 3.1.

Table 3.1 The relationship of a_k and r_k in 1+D PR1 channel

a_k	a_{k-1}	r_k
-1	-1	-2
1	-1	0
-1	1	0
1	1	2

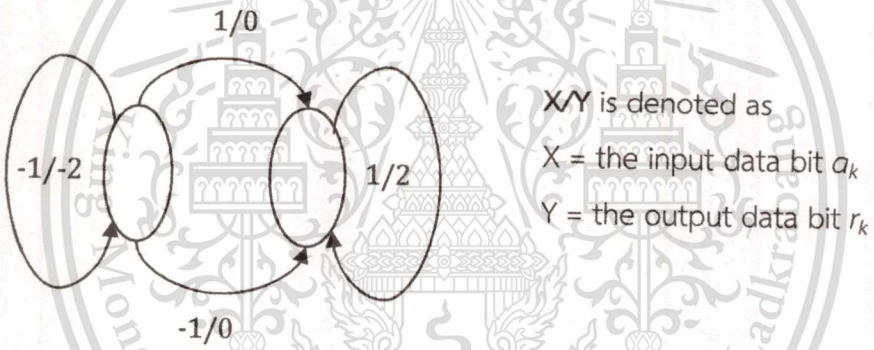


Figure 3.6 Finite state machine (FSM) diagram of PR1, H(D) = 1+D.

3.4.2 Trellis diagram

Figure 3.6 can be written to trellis diagram as shown in Figure 3.7. From a FSM and a state table from table, the trellis diagram is assumed that a finite state machine starts at start state. Each branch in trellis denotes to a possible movement from a_{k-1} state at time $k-1$ to a_k state at time k. We can create the state transition diagram from time $k-1$ to time k and illustrate in Figure 3.7. Here, the detector estimates the maximum likelihood path on the trellis diagram which constricted by using the state transition diagram.

This material is reserved for educational use only, not allowed for commercial use.
Forbidden to modify the content, and cite the document when use.

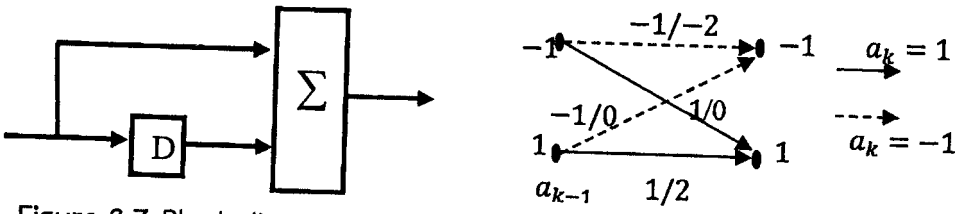


Figure 3.7 Block diagram and trellis diagram of the 1+D PR1 channel.

3.4.3 Viterbi Algorithm (VA)

In the PRML system, the Viterbi detector which is an ML detector, is applied to convert the output sequence into the corresponding sequence of detected bits. The Viterbi Algorithm (VA) is a detection algorithm which has been used to implement the MLSE to find the maximum likelihood or survivor path. VD detects the possible input sequence from Markov process as

$$p(z|a) = \frac{1}{\left(\sqrt{2\pi\sigma^2}\right)^{L+\upsilon}} \exp\left\{-\frac{1}{2\sigma^2}\sum_{k=0}^{L+\upsilon-1}\left|z_k - r_k\right|^2\right\} \tag{3.22}$$

where σ^2 is variance or noise, υ is memory of the recording channel H(D), and L is the length of input sequence a_k.

(3.22) can reduce to (3.23) by taking a natural logarithm on both sides to obtain, we get;

$$\ln\{p(z|a)\} = \ln\left\{\frac{1}{\left(\sqrt{2\pi\sigma^2}\right)^{L+\upsilon}}\right\} - \frac{1}{2\sigma^2}\sum_{k=0}^{L+\upsilon-1}\left|z_k - r_k\right|^2 \tag{3.23}$$

The first term of the right hand side of (3.23) is the constant term and the term $p(z|a)$ of the left hand side is the maximum when the metric of (3.24) is the minimum.

$$\sum_{k=0}^{L+\upsilon-1}\left|z_k - r_k\right|^2 \tag{3.24}$$

$\left|z_k - r_k\right|^2$ is the mean square distance (MSD) and can find the minimum path by the summation of

This material is reserved for educational use only, not allowed for commercial use.
Forbidden to modify the content, and cite the document when use.

$$\lambda(u,q) = \left| z_k - r_k(u,q) \right|^2 \tag{3.25}$$

and

$$\min(\Phi_{i+1}(q)) = \min(\sum_{i=0}^{k} \lambda_k) \tag{3.26}$$

From (3.23)-(3.26), $\lambda(u,q)$ is the branch matric which moves from *u* state to *q* state at time k+1 and $\min(\Phi_{i+1}(q))$ is the survivor path.

Here is the steps of Viterbi algorithm;

Step 1: calculate the branch matric

Step 2: calculate the path matric

Step 3: determine the maximum likelihood path in trellis diagram which is created from FSM

This material is reserved for educational use only, not allowed for commercial use.
Forbidden to modify the content, and cite the document when use.

CHAPTER 4
SIMULATION RESULTS AND DISCUSSION

We use the MATLAB program to simulate the perpendicular heat assisted magnetic recording (HAMR). In this thesis, we simulate the HAMR system with the areal density of 4 Tb/in^2 and 5 Tb/in^2. The characteristics of the HAMR system compared to the temperature profile T, magnetization field $M(x)$, Karlqvist head field H_h and coercivity field H_c will be studied. In this work, the medium is assumed to be $Fe_{55-x}Ni_xPt_{45}L1_0$, where 10<x<30%, because the linear relationship for remanent magnetization M_r and coercivity H_c with temperature T is resulted in this range, similar to [9]-[10]. The temperature induced by the laser is assumed to be Gaussian in both along-track and cross-track directions with the peak temperature.

There are 8 sections in this chapter. Section 4.1 explains the effects of laser position to the temperature profile. Section 4.2 explains the effect of laser position and temperature to the magnetization filed. Section 4.3 presents the Karlqvist head field of both longitudinal and perpendicular recording. Section 4.4 illustrates the coercivity field with linear temperature-dependent. Section 4.5 illustrates and explains the results of perpendicular HAMR system with the areal density of 4 Tb/in^2. Section 4.6 illustrates and explains the results of perpendicular HAMR system with the areal density of 5 Tb/in^2. The results and performance of target shaping design with the areal density of 4 Tb/in^2 are shown and explained in Section 4.7. Finally, the results and performance of target shaping design with the areal density of 5 Tb/in^2 are shown and discussed in Section 4.8.

4.1 The temperature profile

In HAMR system, the coercivity of media when heated by the laser is the Gaussian distribution. A two-dimensional (2D) Gaussian thermal profile given by (2.19) in Chapter 2 is shown in Figure 4.1. This figure illustrates the distribution of temperature profile in both along-track and cross-track directions. The laser position can be attached to the write head either in the direction of the head movement (up-track or +*x*) or in the opposite direction (down-track or -*x*). The laser position is

This material is reserved for educational use only, not allowed for commercial use.
Forbidden to modify the content, and cite the document when use.

assumed to be at the center of the track in cross-track direction for all cases. To study the effect of laser position on temperature profile in the along-track position, we consider only the x direction. As we move the laser spot position c from the gap center, the temperature profiles deviate from the transition center x_0 as shown in Figure 4.2. The result when we focus on cross-track position also shows the similar results to along-track position as shown in Figure 4.3.

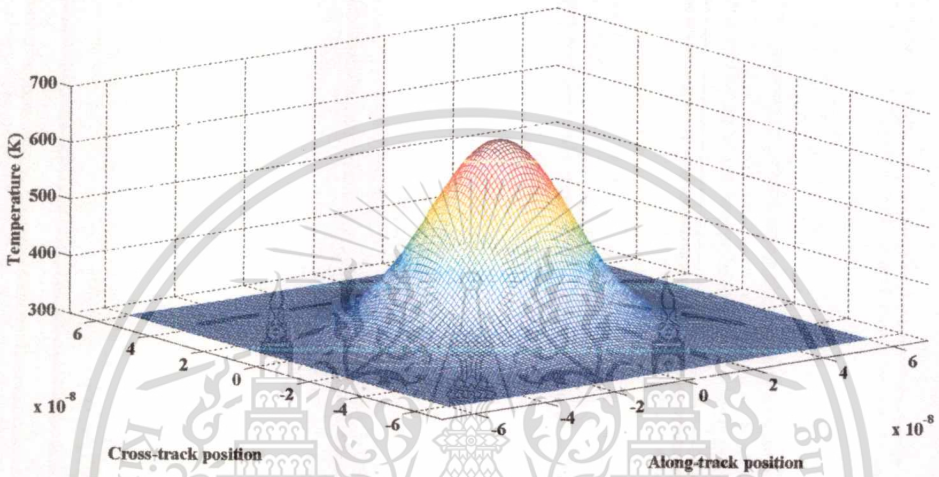


Figure 4.1 Temperature profile using σ_t= 16.2 nm and T_{peak}= 330 °C.

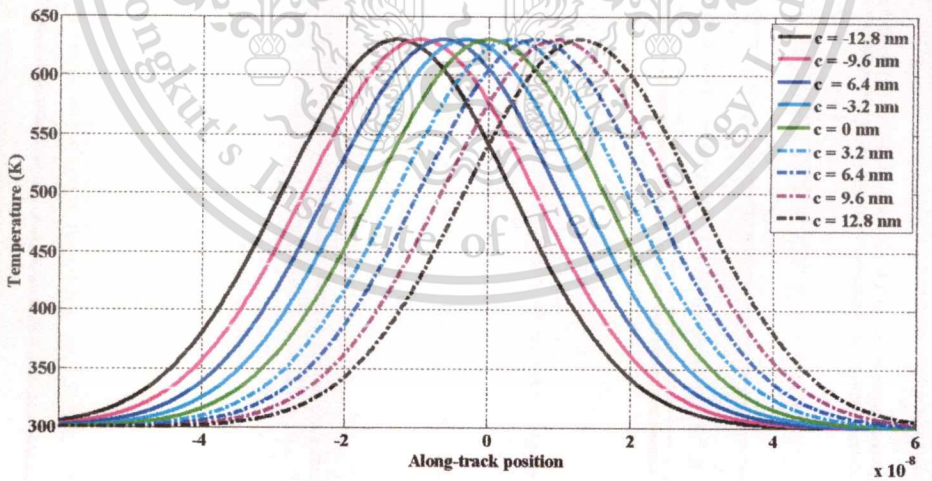


Figure 4.2 The effect of laser position on the temperature profile in the along-track position.

This material is reserved for educational use only, not allowed for commercial use.
Forbidden to modify the content, and cite the document when use.

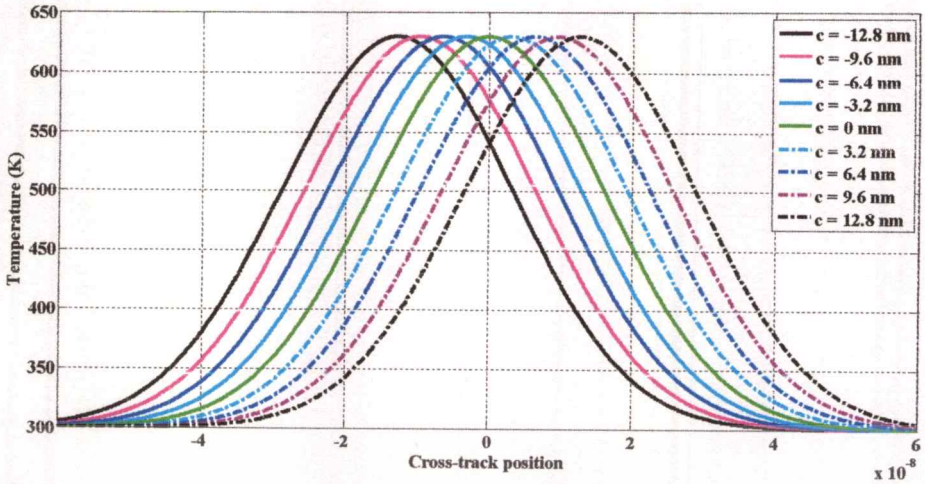


Figure 4.3 The effect of laser position on the temperature profile in the cross-track position.

4.2 The magnetization field

The transition during recording can be described by the arctangent function from (2.9) in Chapter 2. In Figure 4.4, first we use T_{peak}= 0 °C and c = 0 nm for evaluation. The results show the magnetization field $M(x)$ on the media before turning on the laser which is attached to the center gap at the same position of transition center x_0. In this case, $M(x)$ is symmetric around x_0 and it is equal to zero at x_0. Then we turn on the laser to T_{peak}= 330 °C to heat the recording media. In this case, the laser position is still attached to center gap. The result shows that $M(x)$ is decreased and appears symmetric around x_0. Finally, we turn on the laser to T_{peak}= 330 °C and move the laser spot position to the right of gap center (c = 10 nm). The result shows asymmetrical $M(x)$ with x_0. The magnetization $M(x)$ on the up-track position is lower than down-track because the laser is moved to the right of x_0.

4.3 The Karlqvist head field

In this section, we show the head field for both longitudinal and perpendicular [17] in the simulation. The Karlqvist head fields of longitudinal and perpendicular types of HAMR system are illustrated in Figures 4.5 and 4.6.

This material is reserved for educational use only, not allowed for commercial use.
Forbidden to modify the content, and cite the document when use.

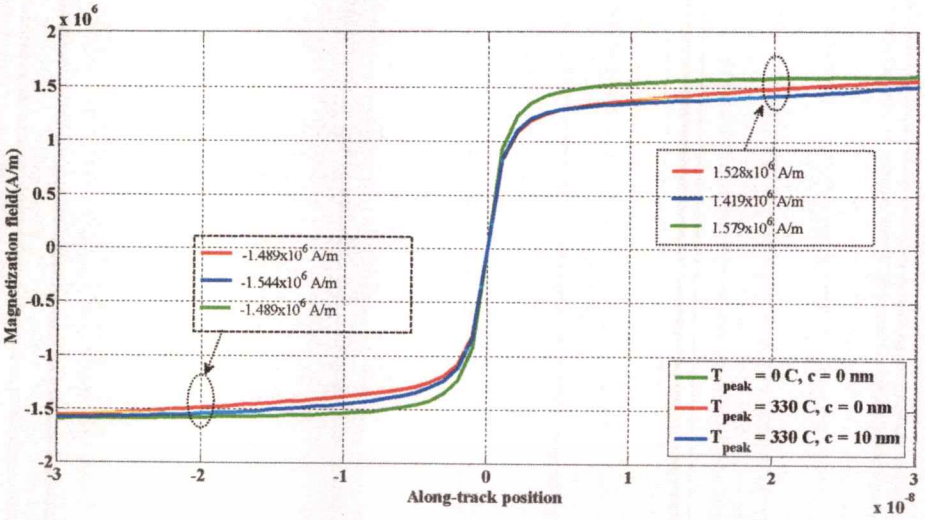


Figure 4.4 The effect of peak temperature and laser position on the magnetization field.

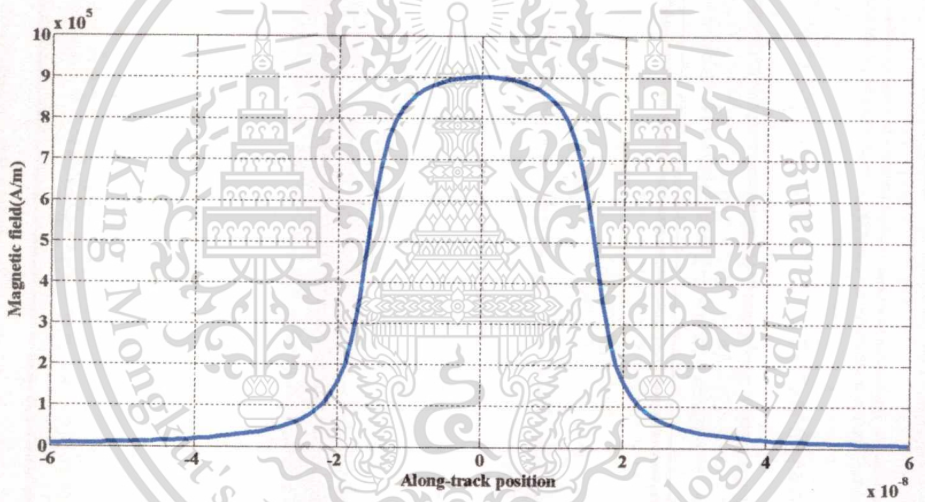


Figure 4.5 Karlqvist head fields of longitudinal HAMR system.

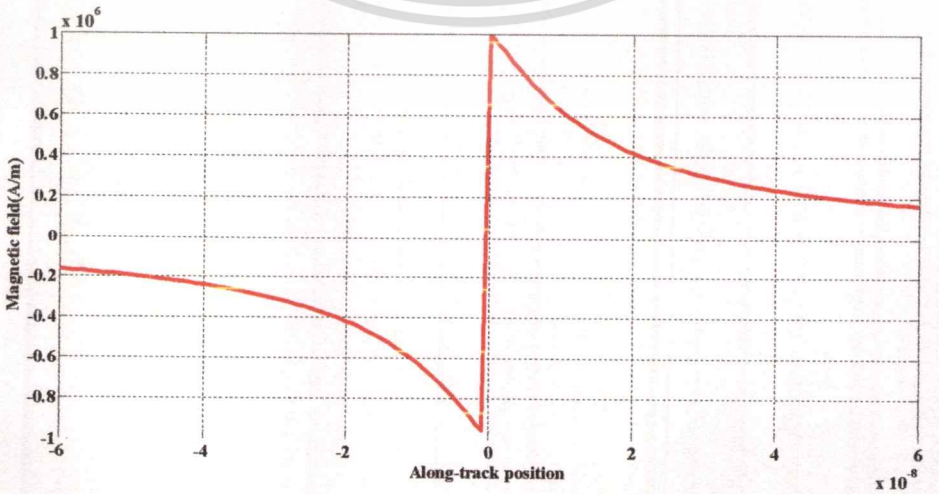


Figure 4.6 Karlqvist head fields of perpendicular HAMR system.

This material is reserved for educational use only, not allowed for commercial use.
Forbidden to modify the content, and cite the document when use.

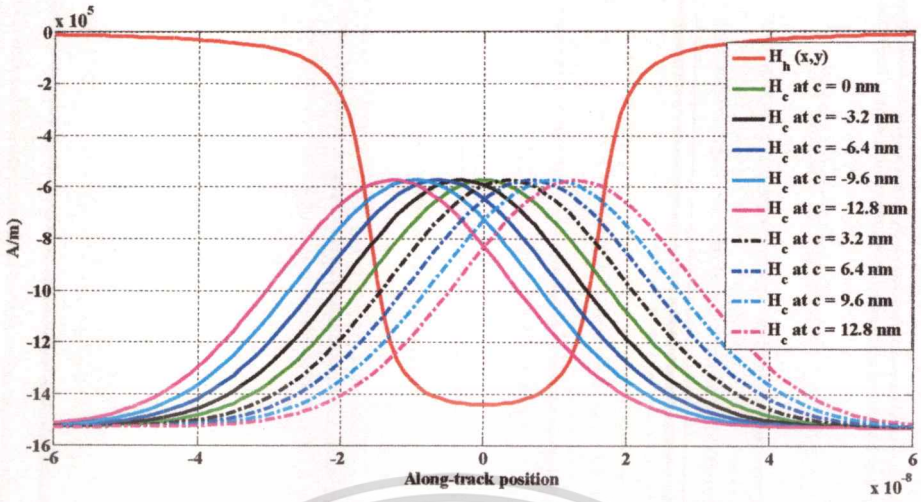


Figure 4.7 The coercivity field with various laser spot positions.

4.4 The coercivity field

In this section, the coercivity field with linear temperature-dependent ($H_{c,0}$ = -2900 and $H_{c,const}$ =2.4x10^6) is illustrated. Figure 4.7 shows how coercivity H_c changes with the laser spot position c. The coercivity field with linear temperature dependence is from (2.17) in Chapter 2. The laser can be positioned either in the direction of the head movement (up-track or $+x$) or opposite to it (down-track or $-x$). The results from this simulation show that the intersections between H_c and H_h of each laser plot position are different. The transition center x_0 is the point at which the H_h at x_0 is equal to the H_c.

4.5 The results of perpendicular HAMR simulation at the areal density of 4 Tb/in^2

In this section, we will illustrate and discuss about the effect of parameter setting in our simulation at the areal density of 4 Tb/in^2. Using the system parameters that are given Table 4.1, the bit period T_x is 6.4 nm and track width TW is 25.4 nm. The areal density can be computed by

$$Areal\ Density\left[bits/inch^2\right] = \frac{1\,bit}{T_x\left[inch\right] \times TW\left[inch\right]} \tag{4.1}$$

Firstly, we convert T_x from nm to inch, to obtain

This material is reserved for educational use only, not allowed for commercial use.
Forbidden to modify the content, and cite the document when use.

$$2.54\times10^{7}\ nm = 1\ inch$$

$$6.4\ nm = \frac{1\ inch\times 6.4\ nm}{2.54\times10^{7}\ nm} = 2.52\times10^{-7}\ inch$$

Secondly, *TW* is converted from nm to inch, to obtain

$$2.54\times10^{7}\ nm = 1\ inch$$

$$25.4\ nm = \frac{1\ inch\times 25.4\ nm}{2.54\times10^{7}\ nm} = 1.0\times10^{-6}\ inch$$

Then, we use (4.1) to compute

$$\begin{aligned} Areal\ Density\left[bits/inch^2\right] &= \frac{1\ bit}{T_x\left[inch\right]\times TW\left[inch\right]} \\ &= \frac{1\ bit}{\left(2.52\times10^{-7}\ inch\right)\times\left(1\times10^{-6}\ inch\right)} \\ &= 0.39\times10^{13}\left[bit/inch^2\right] \\ &\approx 4.0\left[Terabit/inch^2\right] \end{aligned}$$

In all the simulations, the laser is assumed to be at the center of the track in the cross-track direction but varies in the down-track direction. The parameters which can affect the transition center and transition parameter are the coercivity field H_c, the remanent magnetization M_r, head field H_0 and peak temperature T_{peak}. System parameters are given in Table 4.1.

We will first discuss the results from Figure 4.8. Firstly, we fix M_r temperature-dependent magnetization to study the behavior of x_0 and a by using the various H_c. For M_r=-1000T+1.8x10^6, we found that x_0 is shifted faraway from laser position and a is decreased while H_c increases. At the highest H_c (H_c=-3200T+2.4x10^6), x_0 and a are deteriorated and cannot be used for evaluation. Secondly, we vary M_r to study x_0 and a by using H_c = -3100T+2.4x10^6 for evaluation. Figure 4.9 shows that x_0 is almost flat and small values of a are found at low M_r. Small values of a means narrow transitions, hence, recording bits are packed close together. Then, we use high H_c and low M_r to check the assumption. The result in Figure 4.10 shows that the green line with high H_c and low M_r give the lowest transition parameter. Next, we study x_0 and a by focusing on the head field H_0. In this simulation, we use H_c = -3100T+2.4x10^6, M_r=-

This material is reserved for educational use only, not allowed for commercial use.
Forbidden to modify the content, and cite the document when use.

$700T+1.8x10^6$and vary H_0 in the simulation. The results show that x_0 is shifted far from the laser position and a is wider at high head field as shown in Figure 4.11. Finally, using the high H_c, low M_r and low H_0 to evaluate the system by varying peak temperature (T_{peak}), the results of this experiment show that high T_{peak} will give small a as shown in Figure 4.12.

As discussed before, we select the high H_c, low M_r, low H_0 and high T_{peak} to evaluate the system. We select H_c = $-3100T+2.4x10^6$, M_r=$-700T+1.8x10^6$, H_0=*1.3 Tesla or* $1x10^6$ *A/m* and T_{peak}=*300 ℃* or *600 K* to simulate and find x_0 and a. The transition response $p(x)$ and bit response $h(x)$ can be achieved using (2.27) and (2.28) of Chapter 2 and shown in Figure 4.13. We obtain PW_{50} of 12.793 nm and, hence, ND is about 2. The HAMR playback signal is obtained by the convolution between b_k and p_x and the result is corrupted by the additive white Gaussian noise (AWGN) as in (3.4) of Chapter 3. Figure 4.14 illustrates the playback signal without and with AWGN noise. The HAMR playback signal corrupted by AWGN at 6 dB of the SNR is then filtered using the LPF to eliminate out-of-band noise and also shown in Figure 4.14.

Table 4.1 HAMR system parameters with the areal density of 4 Tb/in^2

Symbol	Parameter	Unit
TW	track width	25.4 nm
N	number of sub-track	10
c_o	laser position	0 nm
H_0	deep gap field	$1x10^6$ A/m
T_{peak}	peak temperature	300 °C or 600 K
σ_t	sigma of temperature profile	16.2 nm
g	gap width between pole head and its image	32 nm
σ_r	sigma of reader sensitivity function	4.23 nm
d	head-medium distance or fly height	6 nm
t	medium thickness	10 nm
T_x	bit period	6.4 nm
C	a system specific constant	1
H_c	dependence of coercivity on temperature	$-3100T+2.4x10^6$ A/m
M_r	dependence of remanent magnetization on temperature	$-700T+1.8x10^6$ A/m
AD	areal density	4 Tb/in^2

This material is reserved for educational use only, not allowed for commercial use.
Forbidden to modify the content, and cite the document when use.

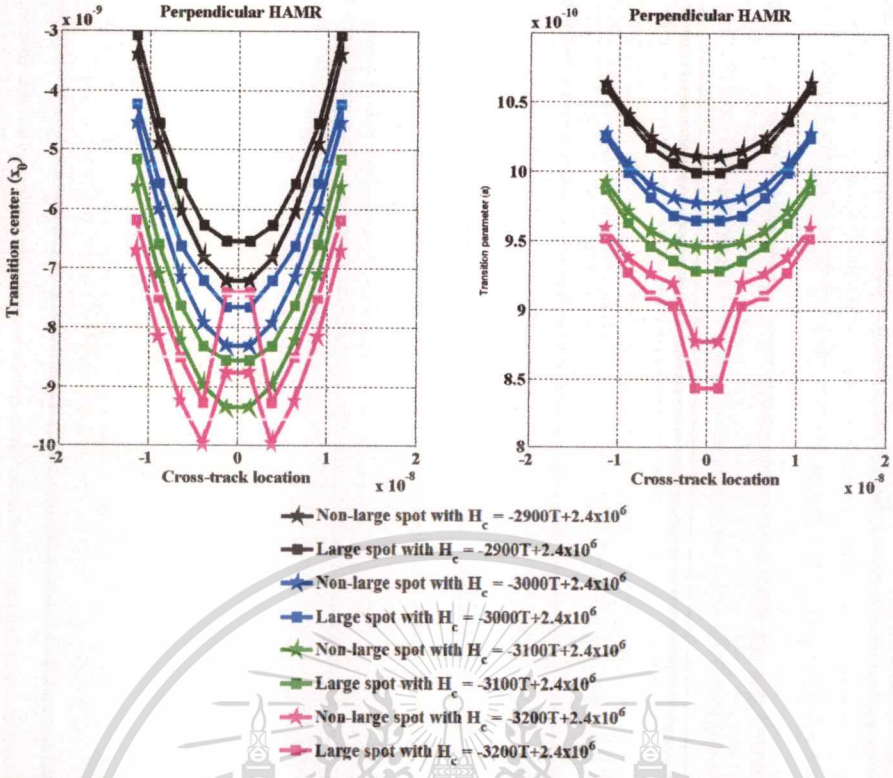


Figure 4.8 Transition center and parameter with various H_c functions at the areal density of 4 Tb/in^2 (M_r=-1000T+1.8x10^6).

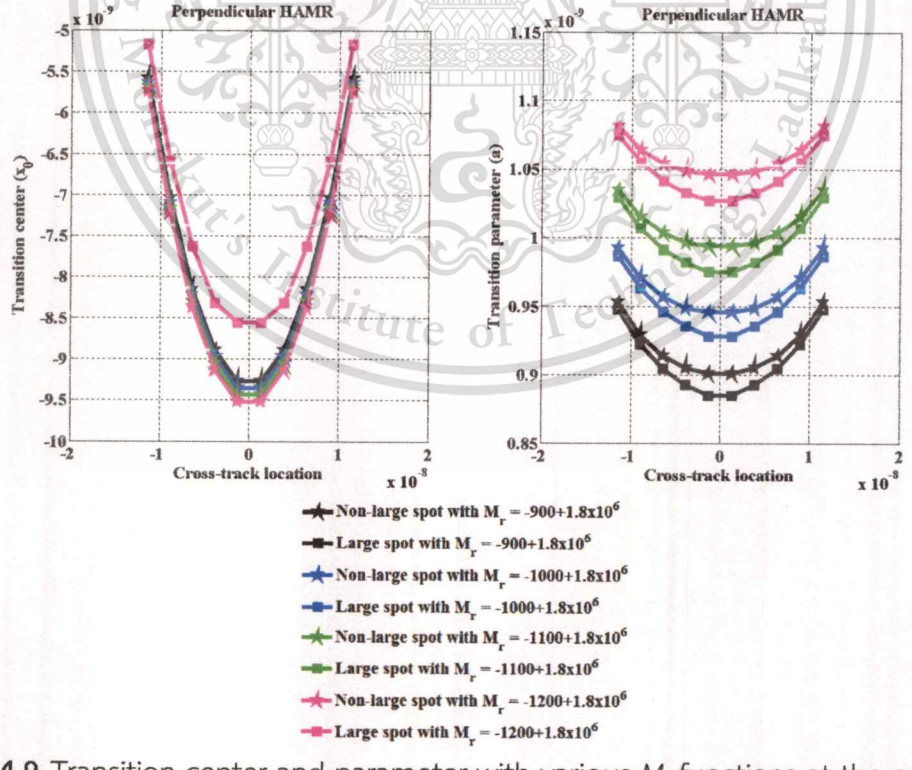


Figure 4.9 Transition center and parameter with various M_r functions at the areal density of 4 Tb/in^2 (H_c = -3100T+2.4x10^6).

This material is reserved for educational use only, not allowed for commercial use.
Forbidden to modify the content, and cite the document when use.

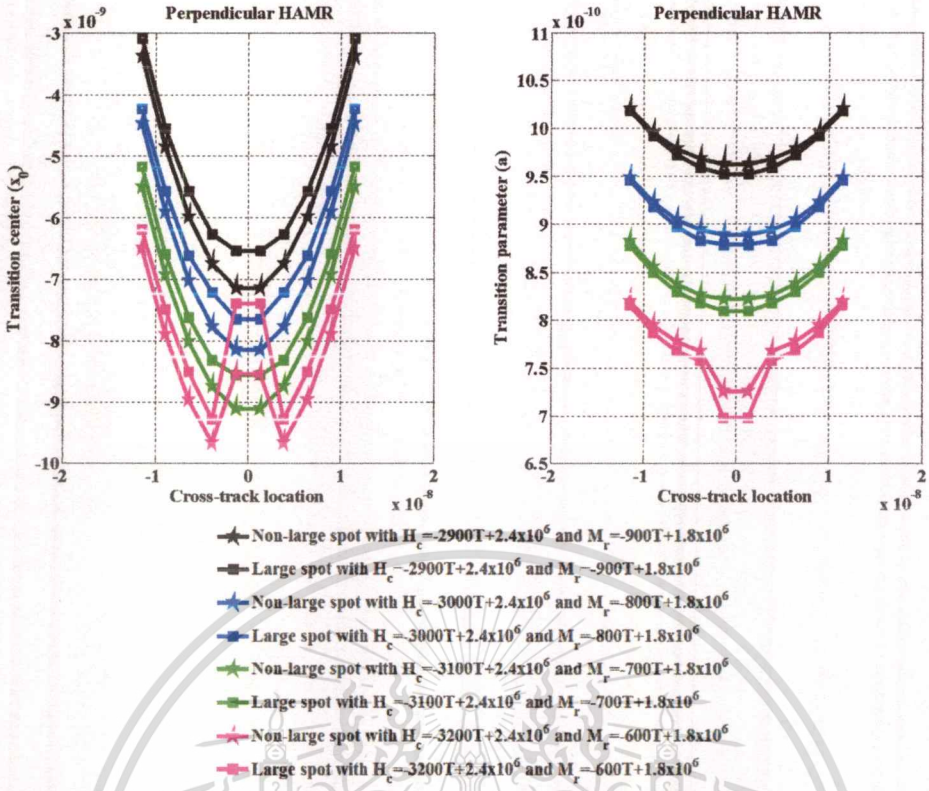


Figure 4.10 Transition center and parameter with various H_c and M_r functions at the areal density of 4 Tb/in^2.

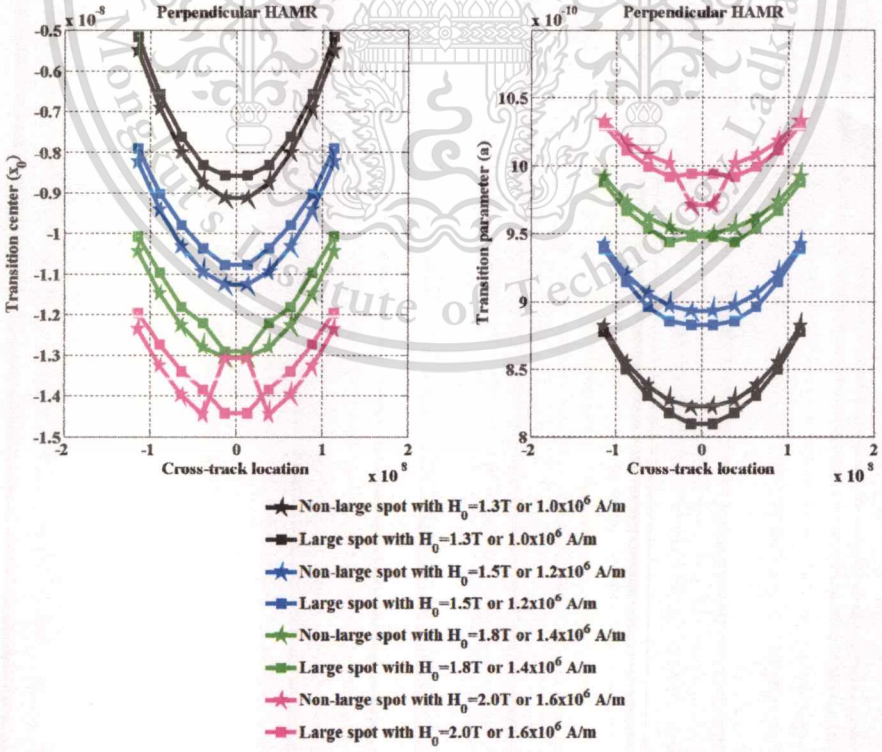


Figure 4.11 Transition center and parameter with various head field at the areal density of 4 Tb/in^2.

This material is reserved for educational use only, not allowed for commercial use.
Forbidden to modify the content, and cite the document when use.

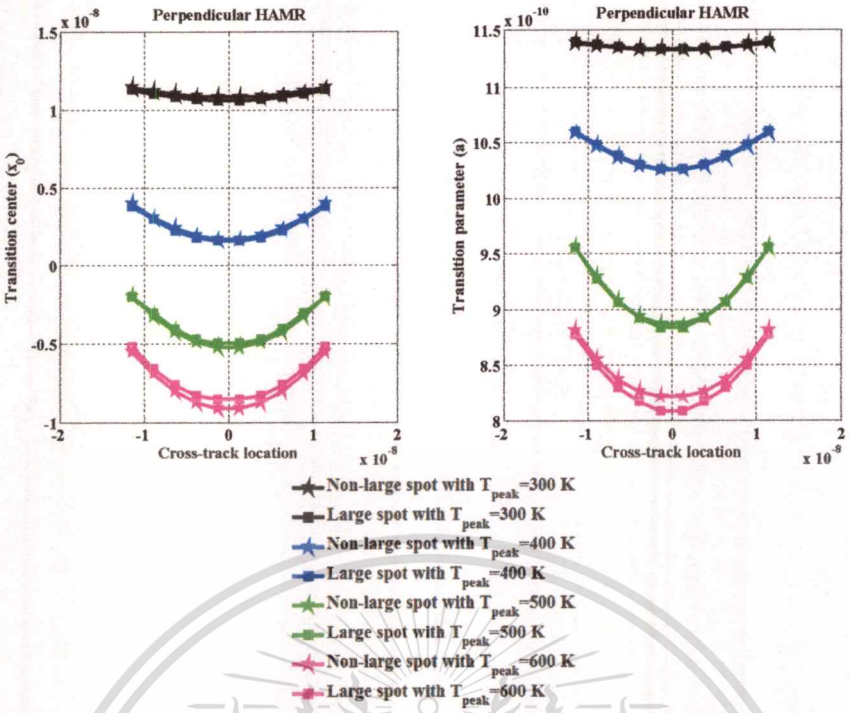


Figure 4.12 Transition center and parameter with various peak temperatures at the areal density of 4 Tb/in^2.

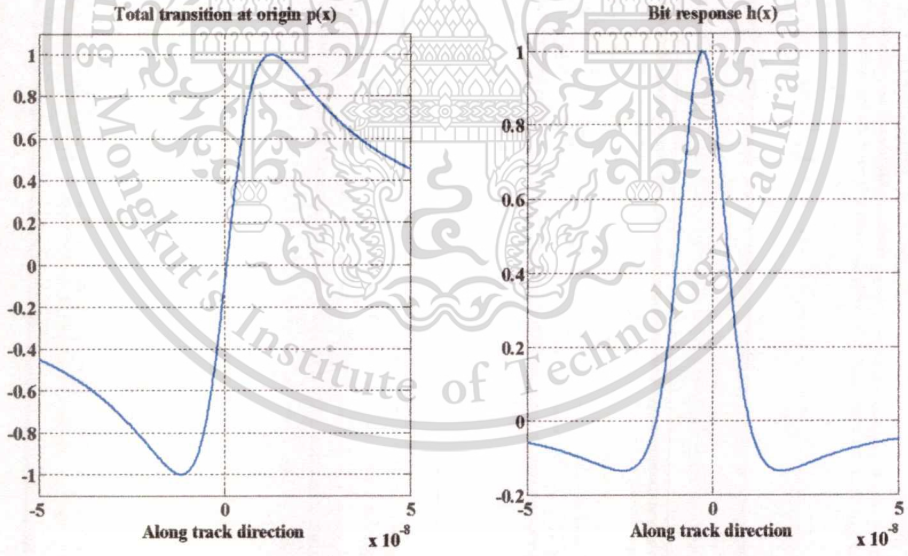


Figure 4.13 Transition response and bit response at the areal density of 4 Tb/in^2.

This material is reserved for educational use only, not allowed for commercial use.
Forbidden to modify the content, and cite the document when use.

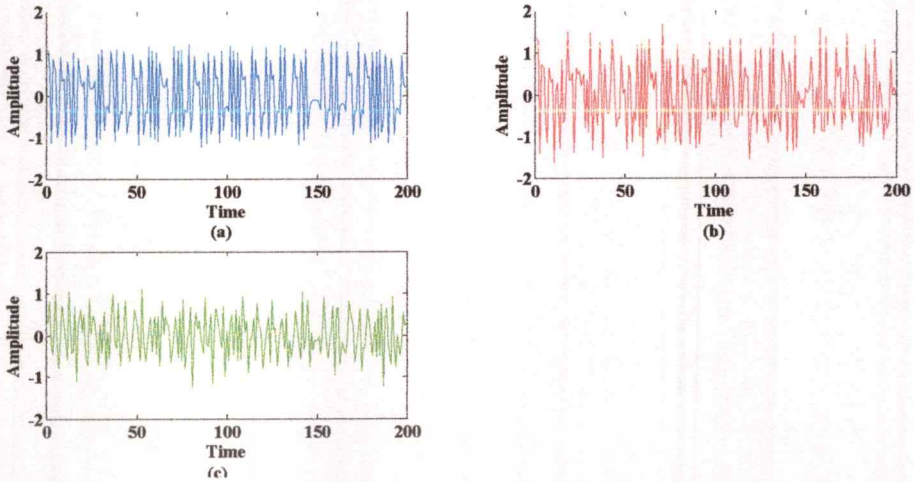


Figure 4.14 Playback signal at the areal density of 4 Tb/in^2 (a) without Noise (b) with AWGN Noise at SNR=6dB and (c) with AWGN Noise after pass LPF.

4.6 The results of perpendicular HAMR simulation at the areal density of 5 Tb/in^2

In this section, we will operate the HAMR system at 5 Tb/in^2. There are two methods to increase the AD from 4 Tb/in^2 to 5 Tb/in^2. For the first method, track width TW is reduced to increase the AD to be 5 Tb/in^2 and shown in Section 4.6.1. For the second method, we reduce the bit period T_x to increase the AD to be 5 Tb/in^2 and show in Section 4.6.2.

4.6.1 The results of perpendicular HAMR simulation at the areal density of 5 Tb/in^2 (reduced track width)

In this section, we will operate the HAMR system at the areal density of 5 Tb/in^2 by using system parameters which are given in Table 4.2. We reduce TW to increase the AD to be 5 Tb/in^2. The AD is can be computed by (4.1). Using the bit period T_x is 6.4 nm and track width TW is 20.0 nm, the AD can be obtained and explained as follows

Firstly, we convert T_x from nm to inch, to obtain

$$2.54\times10^{7}\ nm = 1\ inch$$

$$6.4\ nm = \frac{1\ inch\times 6.4\ nm}{2.54\times10^{7}\ nm} = 2.52\times10^{-7}\ inch$$

Secondly, TW is converted from nm to inch, to obtain

This material is reserved for educational use only, not allowed for commercial use.
Forbidden to modify the content, and cite the document when use.

$$2.54\times10^{7}\ nm = 1\ inch$$

$$20.0\ nm = \frac{1\ inch\times 25.4\ nm}{2.54\times10^{7}\ nm} = 1.0\times10^{-6}\ inch$$

Then, we use (4.1) to compute

$$\begin{aligned} Areal\ Density\left[bits/inch^2\right] &= \frac{1\ bit}{T_x\left[inch\right]\times TW\left[inch\right]} \\ &= \frac{1\ bit}{\left(2.52\times10^{-7}\ inch\right)\times\left(7.874\times10^{-7}\ inch\right)} \\ &= 0.0504\times10^{14}\left[bit/inch^2\right] \\ &\approx 5.0\left[Terabit/inch^2\right] \end{aligned}$$

In all the evaluations, the laser is also assumed to be at the center of the track in the cross-track direction but varies in the down-track direction as same as the Section 4.5. We first discuss the results from Figure 4.15. Firstly, we fix M_r temperature-dependent magnetization to study the behavior of x_0 and a by varying H_c. For M_r=-1000T+1.8x10^6, we found that H_c is increased, x_0 is shifted faraway from laser position and a is decreased while H_c increases. At the highest H_c at H_c=-3000T+2.4x10^6, x_0 and a are distorted and cannot be used for the evaluation. Secondly, we vary M_r to study x_0 and a by using H_c = -2900T+2.4x10^6 for evaluation. Figure 4.16 shows that the values of x_0 is almost flat and the smallest value of a is found at the lowest M_r. Then, we use high H_c and low M_r to check the assumption. The result shows that the blue line with high H_c and low M_r give the lowest transition parameter as illustrates in Figure 4.17. After that, we study x_0 and a by focusing on the head field H_0. The results show that x_0 is shifted faraway from the gap center and a is wider at H_0 as shown in Figure 4.18. Finally, to study the effect of peak temperature T_{peak}, we use high H_c, low M_r and low H_0 to evaluate the system by varying T_{peak}. As the illustrated result in Figure 4.19, high T_{peak} gives small value of a.

As we have discussed, the properly high H_c, low M_r, low H_0 and high T_{peak} are proper to use for system simulation. We select H_c=-2900T+2.4x10^6, M_r=-600T+1.8x10^6, H_0=1.3 Tesla or 1x10^6 A/m and T_{peak}=330 ℃ or 630 K to simulate and find x_0 and a. The transition response $p(x)$ and bit response $h(x)$ which are obtained

This material is reserved for educational use only, not allowed for commercial use.
Forbidden to modify the content, and cite the document when use.

from (2.27) and (2.28) of Chapter 2 can be achieved and shown in Figure 4.20. From the simulation, we obtain PW_{50} of 13.988 nm and, hence, ND is about 2. The HAMR playback signal is obtained by the convolution between b_k and p_x and the result is corrupted by AWGN as in (3.4) of Chapter 3. The playback with and without AWGN is shown in Figure 4.21. Playback signal with AWGN at 6 dB of SNR is then sent to filter using the LPF to eliminate the out-of- band noise and also shown in Figure 4.21.

Table 4.2 HAMR system parameters with the areal density of 5 Tb/in^2 (reduced track width)

Symbol	Parameter	Unit
TW	track width	20 nm
N	number of sub-track	10
c_o	laser position	0 nm
H_0	deep gap field	1x10^6 A/m
T_{peak}	peak temperature	330 °C or 630 K
σ_t	sigma of temperature profile	16.2 nm
g	gap width between pole head and its image	32 nm
σ_r	sigma of reader sensitivity function	4.23 nm
d	head-medium distance or fly height	6 nm
t	medium thickness	10 nm
T_x	bit period	6.4 nm
C	a system specific constant	1
H_c	dependence of coercivity on temperature	-2900T+2.4x10^6 A/m
M_r	dependence of remanent magnetization on Temperature	-600T+1.8x10^6 A/m
AD	areal density	5 Tb/in^2

This material is reserved for educational use only, not allowed for commercial use.
Forbidden to modify the content, and cite the document when use.

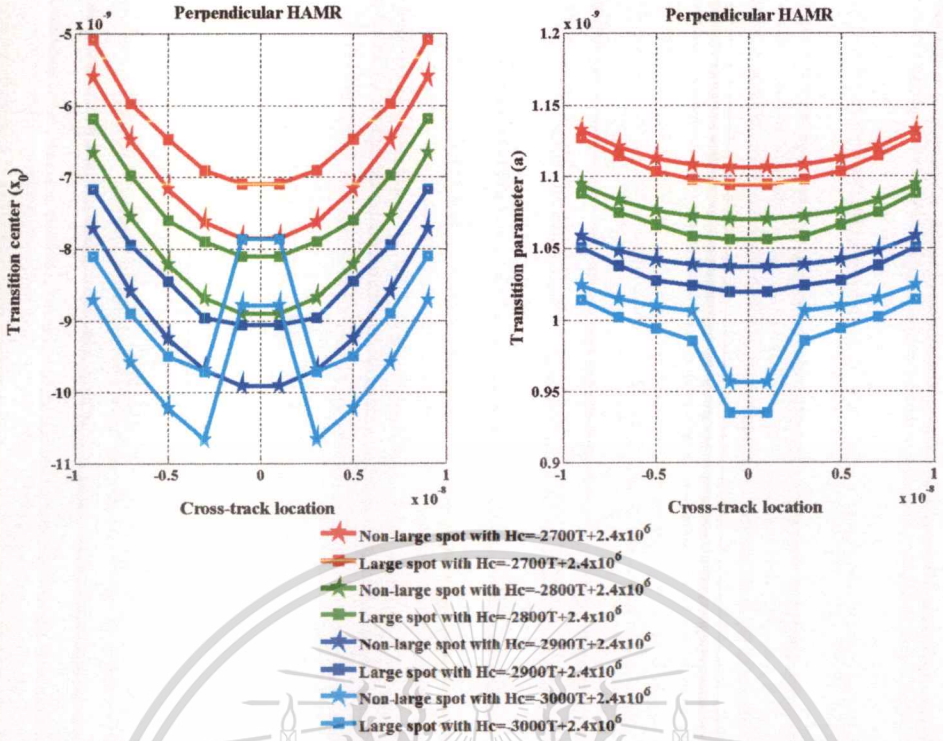


Figure 4.15 Transition center and parameter with various H_c functions at the areal density of 5 Tb/in^2 (reduced track width) with M_r=-1000T+1.8x10^6.

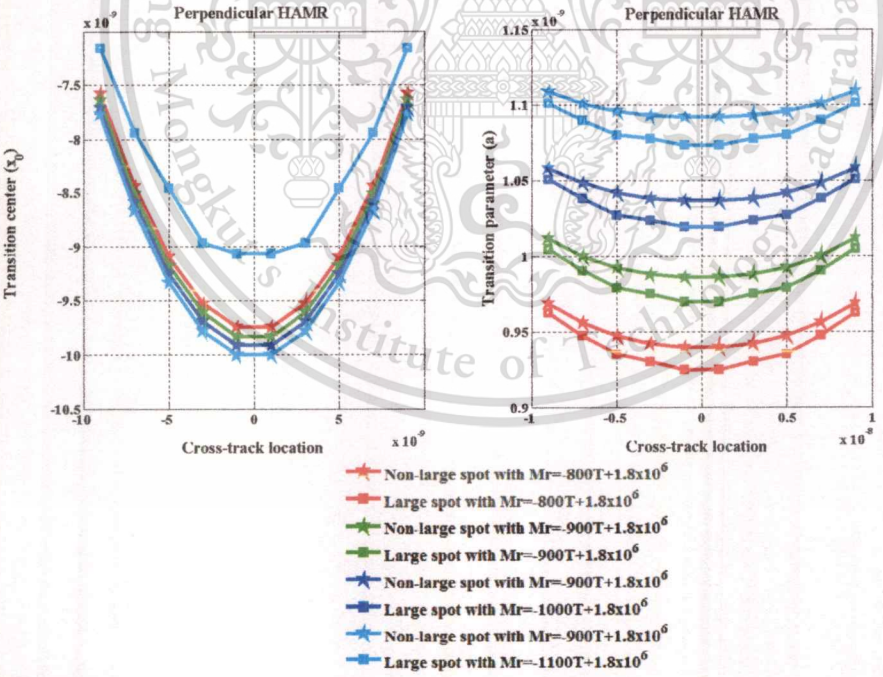


Figure 4.16 Transition center and parameter with various M_r functions at the areal density of 5 Tb/in^2 (reduced track width) with H_c=-2900T+2.4x10^6.

This material is reserved for educational use only, not allowed for commercial use.
Forbidden to modify the content, and cite the document when use.

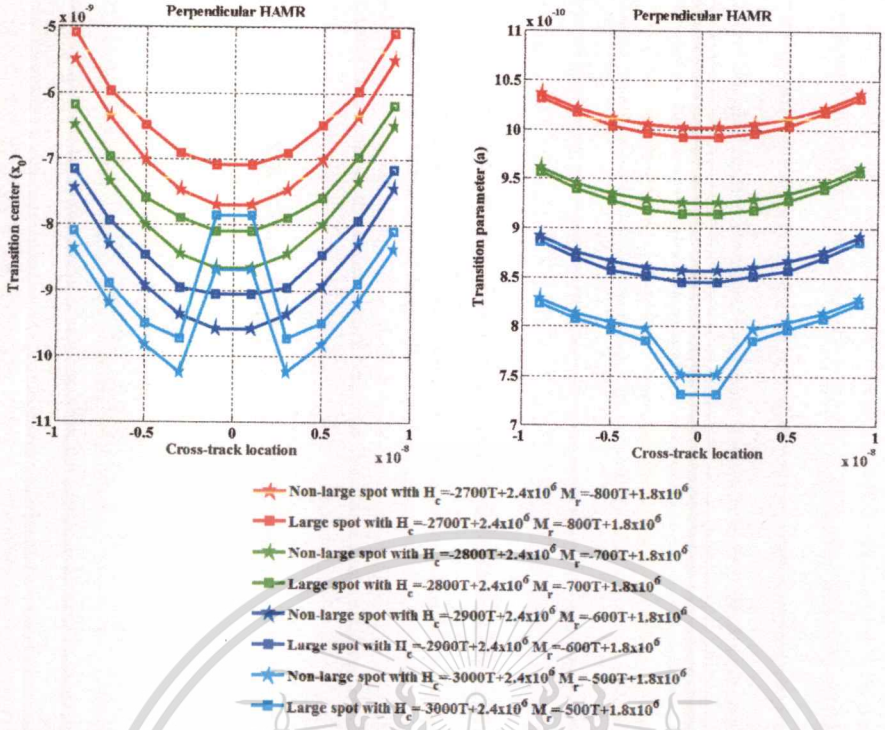


Figure 4.17 Transition center and parameter with various H_c and M_r functions at the areal density of 5 Tb/in^2 (reduced track width).

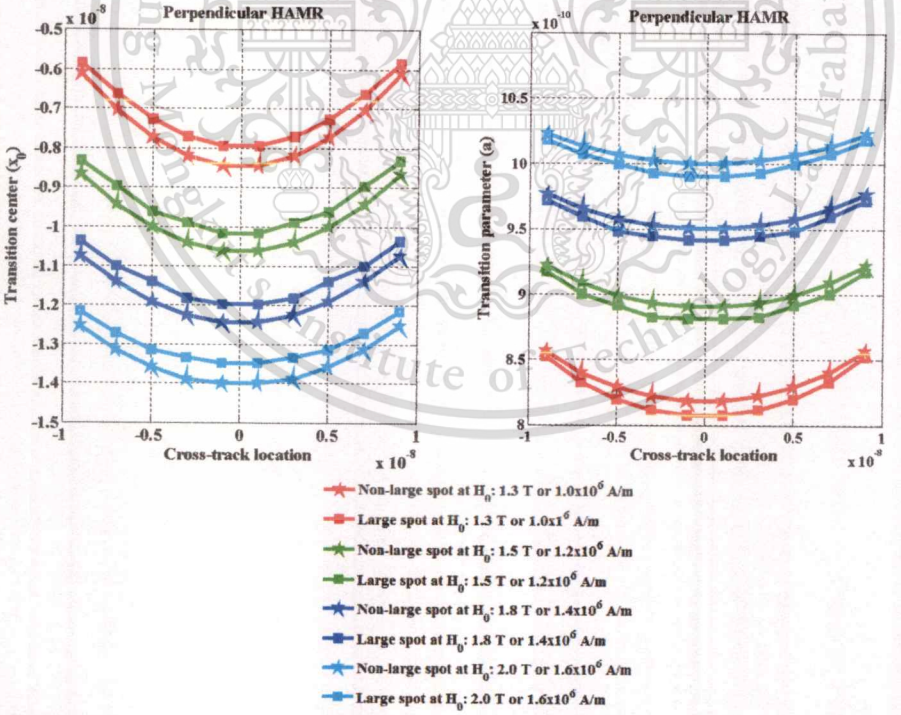


Figure 4.18 Transition center and parameter with various head field at the areal density of 5 Tb/in^2 (reduced track width).

This material is reserved for educational use only, not allowed for commercial use.
Forbidden to modify the content, and cite the document when use.

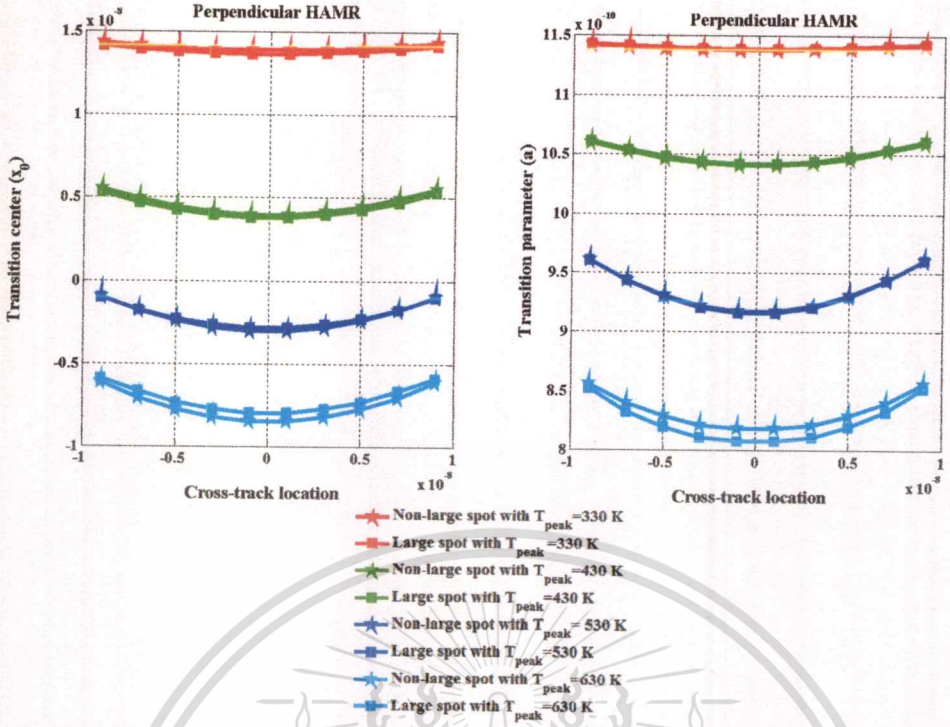


Figure 4.19 Transition center and parameter with various peak temperatures at the areal density of 5 Tb/in^2 (reduced track width).

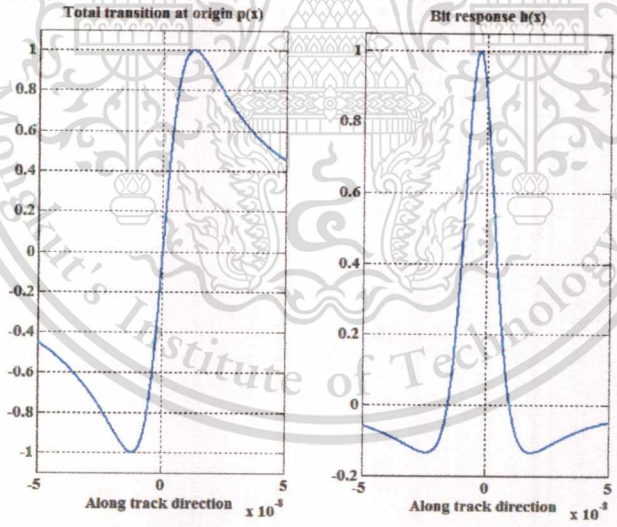


Figure 4.20 Transition response and bit response at the areal density of 5 Tb/in^2 (reduced track width).

This material is reserved for educational use only, not allowed for commercial use.
Forbidden to modify the content, and cite the document when use.

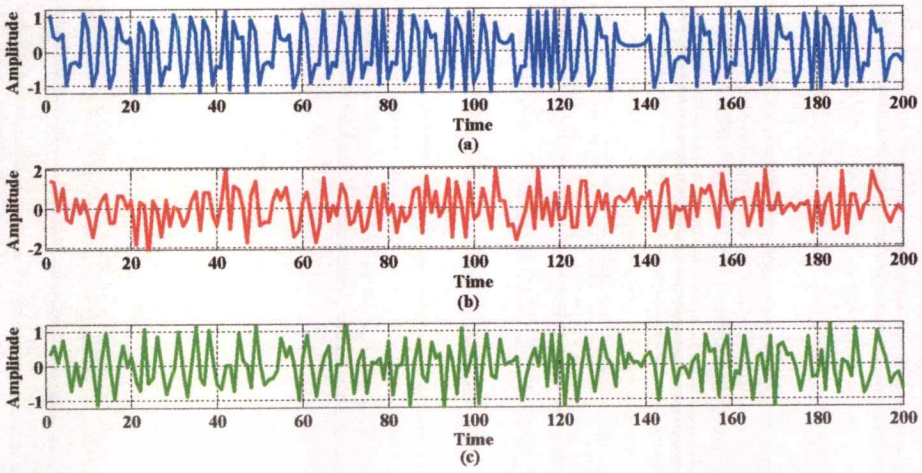


Figure 4.21 Playback signal at the areal density of 5 Tb/in^2 (reduced track width) (a) without Noise (b) with AWGN Noise at SNR=6dB and (c) with AWGN Noise after pass LPF.

4.6.2 The results of perpendicular HAMR simulation at the areal density of 5 Tb/in^2 (reduced bit period)

For this section, we reduce T_x to increase the AD to be 5 Tb/in^2. The AD can be computed by (4.1). Using the same parameters of 4 Tb/in^2 in Table 4.1 except the bit period T_x which is reduced to 5.05 nm, the AD can be increased to 5 Tb/in^2 and explained as follows

Firstly, we convert T_x from nm to inch, to obtain

$$2.54\times10^{7}\ nm = 1\ inch$$

$$5.08\ nm = \frac{1\ inch\times 6.4\ nm}{2.54\times10^{7}\ nm} = 2\times10^{-7}\ inch$$

Secondly, *TW* is converted from nm to inch, to obtain

$$2.54\times10^{7}\ nm = 1\ inch$$

$$25.4\ nm = \frac{1\ inch\times 25.4\ nm}{2.54\times10^{7}\ nm} = 1.0\times10^{-6}\ inch$$

Then, we use (4.1) to compute

This material is reserved for educational use only, not allowed for commercial use.
Forbidden to modify the content, and cite the document when use.

$$Areal\ Density\left[bits/inch^2\right]=\frac{1\,bit}{T_x\left[inch\right]\times TW\left[inch\right]}$$
$$=\frac{1\,bit}{\left(2\times10^{-7}\ inch\right)\times\left(1\times10^{-6}\ inch\right)}$$
$$=0.5\times10^{13}\left[bit/inch^2\right]$$
$$\approx5.0\left[Terabit/inch^2\right]$$

The transition response $p(x)$ and bit response $h(x)$ are shown in Figure 4.22. Here, we obtain PW_{50} of 12.883 nm and ND is about 2.57. The playback signals without and with AWGN at 6 dB of SNR are shown in Figure 4.23. The playback signal after LPF is also shown in Figure 4.23.

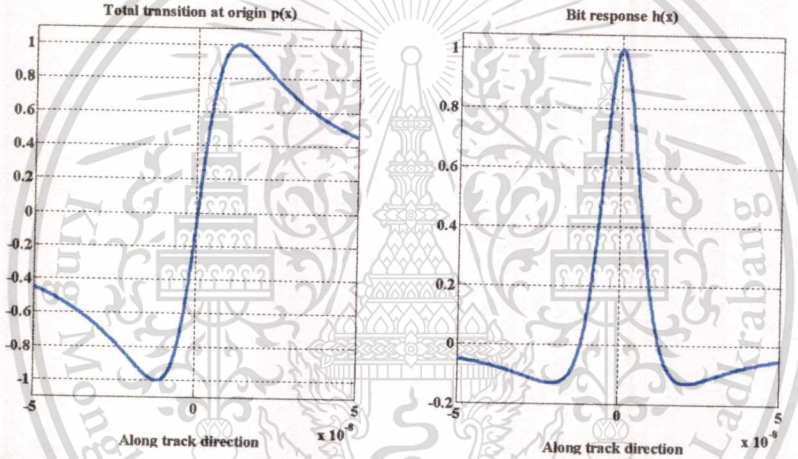


Figure 4.22 Transition response and bit response of HAMR at the areal density of 5 Tb/in^2 (reduced bit period).

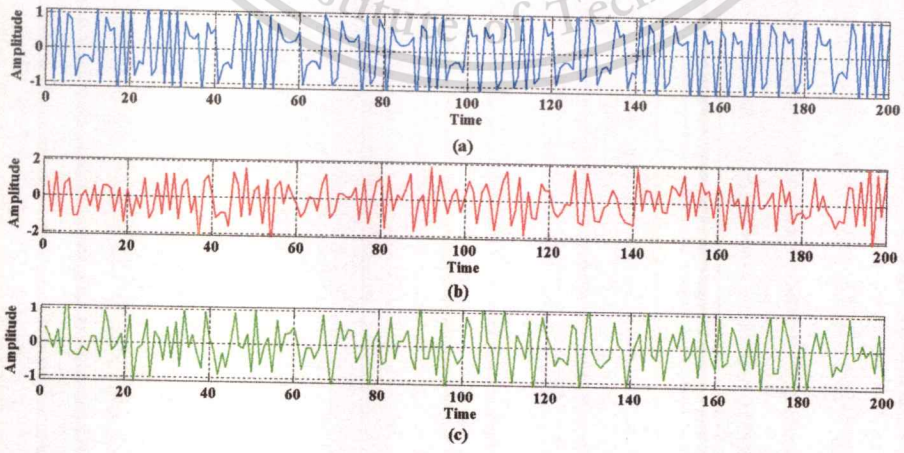


Figure 4.23 Playback signal at the areal density of 5 Tb/in^2 (reduced bit period) (a) without Noise (b) with AWGN Noise at SNR=6dB and (c) with AWGN Noise after pass LPF.

This material is reserved for educational use only, not allowed for commercial use.
Forbidden to modify the content, and cite the document when use.

4.7 The results and performance of target shaping design of the HAMR system at 4 Tb/in^2

In this section, we show the simulation results of and performance of target shaping design of the HAMR system at 4 Tb/in^2.

Firstly, we use the fixed target constraint to minimize the MSE by setting the various number of equalizer taps. The number of equalizer taps are from 3 to 21 taps. The result show that among the partial-response targets considered, PR1 gives the lowest MMSE from all the targets for this case as in Figure 4.24 although the MSE should be further reduced. The MMSE value of PR1 at 11-tap equalizer is equal to 0.506. The 11-tap equalizer coefficients are [0.024 -0.024 0.289 0.151 1.304 2.665 1.404 0.432 0.187 0.060 0.008]. The frequency responses of four PR targets are shown in Figure 4.25. They are all dc-full targets. Next, we compare the MSE using four target constraints for evaluation and the range is from 3 to 21 taps. There are the monic (h_0 = 1) constraint, h_1 = 1 constraint, the unit energy constraint and the fixed target constraint (PR2). All constraints use 3 target taps and 11 equalizer taps. The results from the simulation show that the unit energy gives the lowest MMSE as shown in Figure 4.26. The coefficients and MMSE values of these four target constraints using 3 target taps with 11-tap equalizer are listed in Table 4.4. The frequency responses of three GPR targets versus PR2 [1 2 1] are shown in Figure 4.27. As we can see in Figure 4.27, the frequency response of GPR targets of our system is similar to the frequency response of LMR [14]. That is why four PR targets give high MMSE values and therefore they are not suitable for target design.

Since the unit-energy constraint gives the lowest MSE value, we select the unit energy constraint to evaluate and find the minimum MSE with the various number of target taps. The number of equalizer taps are also in the range of 3 and 21 taps as in the previous simulation. For the 11-tap equalizer, the 10-tap target gives the minimum MSE as shown in Figure 4.28. The 11-tap equalizer coefficients are [-0.027 0.042 -0.111 0.145 -0.387 0.099 0.730 -0.902 0.102 0.613 -0.451] and 10-tap target coefficients are [-0.253 0.420 0.013 -0.587 0.543 0.010 -0.299 0.161 -0.054 0.034]. The MMSE value is 0.05789.

This material is reserved for educational use only, not allowed for commercial use.
Forbidden to modify the content, and cite the document when use.

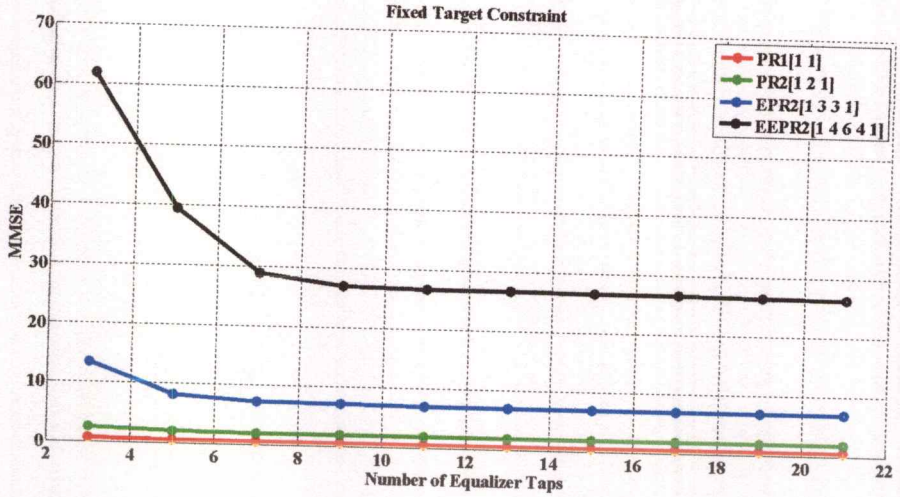


Figure 4.24 MMSE of fixed-target constraint with various equalizer taps of the HAMR system at 4 Tb/in^2.

Table 4.3 The target coefficients and MMSE values of fixed targets at 11-tap equalizer of the HAMR system at 4 Tb/in^2.

Fixed targets	Target coefficients	MMSE
PR1	[1 1]	0.506
PR2	[1 2 1]	1.854
EPR2	[1 3 3 1]	6.998
EEPR2	[1 4 6 4 1]	26.772

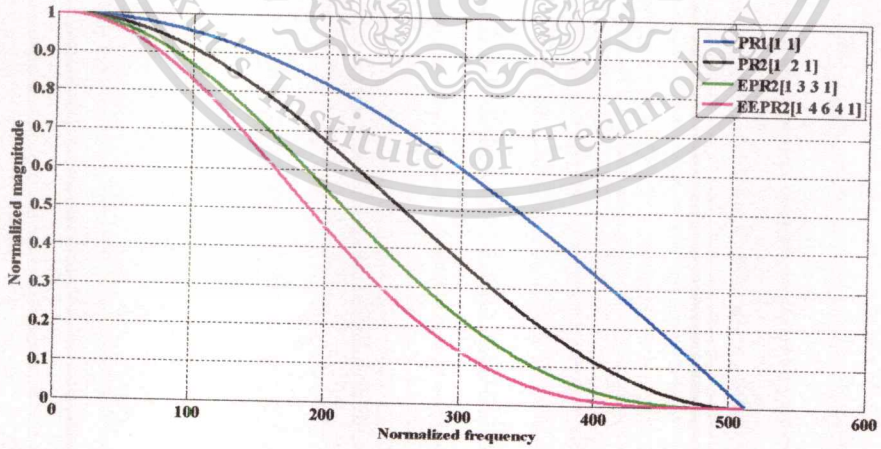


Figure 4.25 Frequency responses of PR targets of the HAMR system at 4 Tb/in^2.

This material is reserved for educational use only, not allowed for commercial use.
Forbidden to modify the content, and cite the document when use.

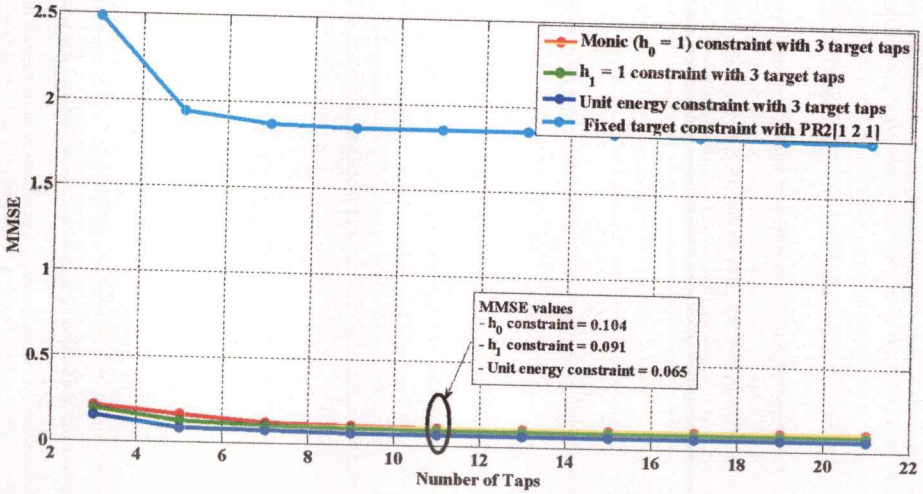


Figure 4.26 MMSE of various targets constraint using 3 target taps with 11-tap equalizer of the HAMR system at 4 Tb/in^2.

Table 4.4 The target coefficients and MMSE values of various constraints using 3 target taps with 11-tap equalizer of the HAMR system at 4 Tb/in^2.

Target constraints	Target coefficients	MMSE
Monic constraint (h_0=1)	[1 -0.440 -0.227]	0.104
h_1=1 constraint	[-0.383 1 -0.388]	0.091
Unit energy constraint	[0.412 -0.801 0.433]	0.065
Fixed target constraint (PR2)	[1 2 1]	1.854

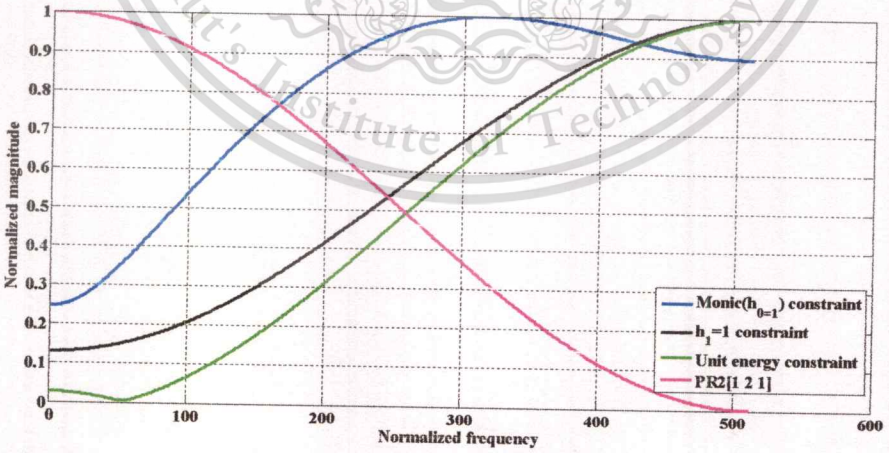


Figure 4.27 Frequency responses of GPR targets versus fixed-target (PR2) of the HAMR system at 4 Tb/in^2.

This material is reserved for educational use only, not allowed for commercial use.
Forbidden to modify the content, and cite the document when use.

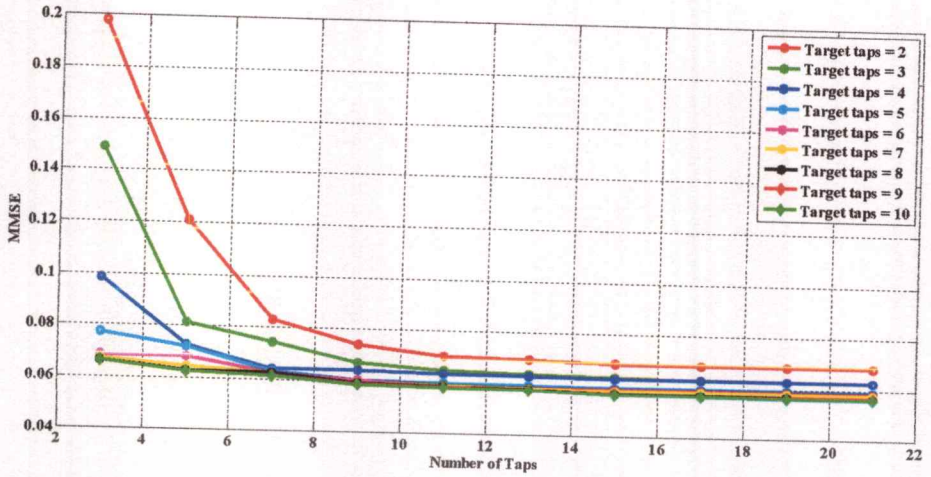


Figure 4.28 MMSE of unit energy constraint equalizers with the number of target taps of the HAMR system at 4 Tb/in^2.

The coefficients and MMSE values of unit-energy constraint of 11-tap equalizers with the target's length from 2 to 10 are listed in Table 4.5. At the same SNR (SNR =15 dB), the bit error rate (BER) of the monic (h_0 = 1) constraint is 2×10^{-4}, BER of the h_1 = 1 constraint is 1.4×10^{-3}, BER of the unit energy constraint is 2.5×10^{-3} and BER of the fixed target constraint (PR2) is 2.25×10^{-1}. Although the lowest MMSE is from the unit energy constraint, but the BER of the monic constraint presents the best system performance as shown in Figure 4.29.

Table 4.5 The coefficients and MMSE values of unit-energy constraint of 11-tap equalizers with various target taps of the HAMR system at 4 Tb/in^2.

Length	Coefficients of the unit energy constraint	MMSE
2	[-0.706 0.708]	0.07004
3	[0.412 -0.8010.433]	0.06462
4	[0.133 0.245 -0.815 0.508]	0.06350
5	[-0.365 0.527 0.111 -0.658 0.379]	0.05998
6	[-0.245 0.538 -0.273 -0.381 0.603 -0.259]	0.05912
7	[0.273 -0.538 0.184 0.472 -0.586 0.186 0.024]	0.05908
8	[0.221 -0.499 0.246 0.401 -0.637 0.258 0.075 -0.055]	0.05869
9	[0.249 -0.479 0.115 0.522 -0.610 0.132 0.158 -0.087 0.024]	0.05851
10	[-0.253 0.4200.013 -0.587 0.543 0.010 -0.299 0.161 -0.054 0.034]	0.05789

This material is reserved for educational use only, not allowed for commercial use.
Forbidden to modify the content, and cite the document when use.

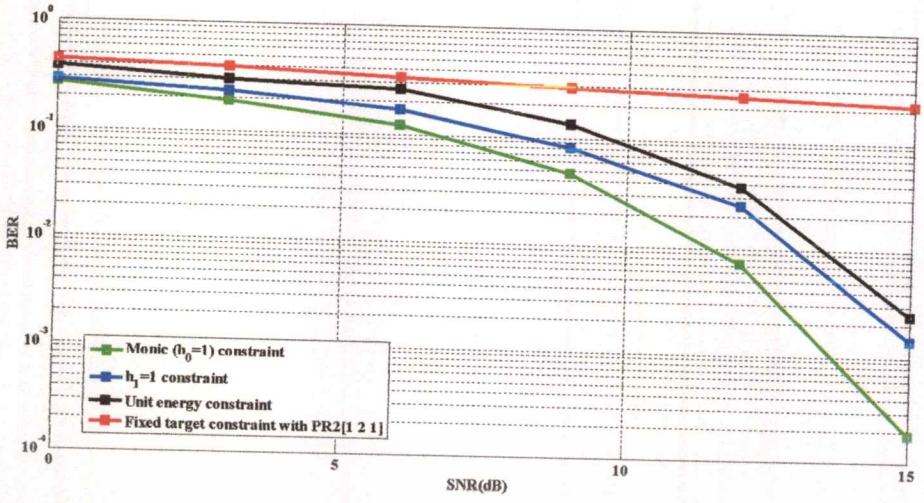


Figure 4.29 Bit error rates (BER) of the HAMR system at 4 Tb/in^2.

4.8 The results and performance of target shaping design of the HAMR system at 5 Tb/in^2

We will first illustrate and describe the result and performance of target shaping design of the HAMR system at 5 Tb/in^2 (reduced track width) in Section 4.8.1. Then, in Section 4.8.2, the results and performance of target shaping design of the HAMR system at 5 Tb/in^2 (reduced bit length) will be discussed.

4.8.1 The result and performance of target shaping design of the HAMR system at 5 Tb/in^2 (reduced track width)

For MMSE equalizer design of the HAMR system at 5 Tb/in^2 of this section, we use the fixed target constraint to minimize the MSE by setting the various number of equalizer taps. Equalizer taps are in the range of 3 and 21 taps. PR1 gives the lowest MMSE from all targets for this case. The results are shown in Figure 4.30. The target coefficients and MMSE values are listed in Table 4.6. The MMSE value at 11-tap equalizer is equal to 0.526. The 11-tap equalizer coefficients are [0.044 -0.036 0.252 0.128 1.320 2.641 1.356 0.404 0.166 0.033 -0.010].

Next, we compare the minimum MSE using four target constraints for evaluation and the range of the equalizer taps is from 3 to 21 taps. We use 3-tap target to simulate this comparison. The result shows that the unit energy constraint has the lowest MMSE, as in Figure 4.31. The 3-tap target with 11-tap equalizer has the MSE equal to 0.065. The h_0=1 constraint gives the MMSE of 0.105. For h_1 = 1 constraint, the minimum MSE of this targets is 0.091, and the fixed-target constraint using PR2 [1

This material is reserved for educational use only. Forbidden to modify the content, and cite the document when use.

2 1] has the highest MMSE value equal to 1.890. The target coefficients and MMSE values are shown in Table 4.7. The frequency responses of GPR targets versus PR2 target are shown in Figure 4.32.

Since the unit energy constraint gives the lowest MMSE value, we select the unit energy constraint to evaluate and find the MMSE with the various number of target taps. Equalizer taps are also in the range of 3 and 21 taps as the previous simulation. For the 11-tap equalizer, the 10-tap target gives the minimum MSE as shown in Figure 4.33. The coefficient and MMSE of unit-energy constraint of 11-tap equalizers with the target's length from 2 to 10 are listed in Table 4.8. The 11-tap equalizer coefficients are [-0.043 0.050 -0.126 0.186 -0.466 0.228 0.616 -0.956 0.360 0.413 -0.438] and 10-tap target coefficients are [-0.261 0.475 -0.109 -0.491 0.607 -0.142 -0.212 0.132 -0.039 0.021]. The MMSE value is 0.055.

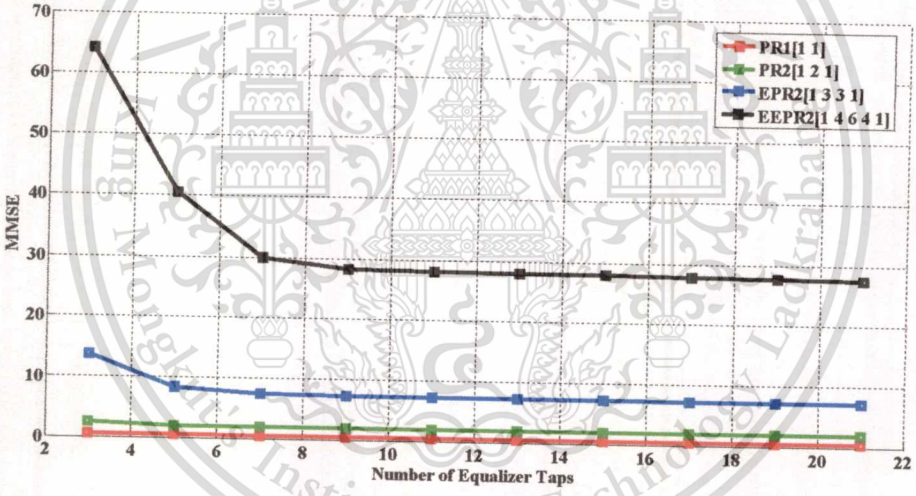


Figure 4.30 MMSE of fixed-target constraint with various equalizer taps of the HAMR system at 5 Tb/in^2 (reduced track width).

Table 4.6 The target coefficients and MMSE values of fixed target constraint at 11-tap equalizer of the HAMR system at 5 Tb/in^2 (reduced track width).

Fixed targets	Target coefficients	MMSE
PR1	[1 1]	0.526
PR2	[1 2 1]	1.933
EPR2	[1 3 3 1]	7.314
EEPR2	[1 4 6 4 1]	27.968

This material is reserved for educational use only, not allowed for commercial use.
Forbidden to modify the content, and cite the document when use.

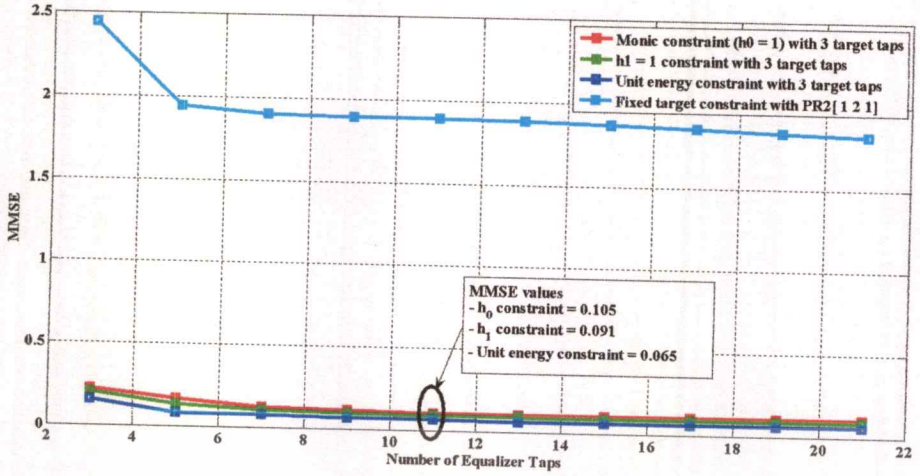


Figure 4.31 MMSE of various targets constraint using 3 target taps with 11-tap equalizer of the HAMR system at 5 Tb/in^2 (reduced track width).

Table 4.7 The target coefficients and MMSE values of various targets constraint using 3 target taps with 11-tap equalizer of the HAMR system at 5 Tb/in^2 (reduced track width).

Target constraint	Target coefficient	MMSE
Monic constraint (h_0=1)	[1 -0.408 -0.258]	0.105
h_1=1 constraint	[-0.381 1 -0.388]	0.091
Unit energy constraint	[0.403 -0.804 0.438]	0.065
Fixed target constraint (PR2)	[1 2 1]	1.890

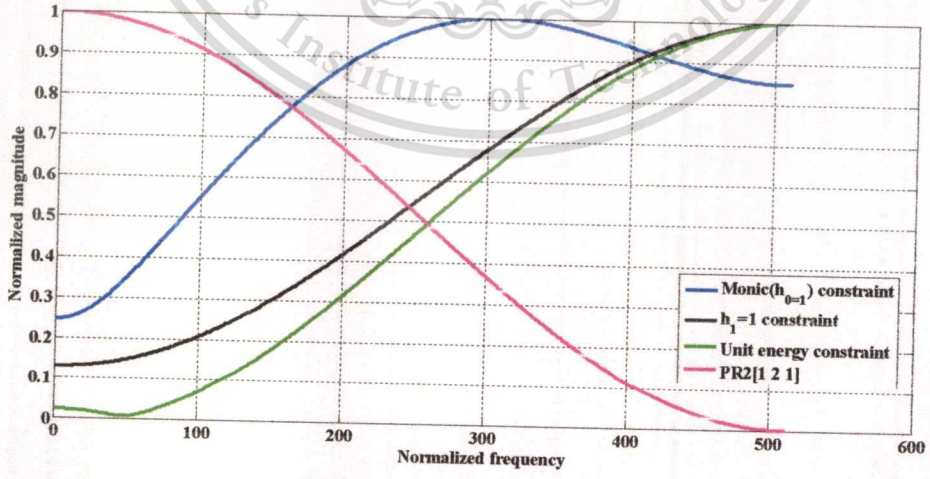


Figure 4.32 Frequency responses of GPR targets versus fixed-target (PR2) of the HAMR system at 5 Tb/in^2 (reduced track width).

This material is reserved for educational use only, not allowed for commercial use.
Forbidden to modify the content, and cite the document when use.

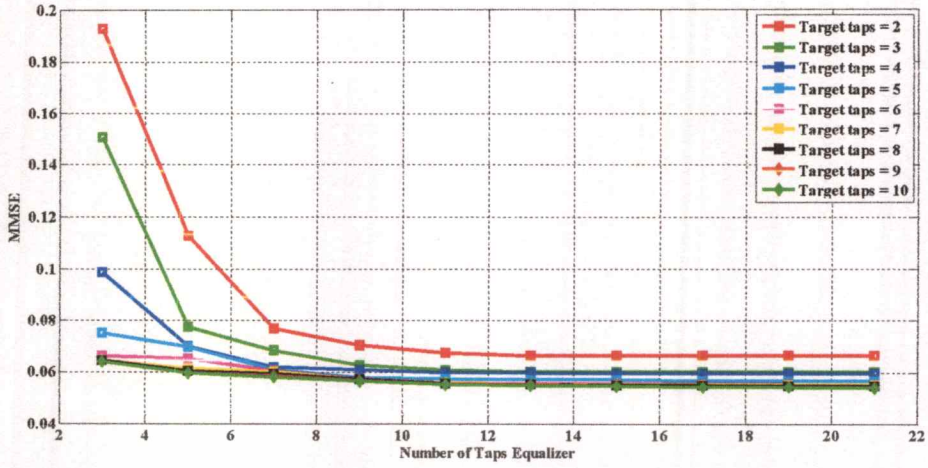


Figure 4.33 MMSE of unit-energy constraint equalizers with the number of target taps of the HAMR system at 5 Tb/in^2 (reduced track width).

Table 4.8 The coefficients and MMSE values of unit-energy constraint of 11-tap equalizers with various target taps of the HAMR system at 5 Tb/in^2 (reduced track width).

Length	Coefficients of the unit energy constraint	MMSE
2	[-0.706 0.708]	0.06747
3	[0.416 -0.799 0.435]	0.06084
4	[-0.191 0.613 -0.706 0.298]	0.06007
5	[-0.382 0.560 0.050 -0.620 0.392]	0.05728
6	[-0.275 0.560 -0.288 -0.338 0.583 -0.270]	0.05570
7	[0.258 -0.557 0.333 0.279 -0.579 0.313 -0.021]	0.05567
8	[-0.253 0.536 -0.288 -0.321 0.605 -0.306 -0.038 0.046]	0.05536
9	[0.264 -0.525 0.226 0.392 -0.612 0.248 0.094 -0.072 0.015]	0.05529
10	[-0.261 0.475 -0.109 -0.491 0.607 -0.142 -0.212 0.132 -0.039 0.021]	0.05511

At the same SNR (SNR =15 dB), the bit error rate (BER) of the monic (h_0 = 1) constraint is 2x10^{-4}, BER of the h_1 = 1 constraint is 1.3x10^{-3}, BER of the unit energy constraint is 3.0x10^{-3} and BER of the fixed target constraint (PR2) is 2.21x10^{-1}. Although the lowest MMSE is from the unit energy constraint, but the BER of the monic constraint presents the best system performance as shown in Figure 4.34.

This material is reserved for educational use only, not allowed for commercial use.
Forbidden to modify the content, and cite the document when use.

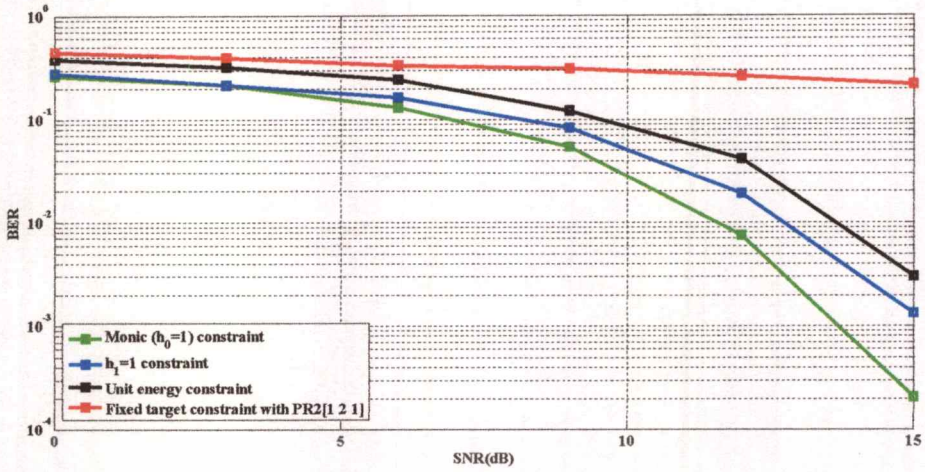


Figure 4.34 Bit error rates (BER) of the HAMR system at 5 Tb/in^2 (reduced track width).

4.8.2 The results and performance of target shaping design of the HAMR system at 5 Tb/in^2 (reduced bit period)

We first use the fixed target constraint to minimize the MSE by setting the various number of equalizer taps which are in the range from 3 to 21 taps. PR1 gives the lowest MMSE from all targets as shown in Figure 4.35 although the MSE should be further reduced. The target coefficient and MMSE values are listed in Table 4.9. The MMSE value at 11-tap equalizer is equal to 0.420. The 11-tap equalizer coefficients are [0.065 0.001 0.298 0.179 1.085 2.386 1.315 0.449 0.224 0.094 0.035].

Next, four target constraints are compared, as in Figure 4.36. We use 3 target taps and 11 equalizer taps to simulate this comparison. The result shows that the unit energy constraint has the lowest minimum MSE as shown in Figure 4.35. The 3-tap target with 11-tap equalizer has the MSE equal to 0.062. The h_0=1 constraint gives the MSE of 0.089. For h_1 = 1 constraint, the minimum MSE of this target is 0.086, and the fixed-target constraint using PR2 [1 2 1] has the highest MSE value which is equal to 1.631. The target coefficients and MMSE values are shown in Table 4.10. The frequency responses of GPR targets versus PR2 target are shown in Figure 4.37.

Then, we select the unit energy constraint to evaluate and find the MMSE with the various number of target taps. The number of equalizer taps are from 3 to 21 taps. For the 11-tap equalizer, the 10-tap target gives the minimum MSE as shown in Figure 4.38. The coefficients and MMSEs of unit-energy constraint of 11-tap equalizers with the target's length from 2 to 10 are listed in Table 4.11. The 11-tap equalizer

This material is reserved for educational use only, not allowed for commercial use.
Forbidden to modify the content, and cite the document when use.

coefficients are [-0.020 0.026 -0.061 0.030 -0.208 -0.359 0.783 0.179 -0.888 0.218 0.394] and 10-tap target coefficients are [-0.300 0.152 0.564 -0.500 -0.323 0.457 0.017 -0.071 0.001 -0.006]. The MMSE value is 0.047.

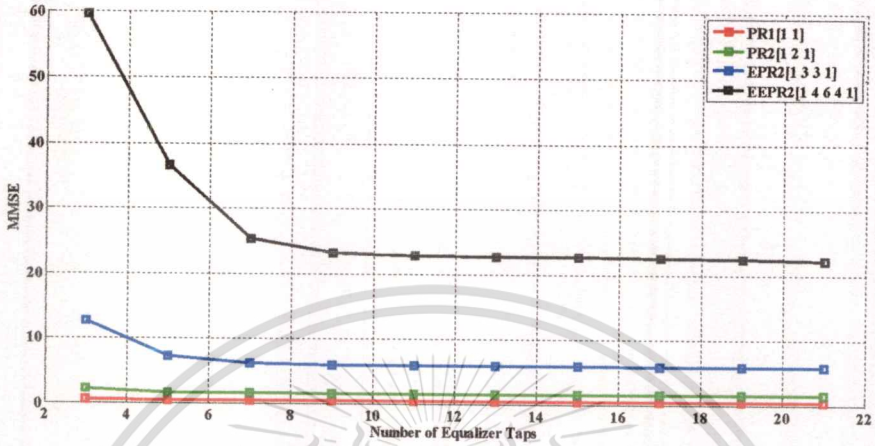


Figure 4.35 MMSE of fixed-target constraint with various equalizer taps of the HAMR system at 5 Tb/in^2 (reduced bit period).

Table 4.9 The target coefficients and MMSE values of fixed targets at 11-tap equalizer of the HAMR system at 5 Tb/in^2 (reduced bit period).

Fixed targets	Target coefficients	MMSE
PR1	[1 1]	0.420
PR2	[1 2 1]	1.553
EPR2	[1 3 3 1]	5.912
EEPR2	[1 4 6 4 1]	22.806

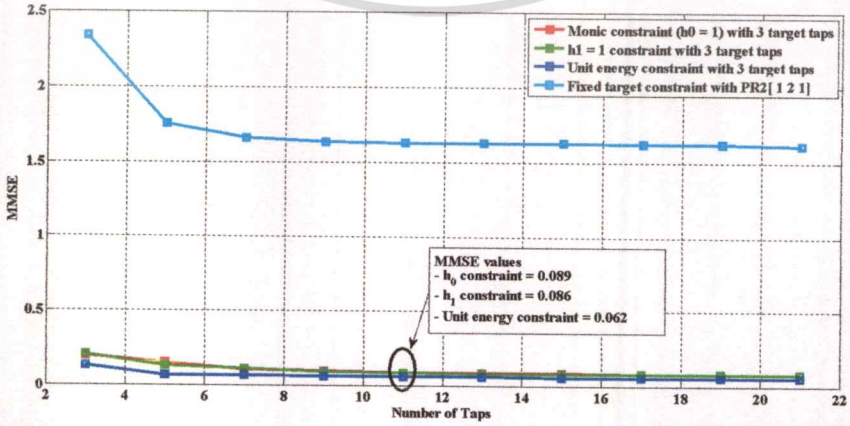


Figure 4.36 MMSE of various constraints using 3 target taps with 11-tap equalizer of the HAMR system at 5 Tb/in^2 (reduced bit period).

This material is reserved for educational use only. Not approved for commercial use.
Forbidden to modify the content, and cite the document when use.

Table 4.10 The target coefficients and MMSE values of various constraints using 3 target taps with 11-tap equalizer of the HAMR system at 5 Tb/in^2 (reduced bit period).

Target constraints	Target coefficients	MMSE
Monic constraint (h_0=1)	[1 -0.350 -0.359]	0.089
h_1=1 constraint	[-0.337 1 -0.375]	0.086
Unit energy constraint	[-0.090 -0.658 0.748]	0.062
Fixed target constraint (PR2)	[1 2 1]	1.631

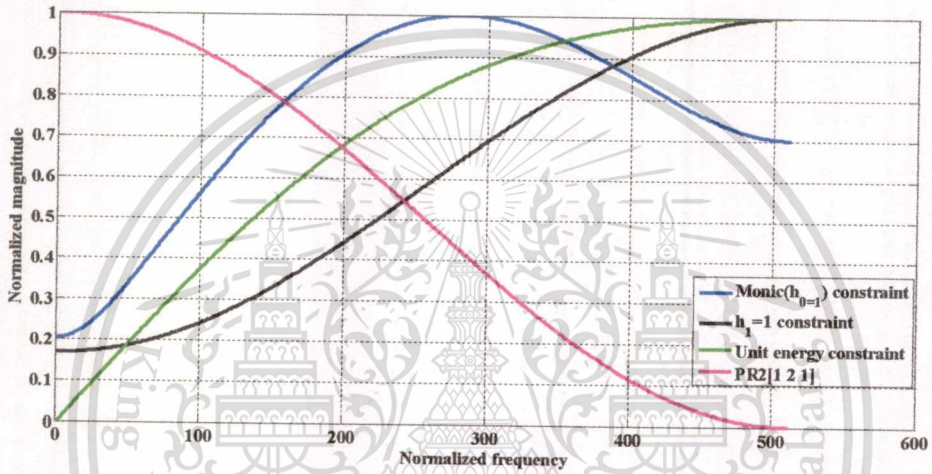


Figure 4.37 Frequency responses of GPR targets versus fixed-target (PR2) of the HAMR system at 5 Tb/in^2 (reduced bit period).

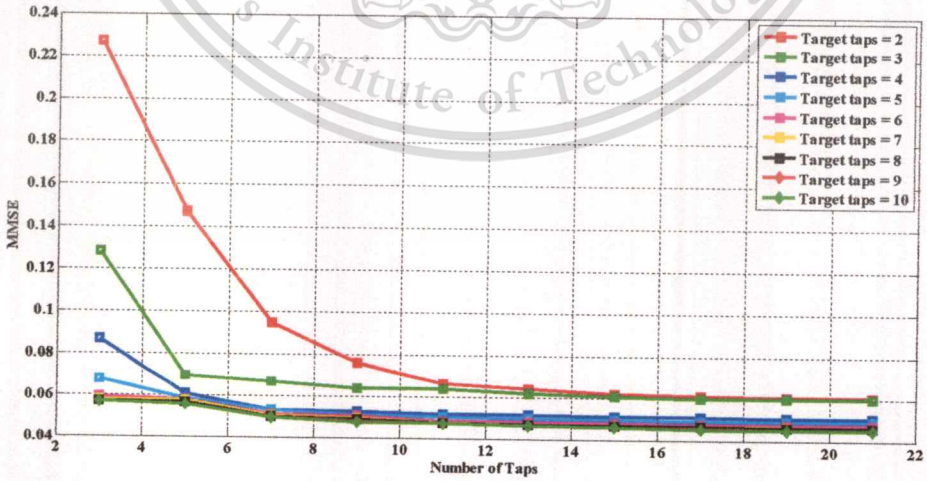


Figure 4.38 MMSE of unit-energy constraint equalizers with the number of target taps of the HAMR system at 5 Tb/in^2 (reduced bit period).

This material is reserved for educational use only, not allowed for commercial use.
Forbidden to modify the content, and cite the document when use.

Table 4.11 The coefficients and MMSE values of unit-energy constraint of 11-tabs equalizers with various target taps of the HAMR system at 5 Tb/in^2 (reduced bit period).

Length	Coefficients of the unit energy constraint	MMSE
2	[-0.703 0.711]	0.066344
3	[-0.249 -0.549 0.798]	0.063539
4	[0.486 -0.372 -0.574 0.544]	0.051510
5	[0.345 -0.548 -0.125 0.673 -0.336]	0.050377
6	[0.331 -0.153 -0.634 0.476 0.344 -0.346]	0.048229
7	[0.330 -0.263 -0.504 0.624 0.133 -0.394 0.075]	0.047664
8	[-0.305 0.166 0.560 -0.515 -0.304 0.452 0.005 -0.063]	0.047213
9	[0.309 -0.186 -0.545 0.543 0.264 -0.453 0.018 0.052 0.006]	0.047205
10	[-0.300 0.152 0.564 -0.500 -0.323 0.457 0.017 -0.071 0.001 -0.006]	0.047192

At the same SNR (SNR =18 dB), the bit error rate (BER) of the monic (h_0 = 1) constraint is 1×10^{-4}, BER of the h_1 = 1 constraint is 8×10^{-4}, BER of the unit energy constraint is 1.80×10^{-3} and BER of the fixed target constraint (PR2) is 1.78×10^{-1}. The BER of the monic constraint gives the best system performance even though the lowest MMSE is from the unit energy constraint. The BER of all target constraints are shown in Figure 4.39.

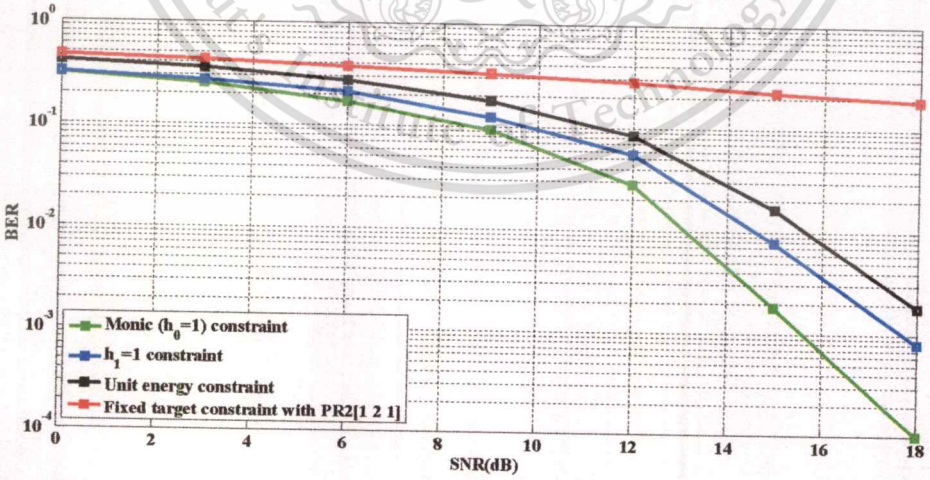


Figure 4.39 Bit error rates (BER) of the HAMR system at 5 Tb/in^2 (reduced bit period).

This material is reserved for educational use only, not allowed for commercial use.
Forbidden to modify the content, and cite the document when use.

As we can see from the simulation results, the frequency responses of GPR targets of the HAMR systems at 4 Tb/in^2, 5 Tb/in^2 (reduced track width) and 5 Tb/in^2 (reduced bit period) are similar to the frequency response of LMR [14] and they provide lower MMSE values than PR targets of the form $H(D) = (1+D)^n$. Since the frequency response of four PR targets are all dc-full. Although the lowest MMSE of all systems is from the unit energy constraint, the monic constraint gives the best BER. However, we know that the BER performance of VD also depends on the noise correlations and the data patterns. So, the lower MMSE does not necessarily provide the lower BER [23].

This material is reserved for educational use only, not allowed for commercial use.
Forbidden to modify the content, and cite the document when use.

CHAPTER 5

CONCLUSION AND SUGGESTION FOR FUTURE WORK

5.1 Conclusion

In this thesis, we use the thermal William-Comstock equation to model the perpendicular heat assisted magnetic recording with non-large thermal laser spot approximation by using linear relationship for M_r and H_c with T to investigate and understand the HAMR system performance. The characteristics of HAMR system compared to the temperature profile T, magnetization field $M(x)$, Karlqvist head field H_h and coercivity field H_c have been studied. The HAMR system behavior of the areal density 4 Tb/in^2, 5 Tb/in^2 (reduced track width) and 5 Tb/in^2 (reduced bit period) are operated.

The microtrack model is used for 2D process of heating and magnetization of a medium determine the transition characteristics in HAMR by dividing recorded track into N individual sub-tracks of equal width with the different transition parameters. The TWC equation is then applied to determine the transition center x_0 and parameter a on each individual sub-track,

Using the HAMR system parameters at the areal density of 4 Tb/in^2, 5 Tb/in^2 (reduced track width) and 5 Tb/in^2 (reduced bit period), the simulation results show that the proper high H_c, low M_r, low H_0 and high T_{peak} provide the good transition parameters. The transition response $p(x)$ and bit response $h(x)$ can be achieved. The parameter PW_{50} with the areal density of 4 Tb/in^2 is equal to 12.793 nm, hence, ND is about 2. We get PW_{50} at the areal density of 5 Tb/in^2 (reduced track width) equal to 13.988 nm and hence ND is about 2. For the areal density of 5 Tb/in^2 (reduced bit period), PW_{50} is 12.883 nm and we get the ND equal to 2.57. The playback signal of HAMR can be obtained by the convolution between the transition bit b_k and the transition response p_x. The playback signal is then corrupted by the additive white Gaussian noise (AWGN). From the results of the simulation, the playback signal of HAMR can be affected from various parameters such as the coercivity H_c, the remanent magnetization M_r, the head field H_0 and the peak temperature T_{peak}.

This material is reserved for educational use only. Commercial use is prohibited.
Forbidden to modify the content, and cite the document when use.

Moreover, we design the MMSE equalizer for heat-assisted magnetic recording by using the minimum-mean squared error (MMSE) method to minimize the mean-squared error (MSE) between the desired outputs and the equalizer outputs. We have compared the monic (h_0 = 1) constraint, h_1 = 1 constraint, the unit energy constraint and the fixed target constraint (PR2) to find the lowest MMSE. From the simulation results, the frequency response of GPR targets of the HAMR systems at 4 Tb/in^2, 5 Tb/in^2 (reduced track width) and 5 Tb/in^2 (reduced bit period) are similar to the frequency response of LMR and provide the lower MMSE than PR targets. Although the lowest MMSE of all systems is from the unit energy constraint, the monic constraint gives the best BER. Therefore, the monic constraint outperforms other constraints.

5.2 The suggestion for further work

In this work, we assume that the HAMR medium is ideal which has no jitter noise in the position of transition. There is only additive white Gaussian noise (AWGN) which is included to the playback signal. As the bit size continues to reduce, each bit in HAMR media is expected to contain only a few grains. Media noise from the jitter between transitions is expected. For the future works, the transition jitter noise should be added to the simulation system of the HAMR to study the effects the imperfect media.

This material is reserved for educational use only, not allowed for commercial use.
Forbidden to modify the content, and cite the document when use.

REFERENCES

[1] O. Heinonen and K.Z Gao, "Extension of Perpendicular Recording," *Journal of Magnetism and Magnetic Material*, vol. 320, no. 22, pp.2885-2888. Aug. 2008.

[2] Y. Shiroishi, K. Fukuda et al., "Future Options for HDD Storage," *IEEE Trans. Magn.*, vol. 45, no. 10, pp. 3816-3822, Oct. 2009.

[3] E.M. Kurtas, M.F. Erden et al., "Future Read Channel Technologies and Challenges for High Density Data Storage Applications," Acoustics, Speech, and Signal Processing, Proceedings of *ICASSP* 2005, pp. 737-740.

[4] T. Rausch, J.A. Bain, D.D. Stancil, and T.E. Schelsinger, "Thermal Williams-Comstock Model for Predicting Transition Lengths in Heat-Assisted Magnetic Recording System," *IEEE Trans. Magn.*, vol. 40, no. 1, pp. 137-147, Jan. 2004.

[5] M.F. Erden, T. Rausch, W.A. Challener, "Cross-track Location and Transition Parameter Effects in Heat-Assisted Magnetic Recording," *IEEE Trans. Magn.*, vol. 41, no. 6, pp.2189-2194, Jun. 2005.

[6] R. Radhakrishnan, M.F. Erden et al., "Transition Response Characteristics of Heat-Assisted Magnetic Recording and Their Performance With MTR Codes," *IEEE Trans. Magn.*, vol. 43, no. 6, pp. 2298-2300, Jun. 2007.

[7] R. Radhakrishnan, B. Vasic, M.F. Erden et al., "Characterization of Heat-Assisted Magnetic Recording Channels," *DIMACS* Series in Discrete Mathematics and Theoretical Computer Science, vol. 73, pp. 25-41, 2007.

[8] M.H. Kryder, E.C. Gage et al., "Heat-Assisted Magnetic Recording," *Invited Paper Proceedings of the IEEE*, vol. 96, no. 11: 1810-1835, Nov. 2008.

[9] R. Wongsathan and P. Supnithi, "Channel Response of HAMR with Linear Temperature-Dependent Coercivity and Remanent Magnetization," in *Conf. Rec. 2012 IEEE Int Conf. ECTI-CON*, 2012, pp. 1-4.

[10] J.U. Thiele, K.R. Coffey, M.F. Toney, J.A. Hedstrom, and A.J. Kellock, "Temperature Dependent Magnetic Properties of Highly Chemically Ordered Fe55−xNixPt45L10 Films," *J. Appl. Phys.*, vol. 91, no. 10, pp. 6595-6600, May 2002.

[11] P. Kovintavewat, I. Ozgunes, E. Kurtas, J.R. Barry and S.W. McLaughlin, "Generalized Partial-Response Targets for Perpendicular Recording with Jitter Noise," *IEEE Trans. Magn.*, vol.38, no.5, pp. 2340-2342, Sep. 2002.

This material is reserved for educational use only, not allowed for commercial use.

Forbidden to modify the content, and cite the document when use.

[12] H.N. Bertram, *Theory of Magnetic Recording*, Cambridge, U.K.: Cambridge Univ. Press 1994, ch. 5, pp. 107-138.

[13] B. Vasic and E.M. Kurtas, *Coding and Signal Processing for Magnetics Recording Systems*, Boca Raton, CRC PRESS 2005, ch. 2, pp. 2.2-1-2.2-26.

[14] P. Kovintavewat, *Signal Processing for Digital Data Storage Volume II: Receiver Design,* National Electronics and computer Technology Center (NECTEC) 2007, ch. 3, pp. 43-64.

[15] M. L. Plumer, J. V. Ek, and W. C. Cain, "New Paradigms in Magnetic Recording," Physics in Canada, vol. 67, no. 1, pp. 25-29, Mar. 2011.

[16] P. Kovintavewat, *Signal Processing for Digital Data Storage Volume I: Basic Read-Write Channel*, National Electronics and computer Technology Center (NECTEC) 2007.

[17] P. Kovintavewat, *Signal Processing for Digital Data Storage Volume III: Advanced Receiver Design*, National Electronics and computer Technology Center (NECTEC) 2007.

[18] K. Boonserm and P. Supnithi, "GUI-Based Read Channel Simulation Tools in Magnetic Recording System" in *the 23nd Int Conf. ITC-CSCC*, 2008, pp. 925-928.

[19] Kavcic, A. and A. Patapoutian, "The Read Channel," Proceedings of the *IEEE*, vol. 96, no. 11, pp. 1761-1774, Nov 2008.

[20] J. Moon, "The Role of Signal Processing in Data-Storage," *IEEE* Signal processing magazine, pp.54-72, July 1998.

[21] G. D. Forney Jr. "Maximum-Likelihood Sequence Estimation of Digital Sequences in the Presence of Intersymbol Interference," *IEEE* Proceeding, vol. 61, no. 3, pp. 363-378. Mar 1972.

[22] S. K. Nair, H. Shafiee and J. Moon. "Equalization and Detection in Storage Channels," *IEEE* Trans. Mag., vol.32, no. 5, pp. 5206-5217, Sep 1996.

[23] J. Moon and W. Zeng. "Equalization for Maximum Likelihood Detectors," *IEEE* Trans. Magn., vol.31, no. 2, pp. 1083-1088, Mar 1995.

This material is reserved for educational use only, not allowed for commercial use.
Forbidden to modify the content, and cite the document when use.

APPENDICES

King Mongkut's Institute of Technology Ladkrabang

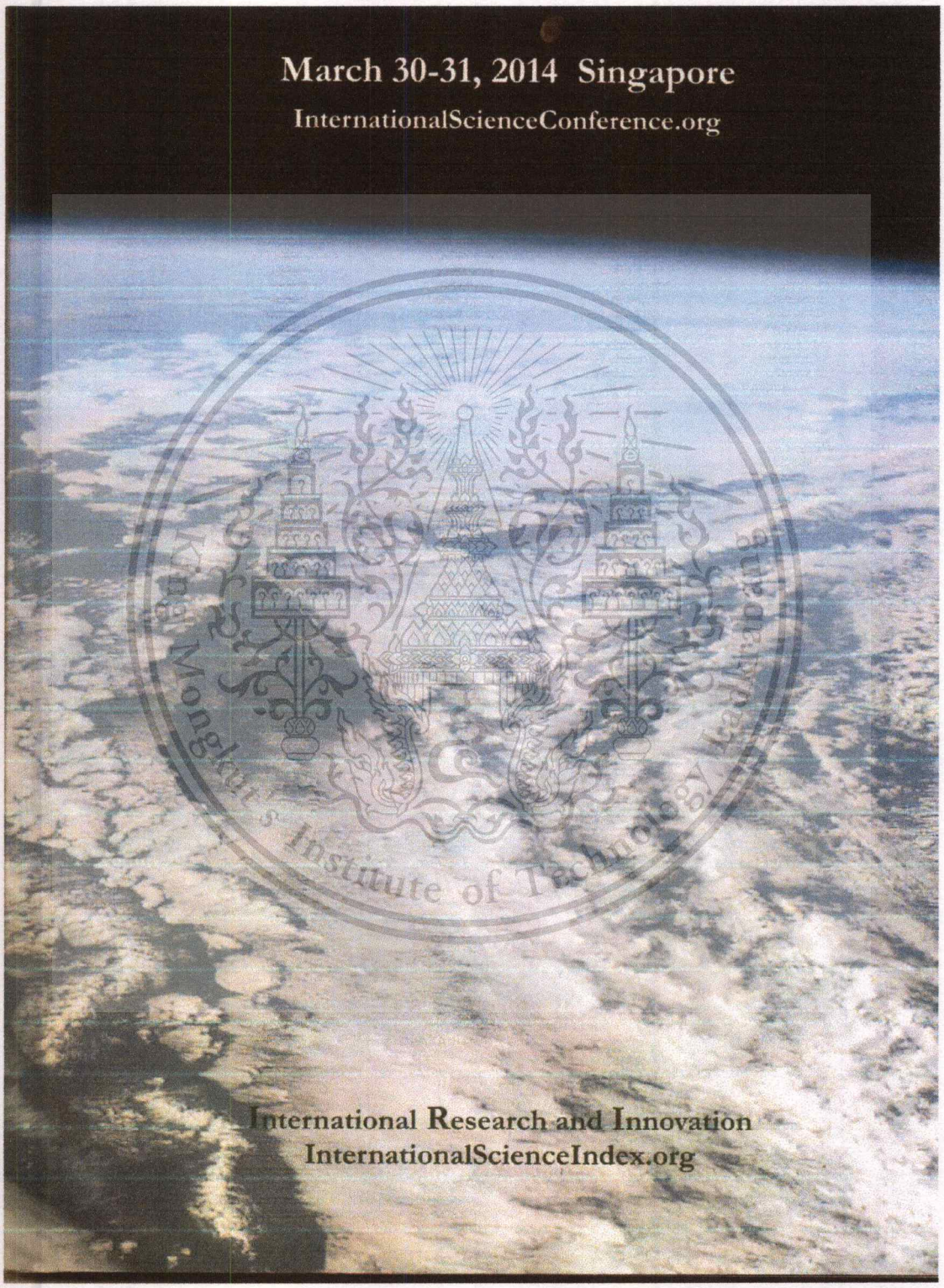
This material is reserved for educational use only, not allowed for commercial use.
Forbidden to modify the content, and cite the document when use.

APPENDIX A

CONFERENCE PROCEEDING

King Mongkut's Institute of Technology Ladkrabang

This material is reserved for educational use only, not allowed for commercial use.
Forbidden to modify the content, and cite the document when use.



This material is reserved for educational use only, not allowed for commercial use.
Forbidden to modify the content, and cite the document when use.

International Science Index Vol:8 No:3 2014

Target and Equalizer Design for Perpendicular Heat-Assisted Magnetic Recording

P. Tueku, P. Supnithi, R. Wongsathan

Abstract—Heat-Assisted Magnetic Recording (HAMR) is one of the leading technologies identified to enable areal density beyond 1 Tb/in^2 of magnetic recording systems. A key challenge to HAMR designing is accuracy of positioning, timing of the firing laser, power of the laser, thermo-magnetic head, head-disk interface and cooling system. We study the effect of HAMR parameters on transition center and transition width. The HAMR is model using Thermal Williams-Comstock (TWC) and microtrack model. The target and equalizer are designed by the minimum mean square error (MMSE). The result shows that the unit energy constraint outperforms other constraints.

Keywords—Heat-Assisted Magnetic Recording, Thermal Williams-Comstock equation, Microtrack model, Equalizer.

I. Introduction

THE proliferation of digital content creation and consumption brings an increasing demand for data storage devices, such as the hard disk drive (HDD). This demand drives requires increasing storage capacity, which in turns drives increasing growth in areal density (AD). AD is defined as the number of bits stored in a bit area of medium and it is determined by the average size of the grains and the number of grains that is used to store 1 bit of information. To increase the AD, the magnetic grain size must be reduced and to maintain the right levels of signal to noise ratio (SNR), the number of grains per bit must be constant. However, small grains will face thermal instability problem. To remedy this issue, media need to have high coercivity (H_c) which means anisotropy (K_u) is high and, therefore, it is difficult to write data bits because the current write field limitation. Heat-assisted magnetic recording (HAMR) channel model has been developed and the thermal Williams-Comstock (TWC) model has been used to predict the limitation. HAMR is one of the four enabling technologies which surpass the critical point of storage density limit known as the super-paramagnetic limit at 1 Tb/in^2 AD, as in [1]-[3].

New write mechanism has been researched by many researchers around the world. It is able to utilize higher anisotropy to produce smaller grain sizes and to secure a signal to noise ratio (SNR) and bit error rate (BER). HAMR can overcome the write field limitation (2.45T) by temporarily reducing H_c during the write process by heating the medium. That means K_u is also reduced and the energy barrier to write on the medium is also decreased. The medium is then rapidly cooled down to the room temperature after magnetization completed, where thermal stability is acceptable.

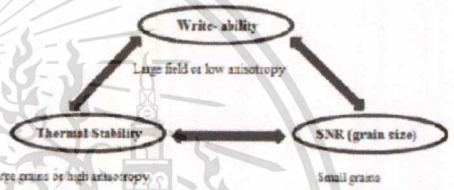


Fig. 1 The write-ability trilemma: the available from writer has to be trade off against thermal stability (large grains or high anisotropy) and media SNR (small grains) [1]

HAMR system has many thermal issues compared to the conventional magnetic recording. Hence, each work step and the whole system need to be researched and clarified, as well as improving the stability and reliability of the system against thermal issues. The HAMR channel model has recently been investigated and the read process of the conventional read channel models employed in current magnetic recording systems has been used to produce the HAMR playback signals, as in [4]-[11].

The organization of this paper is as follows. In Section II, we will describe the principles of perpendicular HAMR systems using the Thermal Williams-Comstock (TWC) model, transition parameters and the microtrack modeling to determine the transition characteristics of both large and non-large spot laser. Next in Section III, we will propose the target and equalizer by the minimum-mean squared error (MMSE) method. Then, the simulation and results is discussed in section IV. Finally, the conclusion will be made in Section V.

II. Perpendicular Heat-Assisted Magnetic Recording

References [4], [5] show the longitudinal HAMR with large spot approximation is used to simplify the equation but it is only valid if the assumptions are fulfilled. Large spot approximation is also used for the perpendicular HAMR, as in [6]. References [7], [9] show the perpendicular channels with non-large spot approximation are used to simulate the channel model. A linear relationship for remanent magnetization M_r and coercivity H_c with temperature is assumed to be used in

P. Tueku is with the International College, King Mongkut's Institute of Technology Ladkrabang, Bangkok 10520 Thailand (phone: 663-527-7345; fax: 663-527-7955; e-mail: S2600622@kmitl.ac.th).

P. Supnithi is with the School of Telecommunications Engineering, King Mongkut's Institute of Technology Ladkrabang, Bangkok 10520 Thailand (e-mail: ksupornc@kmitl.ac.th).

R. Wongsathan is with the Faculty of Engineering, King Mongkut's Institute of Technology Ladkrabang, Bangkok 10520 Thailand (e-mail: s4610146@kmitl.ac.th).

This material is reserved for educational use only, not allowed for commercial use.
Forbidden to modify the content, and cite the document when use.

[4]-[7] and [9] but as in [10], the non-linear relationship for M_r and H_c with temperature T is assumed instead. In this paper, we use the TWC equation for perpendicular HAMR with non-large spot approximation by using linear relationship for M_r and H_c with T to investigate and understand the HAMR system performance.

A. Williams-Comstock (WC) Model

In 1971, Mason Williams and Larry Comstock developed the William-Comstock (WC) model to predict the transition width in longitudinal magnetic recording, as in [13]. They provide a simple analysis of the write process. WC model is a well-known approximate analytical model which describes the transition characteristics in a conventional magnetic recording system. In the model, the "zigzag" nature of magnetic transition is ignored and the shape of magnetic transition is presumed to be described by the arctangent function. The transition center x_0 and the transition parameter a are the two main parameters which can be derived from this model.

The relationship between the applied field H_a and the resultant magnetization M in the medium is given by the hysteresis loop of the medium and can be written as $M=F_{loop}(H_a)$, where F_{loop} represents the hysteresis loop. The applied magnetic field during the transition formation can be described by the contribution from the head field H_h and the demagnetization field H_d from the recorded transition, i.e.,

$$H_a(x) = H_h(x) + H_d(x) \tag{1}$$

In the down track direction (x-direction), M can be determined by solving

$$M(x) = M\left[H_a(x)\right] = M\left[H_h(x) + H_d(x)\right] \tag{2}$$

where H_d is dependent on M in (2), and so (2) can only be solved by iteration. Williams and Comstock noted that is possible to solve the derivative of (2) by evaluating at the transition center x_0 where the applied field at x_0 is equal to the coercivity H_c. The WC slope equation can be derived from (2)

$$\left.\frac{dM(x)}{dx}\right|_{x_0} = \left.\frac{dM(H)}{dH_a}\right|_{H_c} \left.\frac{dH_a(x)}{dx}\right|_{x_0} = \left.\frac{dM(H)}{dH_a}\right|_{H_c} \left[\left.\frac{dH_h(x)}{dx}\right|_{x_0} + \left.\frac{dH_d(x)}{dx}\right|_{x_0}\right] \tag{3}$$

The magnetization transition during recording can be described by the arctangent function, both the magnetization gradient dM/dx and demagnetization field gradient dHd/dx can be expressed analytically in terms of only one unknown quantity, namely, the transition parameter a. Furthermore, the head field gradient dHh/dx and magnetization gradient with applied field $dM(H)/dHa$ can be evaluated from the analytic Karlqvist head field expressions and the M–H loop for the medium. These assumptions allow (3) to be solved analytically, giving an expression for a containing all the relevant factors in the write process.

B. Thermal Williams-Comstock (TWC) Model

$F_{loop}(H_a)$ in WC model does not account for the effects of heating in HAMR system. In 2004, WC model was extended by incorporating thermal gradients of coercivity H_c and magnetization M for a longitudinal HAMR system and is known as the Thermal Williams–Comstock (TWC) model, as in [4]. The effective field (h) is introduced to account for heating behavior, i.e.,

$$h(x) = \frac{H_a(x)}{H_c(T(x))}. \tag{4}$$

The dependence of M on the temperature captured by h in Eq. 4 is substituted into $M=F_{loop}(h)$. Evaluating the derivative of $M(x)$ at x_0, where the applied field is equal to coercivity $H_a=H_c$, we obtain

$$\left.\frac{dM(x)}{dx}\right|_{x_0} = \left.\frac{dM(h)}{dh}\right|_{H_c} \left.\frac{dh(x)}{dx}\right|_{x_0} \tag{5}$$

The derivative at the H_c is simply the linear slope and S^* is coercivity squareness factor.

$$\left.\frac{dM(x)}{dx}\right|_{H_c(T(x_0))} = \frac{M_r(T(x_0))}{(1-S^*(T(x_0)))} = \left.\frac{H_c(T(x_0))dM(H)}{dH_a}\right|_{H_c(T(x_0))} \tag{6}$$

The thermal Williams-Comstock slope equation can then be derived from (3) giving

$$\left.\frac{dM(x)}{dx}\right|_{x_0} = \left.\frac{dM(H)}{dH_a(T(x_0))}\right|_{H_c(T(x_0))} \times \left[\left.\frac{dH_h(x)}{dx}\right|_{x_0} + \left.\frac{dH_d(x)}{dx}\right|_{x_0} - \left.\frac{dH_c(T(x_0))}{dT}\right|_{T(x_0)} \left.\frac{dT}{dx}\right|_{x_0}\right] \tag{7}$$

Since dM/dx and dH_d/dx depend on a, a can be solved by using (4). To obtain dM/dx, it is assumed that the transition during recording can be described by the arctangent function from which dM/dx can be derived.

$$M(x) = \frac{2M_r(T(x))}{\pi} \tan^{-1}\frac{x-x_0}{a} \tag{8}$$

and dM/dx at x_0 can be solved by differentiating (8), i.e.,

$$\left.\frac{dM(x)}{dx}\right|_{x_0} = \frac{2M_r(T(x_0))}{\pi a} \tag{9}$$

This material is reserved for educational use only, not allowed for commercial use.
Forbidden to modify the content, and cite the document when use.

International Science Index Vol:8 No:3 2014

The term $dM(h)/dh$ from (5) at x_0 can be solved as slope of hysteresis loop is always positive at either transition is made from positive or negative H_c

$$\left.\frac{dM(h)}{dh}\right|_{H_c(T(x_0))} = \left|\frac{1}{H_c(T(x_0))} \times \frac{M_r(T(x_0))}{1-S^*}\right| \quad (10)$$

The term dH_h/dx of perpendicular recording at x_0 can be solved by using and the symmetry of the longitudinal Karlqvist head field component. The perpendicular head field can be derived by facilitating to turned sideways of longitudinal as

$$H_h = \frac{H_0}{\pi}\left[\tan^{-1}\left(\frac{y+g/2}{x}\right) - \tan^{-1}\left(\frac{y-g/2}{x}\right)\right], \quad (11)$$

and

$$\left.\frac{H_h(x)}{dx}\right|_{x_0} = -\frac{gH_0}{\pi\left(x^2+(g/2)^2\right)}, \quad (12)$$

where H_0 is the deep gap field, g is the gap width between pole head and its image ($g = 2d+2t$), t is the medium thickness and the field is evaluated at the center of medium ($y = t/2$). The parameter H_d for perpendicular recording is obtained by convolving the unit step response at the original and the magnetization gradient, i.e.,

$$H_{d_perp} = -\frac{\partial M(x)}{\partial x} * H_y^{step} = -\frac{\partial M(x)}{\partial x} * \frac{1}{\pi}\tan^{-1}\left(\frac{2x}{t}\right) \quad (13)$$

$$\frac{dH_d(x)}{dx} = -\frac{4}{\pi^2}\int_{-\infty}^{\infty}\frac{M_r(T(x'))a}{a^2+(x'-x_0)^2}\frac{t}{t^2+4(x-x')^2}dx' + \frac{4}{\pi^2}\int_{-\infty}^{\infty}\tan^{-1}\left(\frac{x'-x_0}{a}\right)\left.\frac{dM_r(T(x'))}{dT}\right|_{T(x')}\frac{dT(x')}{dx'}\frac{t}{t^2+4(x-x')^2} \quad (14)$$

Here, H_c and M_r are linearly temperature-dependent (T), i.e.

$$H_c = -H_{c0}T(x,y) + H_{c,const} \quad (15)$$

$$M_r = -M_{r0}T(x,y) + M_{r,const} \quad (16)$$

where H_{c0} and M_{r0} are the temperature sensitivities of H_c and M_r, $H_{c,const}$ and $M_{r,const}$ are H_c and M_r at 0 Kelvin (K). So dH_c/dT is $-H_{c0}$ and dM_r/dT is $-M_{r0}$. A two-dimensional (2D) Gaussian thermal profile is given as

$$T(x,z) = T_{peak}\exp\left(-\frac{(x-c_0)^2}{2\sigma_t^2}\right)\exp\left(-\frac{z^2}{2\sigma_t^2}\right) + 300 \text{ (K)} \quad (17)$$

where T_{peak} is the peak temperature in the medium above room temperature in degree Celsius, c_0 is the laser spot position, x is defined to the position in down-track direction and z is defined to the position in cross-track direction. Differentiating (17), we have

$$\frac{T(x,z)}{dx} = T_{peak}\left(-\frac{(x-c_0)}{\sigma_t^2}\right)\exp\left(-\frac{(x-c_0)^2}{2\sigma_t^2}\right)\exp\left(-\frac{z^2}{2\sigma_t^2}\right) \quad (18)$$

C. Transition Center (x_0) and Transition Parameter (a)

The position x_0 is defined as the point where the medium reverses its direction of magnetization and a is measured and related to the width of the magnetization transition. Achieving the narrowest possible transition (smallest a) allows placing recording bits close together and hence results in high linear density. The position x_0 of perpendicular HAMR with large spot and linear relationship for H_c and M_r can be calculated, as in [9],

$$x_0 = \frac{g + \sqrt{g^2 - a\tan^2\left(\pi\frac{H_c(T(x_0))}{H_0}\right)\left(y^2-(g/2)^2\right)}}{2\tan\left(\pi\frac{H_c(T(x_0))}{H_0}\right)} \quad (19)$$

and a can be also calculated from

$$a = -\frac{\gamma}{2} + \frac{1}{2}\sqrt{\gamma^2 - \frac{4H_c(1-S^*)t}{\Delta\pi}}\Bigg|_{x_0} \quad (20)$$

where

$$\Delta \equiv \frac{H_g g}{\pi\left(x_0^2+(g/2)^2\right)} - \frac{dH_c}{dT}\left.\frac{dT}{dx}\right|_{x_0}$$

and

$$\gamma \equiv \frac{2M_r}{\Delta\pi} - \frac{t}{2} + \frac{2H_C(1-S^*)}{\Delta\pi}$$

For non-large spot HAMR, x_0 can be solved by

$$x_{0,j+1} = \frac{g + \sqrt{g^2 - 4\tan^2\left(\pi\frac{H_c(T(x_0))+H_d(x_0,j,a_k)}{H_0}\right)\left(y^2-(g/2)^2\right)}}{2\tan^2\left(\pi\frac{H_c(T(x_0))+H_d(x_0,j,a_k)}{H_0}\right)} \quad (21)$$

and a can be solved by

$$a_{k+1} = \frac{-\beta + \sqrt{\beta^2 + 4\pi(\alpha+\delta)H_c(1-S^*)t}}{2\pi(\alpha+\delta)} \quad (22)$$

where

$$\alpha = \frac{H_g g}{\pi\left(x_{0,j+1}^2+(g/2)^2\right)}, \delta = \frac{dH_d\left(a_k, x_{0,j+1}\right)}{dx} - \frac{dHc}{dx},$$

This material is reserved for educational use only, not allowed for commercial use.
Forbidden to modify the content, and cite the document when use.

$$\beta = -\frac{\pi\alpha t}{2} + 2M_r - \frac{\pi t}{2}\left(\frac{dH_d\left(a_k \cdot x_{0,j+1}\right)}{dx} - \frac{dH_c}{dx}\right) + 2H_c\left(1 - S^*\right)$$

D. Microtrack Model

The microtrack model is used for 2D process of heating and magnetization of a medium to solve the problem of determining the transition characteristics in HAMR by dividing recorded track into N individual sub-tracks of equal width with different transition parameters. The TWC equation is applied to determined x_0 and a in each individual sub-track, as in [4]-[9]. The playback voltage (V) of perpendicular recording is given from [12] by

$$V(x, a_i, x_{0,i}) = -CM_r t \ln\left\{\frac{(g_r/2-(x-x_{0,i}))^2 + (d+a_i+t/2)^2}{(g_r/2+(x-x_{0,i}))^2 + (d+a_i+t/2)^2}\right\} \quad (23)$$

where C is a system specific constant, g_r is the read head gap, and d is the head-medium spacing and t is denote to media thickness.

The overall transition response $p(x)$ can be obtained by weighting the transition response $p_i(x)$ of each sub-track to obtain

$$p_i(x) = \exp\left\{-\frac{\left(x-\frac{N+1}{2}\Delta x+i\Delta x\right)^2}{2\sigma_T^2}\right\} \cdot V(x, a_i, x_{0i}) \quad (24)$$

and

$$p(x) = \frac{1}{N}\sum_{i=1}^{N} p_i(x) \quad (25)$$

where a_i and x_{0i} are the transition parameter and transition center of the i^{th} microtrack, i can be 1 to N and Δx stands for the width of each sub-track. The bit response is then

$$h(x) = 0.5\{p(x) - p(x - T_x)\} \quad (26)$$

where T_x denotes the along-track bit period.

III. Target and Equalizer Design

A. Channel Model

The laser can be positioned either in the direction of the head movement (up-track or $+x$) or opposite to it (down-track or $-x$). However, in this work, the laser is assumed to be at the center of the track in the cross-track direction. The HAMR channel with equalizer design is shown in Fig. 2.

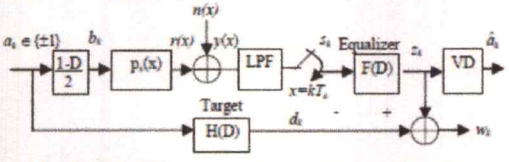


Fig. 2 The HAMR system with target-shaping equalization

where $a_k \in \{\pm 1\}$ is input sequences and filtered by using ideal differentiator (1-D)/2. The sequence of the transitions is $b_k \in \{\pm 1, 0\}$, where $b_k \in \{\pm 1\}$ represents the positive and negative transitions, and $b_k = 0$ means no transition. The playback signal $r(x)$ is obtained by convolution between b_k and transition response p_k and then corrupted by the additive white Gaussian noise (AWGN). In this simulation, SNR is defined as SNR = $10\log_{10}(1/\sigma^2)$, where σ^2 is the variance of AWGN. The playback signal with AWGN $y(x)$ will be passed to low pass filter (LPF), sampled and then put in equalizer (FD) to equalize the signal in order to facilitate the application of Viterbi detector (VD). Finally, the equalized outputs $z(k)$ are detected by VD.

B. Target and Equalizer Design

In this study, we design targets (HD) and equalizers (FD) by using the minimum-mean squared error (MMSE) method to minimize the mean-squared error (MSE) between desired outputs and equalizer outputs, as in [11], [14]. The target $H(D)$ and its corresponding $F(D)$ can be obtained by minimizing

$$E\left\{w_k^2\right\} = E\left[(z_k - d_k)^2\right] = E\left[\{(z_k * f_k) - (a_k * h_k)\}^2\right] \quad (27)$$

where w_k is the difference between output of equalizer, z_k and the desired output, d_k of designed target, * is the convolution operator and $E\{.\}$ is the expectation operator. h_k and f_k stand for the coefficients of $H(D)$ and $F(D)$. The MMSE can be expressed as

$$\varepsilon^2 = E\left\{w_k^2\right\} = \mathbf{F}^T\mathbf{R}\mathbf{F} + \mathbf{H}^T\mathbf{A}\mathbf{H} - 2\mathbf{F}^T\mathbf{P}\mathbf{H} \quad (28)$$

where $\mathbf{H} = [h_0\ h_1\ h_2 \ldots h_{L-1}]^T$ represents the L-tap GPR target and $\mathbf{F} = [f_{-K}, f_{-K+1} \ldots f_0 \ldots f_K]^T$ represents the K-tap equalizer by where the length of the equalizer is N ($N = 2K+1$). A is an LxL autocorrelation matrix of a_k, R is an MxM autocorrelation matrix of sequence s_k, and P is an MxL cross-correlation matrix sequence of a_k and s_k. During the minimization process, the specified constraint must be used to avoid the trivial solution of $\mathbf{F} = 0$ and $\mathbf{H} = 0$.

Firstly, by minimizing (28) subject to a monic constraint, we fix h_0=1 and compute

$$\varepsilon^2 = \mathbf{F}^T\mathbf{R}\mathbf{F} + \mathbf{H}^T\mathbf{A}\mathbf{H} - 2\mathbf{F}^T\mathbf{P}\mathbf{H} - 2\lambda\left(\mathbf{I}^T\mathbf{H} - 1\right)$$

$$\lambda = \frac{1}{\mathbf{I}^T\left(\mathbf{A} - \mathbf{P}^T\mathbf{R}^{-1}\mathbf{P}\right)^{-1}\mathbf{I}} \quad (29)$$

$$\mathbf{H} = \lambda\left(\mathbf{A} - \mathbf{P}^T\mathbf{R}^{-1}\mathbf{P}\right)^{-1}\mathbf{I}$$

$$\mathbf{F} = \mathbf{R}^{-1}\mathbf{P}\mathbf{H}$$

where λ is the Lagrange multiplier and $\mathbf{I}$ is an L-element column vector which 1st element is 1 and the rest is 0.

This material is reserved for educational use only, not allowed for commercial use.
Forbidden to modify the content, and cite the document when use.

Secondly, we fix the second target h_1=1 constraint. Column vector **J** that 2nd element is 1 and the others are 0. This is identical to monic constraint solution but **I** is replaced by **J**. Thirdly, the energy $\mathbf{H}^T\mathbf{H}$=1 is fixed to minimize (28) called the unit energy constraint.

$$\varepsilon^2 = \mathbf{F}^T\mathbf{R}\mathbf{F} + \mathbf{H}^T\mathbf{A}\mathbf{H} - 2\mathbf{F}^T\mathbf{P}\mathbf{H} - 2\lambda\left(\mathbf{H}^T\mathbf{H}-1\right) \quad (30)$$

After differentiating and setting the result to 0, the final constraint we use fixed target constraint according to PR form $1\text{-}D^2$ of the PR-4 target for minimizing (28).

IV. Simulation Results

In this work, the medium is assumed to be $Fe_{55-x}Ni_xPt_{45}L1_0$ where 10<x<30% because the linear relationship for remanent magnetization M_r and coercivity H_c with temperature is resulted in this range, as in [9]-[10]. For all cases, the laser is assumed to be at the center of the track in the cross-track direction but varied in the down-track direction. The temperature induced by the laser is assumed to be Gaussian in both dimensions with the peak temperature of 330 °C and track width 20 nm. System parameters are given in Table I.

We first discuss the results from Fig. 3. Firstly, we fix M_r magnetization dependencies on temperature to study the behavior of x_0 and a by using various H_c. With magnetization dependencies on temperature (M_r=-1000T+1.8x10^6), we found that at increasing H_c, x_0 is shifted faraway from laser position and a is decreased. Secondly, we vary M_r to study x_0 and a by using H_c = -2900T+2.4x10^6 for evaluation. Fig. 4 shows that x_0 has almost the same values and small a is found at low M_r. Small a means narrow transitions, hence, recording bits are packed close together.

Next, we study x_0 and a by focusing on the head field (H_0). The results show that x_0 is shifted far from the laser position and a is wider at high head field as shown in Fig. 5. Finally, using high H_c, low M_r and low H_0 to evaluate the system by varying peak temperature (T_{peak}), the results of this experiment show that high T_{peak} will give small a as shown in Fig. 6.

As the discussion before, we select high H_c, low M_r, low H_0 and high T_{peak} to evaluate the system. The transition response $p(x)$ and bit response $h(x)$ can be achieved and shown in Fig. 7. We get PW_{50} equal to 13.988 nm and hence ND is about 2. The HAMR playback signal is obtained by the convolution between b_k and p_x and corrupted from AWGN. The playback with and without AWGN is shown in Fig. 8. Playback signal from LPF is also shown in this Fig. 8.

For MMSE equalizer design, we use the fixed target constraint to minimize the MSE by setting the various number of equalizer taps. Equalizer taps are in the range of 3 to 21 taps. PR1 gives the lowest MMSE from all the targets for this case. The results are shown in Fig. 9. The MMSE value at 11-tap equalizer is equal to 0.526. The 11-tap equalizer coefficients are [0.044 -0.036 0.252 0.128 1.320 2.641 1.356 0.404 0.166 0.033 -0.010]

Next, we compare the MSE using four target constraints for evaluation and the range is from 3 to 21 taps. We use 3-tabs target to simulate this comparison. The result shows that the unit energy constraint has the lowest minimum MSE, as in Fig. 10. The 3-tap target with 11-tap equalizer has the MSE equal to 0.065. The h_1=0 constraint gives the MSE of 0.105. For h_0 = 1 constraint, the minimum MSE of this targets is 0.091, and the fixed-target constraint using PR2 [1 2 1] has the highest MSE value equal to 1.890.

Since the unit-energy constraint gives the lowest MSE value, we select the unit energy constraint to evaluate and find the MSE with the various number of target taps. Equalizer taps are also in the range of 3 to 21 taps as the previous simulation. For the 11-tap equalizer, the 10-tap target gives the minimum MSE as shown in Fig. 11. The 11-tap equalizer coefficients are [-0.043 0.050 -0.126 0.186 -0.466 0.228 0.616 -0.956 0.360 0.413 -0.438] and 10-tap target coefficients are [-0.261 0.475 -0.109 -0.491 0.607 -0.142 -0.212 0.132 -0.039 0.021]. The MMSE value is 0.055.

V. Conclusions

In this paper, we use the thermal William-Comstock equation to model the perpendicular heat assisted magnetic recording with non-large thermal laser spot. The playback signal of HAMR can be affected from various parameters such as H_c, M_r, H_0 and T_{peak}. The simulation results show that the proper high H_c, low M_r, low H_0 and high T_{peak} provide the good transition parameters. Moreover, we design the MMSE equalizer for heat-assisted magnetic recording. The lowest minimum MSE value is obtained from the unit energy constraint.

TABLE I
System Parameters

Symbol	Parameter	Unit
TW	track width	20 nm
N	number of sub-track	10
c_x	laser position	0 nm
H_0	deep gap field	1x10^6 A/m
T_{peak}	peak temperature	330 C°
σ_T	sigma of temperature profile	16.2 nm
g	gap width between pole head and its image	32 nm
σ_s	sigma of reader sensitivity function	4.23 nm
d	head-medium distance or fly height	6 nm
t	medium thickness	10 nm
T_b	bit period	6 nm
C	a system specific constant	1
H_c	dependence of coercivity on temperature	2900T+2.4x10^6 A/m
M_r	dependence of remanent magnetization on Temperature	600T+1.8x10^6 A/m
AD	Areal density	5 Tb/in^2

This material is reserved for educational use only, not allowed for commercial use.
Forbidden to modify the content, and cite the document when use.

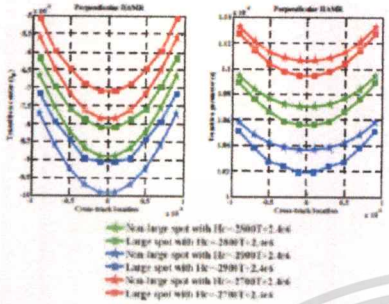


Fig. 3 Transition center and parameter with various H_c dependencies on temperature

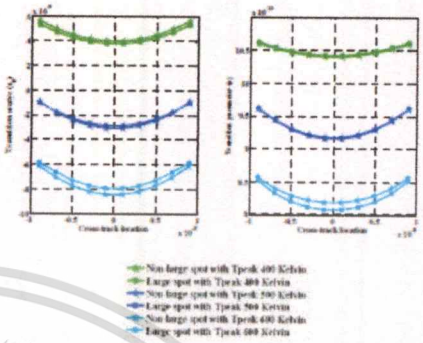


Fig. 6 Transition center and parameter with various peak temperatures

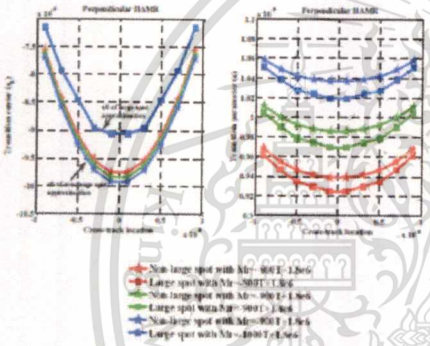


Fig. 4 Transition center and parameter with various M_r dependencies on temperature

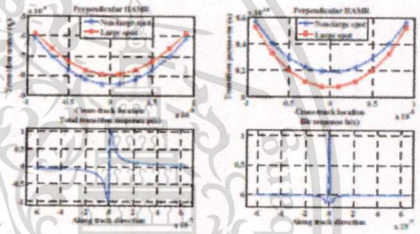


Fig. 7 Transition center, parameter, response and bit response

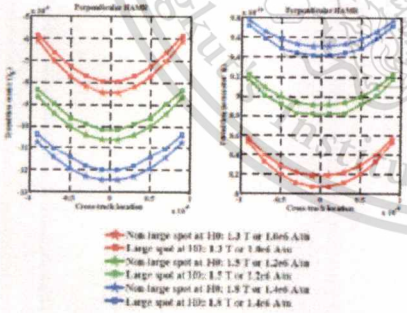


Fig. 5 Transition center and parameter with various head field

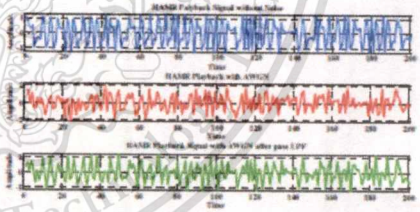


Fig. 8 Playback signal with and without AWGN

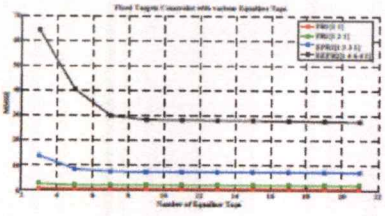


Fig. 9 MMSE of fixed-target constraint with various equalizer taps

This material is reserved for educational use only, not allowed for commercial use.
Forbidden to modify the content, and cite the document when use.

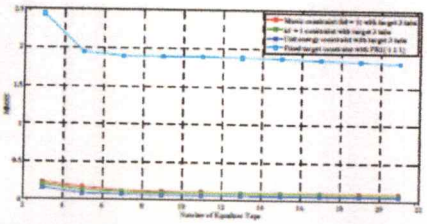


Fig. 10 MMSE of various targets constraint using 3 target taps

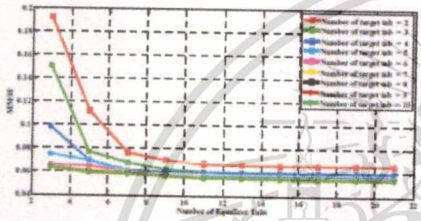


Fig. 11 MMSE of unit-energy constraint equalizers with various target tabs

ACKNOWLEDGMENT

This work was support in part by Faculty of Engineering, King Mongkut's Institute of Technology Ladkrabang. Also, we would like to acknowledge Western Digital (Thailand) Co., Ltd. for granting the scholarship at the International College, King Mongkut's Institute of Technology Ladkrabang.

REFERENCES

[1] O. Heinonen and K.Z. Gao, "Extension of perpendicular recording," *Journal of Magnetism and Magnetic Material*, 2008, pp.2885-2888.

[2] Y. Shiroishi, K. Fukuda et al., "Future Options for HDD Storage," *IEEE Trans. Magn.*, vol. 45, no. 10, pp. 3816-3822, Oct. 2009.

[3] E.M. Kurtas, M.F. Erden et al., "Future read channel technologies and challenges for high density data storage applications, Acoustics, Speech, and Signal Processing," Proceedings of *ICASSP* 2005, pp. 737-740.

[4] T. Rausch, J.A. Bain, D.D. Stancil, and T.E. Schelsinger, "Thermal Williams-Comstock model for predicting transition lengths in heat-assisted magnetic recording system," *IEEE Trans. Magn.*, vol. 40, no. 1, pp. 137-147, Jan. 2004.

[5] M.F. Erden, T. Rausch, W.A. Challener, "Cross-track location and transition parameter effects in heat-assisted magnetic recording," *IEEE Trans. Magn.*, vol. 41, no. 6, pp.2189-2194, Jun. 2005.

[6] R. Radhakrishnan, M.F. Erden et al., "Transition Response Characteristics of Heat-Assisted Magnetic Recording and Their Performance With MTR Codes," *IEEE Trans. Magn.*, vol. 43, no. 6, pp. 2298-2300, Jun. 2007.

[7] R. Radhakrishnan, B. Vasic, M.F. Erden et al., "Characterization of of Heat-Assisted Magnetic Recording Channels," *DIMACS Series in Discrete Mathematic sand Theoretical Computer Science*, vol. 73, pp. 25-41, 2007.

[8] M.H. Kryder, E.C. Gage et al., "Heat-Assisted Magnetic Recording," *Invited Paper Proceedings of the IEEE*, vol. 96, no. 11: 1810-1835, Noember. 2008.

[9] R. Wongsathan and P. Supnithi "Channel response of HAMR with linear temperature-dependent coercivity and remanent magnetization," in *Conf. Rec. 2012 IEEE Int Conf. ECTI-CON*, 2012, pp. 1-4.

[10] J.U. Thiele, K.R. Coffey, M.F. Toney, J.A. Hedstrom, and A.J. Kellock, "Temperature dependent magnetic properties of highly chemically ordered $Fe_{55-x}Ni_xPt_{45}L1_0$ films," *J. Appl. Phys.*, vol. 91, no. 10, pp. 6595-6600, May 2002.

[11] P. Kovintavewat, I. Ozgunes, E. Kurtas, J.R. Barry and S.W. McLaughlin, "Generalized Partial-Response Targets for Perpendicular Recording with Jitter Noise," *IEEE Trans. Magn.*, vol.38, no.5, pp. 2340-2342, Sep. 2002.

[12] H.N. Bertram, *Theory of Magnetic Recording*. Cambridge, U.K.: Cambridge Univ. Press 1994, ch. 5, pp. 107-138.

[13] B. Vasic and E.M. Kurtas, *Coding and Signal Processing for Magnetics Recording Systems*, Boca Raton, CRC PRESS 2005, ch. 2, pp. 2.2-1-2.2-26.

[14] P. Kovintavewat, *Signal Processing for Digital Data Storage Volume II: Receiver Design*, National Electronics and computer Technology Center(NECTEC) 2007, ch. 3, pp. 43-64.

This material is reserved for educational use only, not allowed for commercial use.

Forbidden to modify the content, and cite the document when use.

Target and Equalizer Design for Perpendicular Heat-Assisted Magnetic Recording with Media Jitter Noise

Panatda Tueku[1], Rati Wongsathan[2] and Pornchai Supnithi[2]
[1]International College, King Mongkut's Institute of Technology Ladkrabang
[2]Faculty of Engineering, King Mongkut's Institute of Technology Ladkrabang
Bangkok 10520, Thailand
Email: s2600622@kmitl.ac.th, s4610146@kmitl.ac.th, ksupornc@kmitl.ac.th

***Abstract*—Heat-Assisted Magnetic Recording (HAMR) is one of the leading technologies identified to enable areal density beyond 1 Tb/in² of magnetic recording systems. We study the effect of HAMR parameters on transition center and transition width. The HAMR is modeled using Thermal Williams-Comstock (TWC) and microtrack model. As the bit size continues to reduce and each bit in the HAMR media is expected to have a few magnetic grain that results in a very zigzagged transition from one bit to adjacent bit, the HAMR media is expected to have the high media jitter noise. The target and equalizer are designed by the minimum mean square error (MMSE) and proposed to mitigate the media jitter noise problem and for improving the bit error rate performance. The results show that the monic constraint outperforms other constraints.**

***Keywords*—Heat-Assisted Magnetic Recording, Thermal Williams-Comstock equation, Microtrack model, Media Jitter Noise, Equalizer.**

I. Introduction

The proliferation of digital content creation and consumption brings an increasing demand for data storage devices, such as the hard disk drive (HDD). This demand requires increasing storage capacity, which in turns drives increasing growth in areal density (AD). To increase the AD, the volume (V) of magnetic grain size must be reduced. However, small grains will face the thermal stability problem. To remedy this issue, media need to have high coercivity (H_c) which means anisotropy (K_u) is high and, therefore, it is difficult to write data bits because the current write field limitation by the material and design of write heads (2.4 T). HAMR is one of the leading technologies identified to enable the AD beyond 1 Tb/in² by choosing the high H_c media which means high K_u such as iron platinum alloy while writing by a tiny focused laser at the location of transition. This briefly reduces the high H_c and the energy barrier to write on the medium is also decreased below the available applied field (H_a) for the magnetization process to take place. The medium is then rapidly cooled down after magnetization to the room temperature after magnetization is completed, where thermal stability is acceptable [1]-[3]. The HAMR channel model has recently been investigated and the read process of the conventional read channel models employed in current magnetic recording systems has been used to produce the HAMR playback signals, as in [4]-[9].

The organization of this paper is as follows. In Section II, we will briefly describe the principles of perpendicular HAMR systems using the Thermal Williams-Comstock (TWC) model, transition parameters and the microtrack modeling. Next in Section III, we will propose the target and equalizer by the minimum-mean squared error (MMSE) method. Then, the simulation and results will be discussed in Section IV. Finally, the conclusions will be made in Section V.

II. Perpendicular Heat-Assisted Magnetic Recording

References [4]-[5] show the longitudinal HAMR with large spot approximation is used to simplify the equation, but it is only valid if the assumptions are fulfilled. Large spot approximation is also used for the perpendicular HAMR [6]. References [7], [9] show the perpendicular channels with non-large spot approximation are used to simulate the channel model. A linear relationship for remanent magnetization (M_r) and coercivity (H_c) with temperature is assumed to be used in [4]-[7] and [9], but as in [10], the non-linear relationship for M_r and H_c with temperature (T) is assumed instead. In this paper, we use the thermal Williams-Comstock (TWC) equation for perpendicular HAMR with non-large spot approximation by using linear relationship for M_r and H_c with T to investigate and understand the HAMR system performance.

A. Thermal Williams-Comstock (TWC) Model

Thermal Williams-Comstock (TWC) model which was extended from Williams-Comstock (WC) model by incorporating the thermal gradient to capture the effect of temperature (T) on coercivity (H_c) and remanent magnetization (M_r) is used to approximate the characteristics of HAMR. The transition center (x_0) and parameter (a) can be derived from TWC model. The position x_0 is defined as the point where the medium reverses its direction of magnetization and a is measured and related to the width of the magnetization transition. Achieving the narrowest possible transition (smallest a) allows placing recording bits close together and hence results in high linear density.

The applied magnetic field (H_a) during the transition formation can be described by the contribution from the head field (H_h) and the demagnetization field (H_d) from the recorded transition, i.e.,

This material is reserved for educational use only, not allowed for commercial use.
Forbidden to modify the content, and cite the document when use.

$$H_a(x) = H_h(x) + H_d(x) \quad (1)$$

where x is the down-track direction. TWC slope equation which can be derived and is given in [4]-[9] as

$$\left.\frac{dM(x)}{dx}\right|_{x_0} = \left.\frac{dM(H)}{dH_a(T(x_0))}\right|_{H_c(T(x_0))} \times \left[\left.\frac{dH_h(x)}{dx}\right|_{x_0} + \left.\frac{dH_d(x)}{dx}\right|_{x_0} - \left.\frac{dH_c(T(x_0))}{dT}\right|_{T(x_0)} \left.\frac{dT}{dx}\right|_{x_0}\right] \quad (2)$$

where $T(x_0)$ is the temperature profile at x_0 and the magnetization changing is assumed to flip from $-M_r$ to $+M_r$. The transition formation can be described as $H_a=H_c$, i.e.,

$$H_h(x_0) + H_d(x_0) = H_c(T(x_0)) \quad (3)$$

The values x_0 of the HAMR system can be solved by using (3) and a can be obtained by (2). The expression of the field gradients in (2) can be derived and found in [9]. To obtain dM/dx, it is assumed that the transition during recording can be described by the arctangent function

$$M(x) = \frac{2M_r(T(x))}{\pi} \tan^{-1}\frac{x - x_0}{a} \quad (4)$$

and dM/dx at x_0 can be solved by differentiating (4), i.e.,

$$\left.\frac{dM(x)}{dx}\right|_{x_0} = \frac{2M_r(T(x_0))}{\pi a} \quad (5)$$

For TWC model, the effective field (h) is introduced [4] to account for heating behavior and given as

$$h(x) = \frac{H_a(x)}{H_c(T(x))} \quad (6)$$

Evaluating the derivative of $M(x)$ at x_0, where the applied field is equal to coercivity $H_a=H_c$, we obtain

$$\left.\frac{dM(x)}{dx}\right|_{x_0} = \left.\frac{dM(h)}{dh}\right|_{H_c} \left.\frac{dh(x)}{dx}\right|_{x_0} \quad (7)$$

The term $dM(h)/dh$ from (7) at x_0 can be solved as the slope of hysteresis loop is always positive at either transition is made from positive or negative H_c.

$$\left.\frac{dM(h)}{dh}\right|_{H_c(T(x_0))} = \left|\frac{1}{H_c(T(x_0))} \times \frac{M_r(T(x_0))}{1 - S^*}\right| \quad (8)$$

The term dH_h/dx of perpendicular recording at x_0 can be solved by using the symmetry of the longitudinal Karlqvist head field component [7], [9]. The perpendicular head field can be derived by facilitating to turned sideways of longitudinal as

$$H_h = \frac{H_0}{\pi}\left[\tan^{-1}\left(\frac{y+g/2}{x}\right) - \tan^{-1}\left(\frac{y-g/2}{x}\right)\right] \quad (9)$$

where H_0 is the deep gap field, g is the gap width between pole head and its image ($g = 2d+2t$), t is the medium thickness and the field is evaluated at the center of medium ($y = t/2$). The parameter H_d for perpendicular recording is obtained by convolving the unit step response at the original and the magnetization gradient and dH_d/dx can be obtained by differentiating H_d as

$$H_{d,perp} = -\frac{\partial M(x)}{\partial x} * H_y^{step} = -\frac{\partial M(x)}{\partial x} * \frac{1}{\pi}\tan^{-1}\left(\frac{2x}{t}\right) \quad (10)$$

$$\frac{dH_d(x)}{dx} = -\frac{4}{\pi^2}\int_{-\infty}^{\infty}\frac{M_r(T(x'))a}{a^2 + (x'-x_0)^2}\frac{t}{t^2 + 4(x-x')^2}dx' + \frac{4}{\pi^2}\int_{-\infty}^{\infty}\tan^{-1}\left(\frac{x'-x_0}{a}\right)\left.\frac{dM_r(T(x'))}{dT}\right|_{T(x')}\frac{dT(x')}{dx'}\frac{t}{t^2 + 4(x-x')^2} \quad (11)$$

Here, H_c and M_r are linearly temperature-dependent (T),i.e.

$$H_c = -H_{c0}T(x,y) + H_{c,const} \quad (12)$$

$$M_r = -M_{r0}T(x,y) + M_{r,const} \quad (13)$$

where H_{c0} and M_{r0} are the temperature sensitivities of H_c and M_r. $H_{c,const}$ and $M_{r,const}$ are H_c and M_r at 0 Kelvin (K). So dH_c/dT is $-H_{c0}$ and dM_r/dT is $-M_{r0}$. A two-dimensional (2D) Gaussian thermal profile is given as

$$T(x,z) = T_{peak}\exp\left(-\frac{(x-c_0)^2}{2\sigma_t^2}\right)\exp\left(-\frac{z^2}{2\sigma_t^2}\right) + 300 \text{ (K)} \quad (14)$$

where T_{peak} is the peak temperature in the medium above room temperature in Celsius, c_0 is the laser spot position, x is defined as the position in down-track direction and z is defined as the position in cross-track direction. Differentiating (14), we have

$$\frac{T(x,z)}{dx} = T_{peak}\left(-\frac{(x-c_0)}{\sigma_t^2}\right)\exp\left(-\frac{(x-c_0)^2}{2\sigma_t^2}\right)\exp\left(-\frac{z^2}{2\sigma_t^2}\right) \quad (15)$$

B. Microtrack Model

The microtrack model is used for 2D process of heating and magnetization of a medium to solve the problem of determining the transition characteristics in HAMR by dividing recorded track into N individual sub-tracks of equal width with different transition parameters. The TWC equation is then applied to determine x_0 and a in each individual sub-track [4]-[9]. The overall transition response $p(x)$ can be obtained by weighting the transition response $p_i(x)$ of each sub-track to obtain

$$p_i(x) = \exp\left(-\frac{\left(-\frac{N+1}{2}\Delta z + i\Delta z\right)^2}{2\sigma_t^2}\right) \cdot V(x, a_i, x_{0i}) \quad (16)$$

and

$$p(x) = \frac{1}{N}\sum_{i=1}^{N} p_i(x) \quad (17)$$

where V is defined as the playback voltage, a_i and x_{0i} are the transition parameter and transition center of the i^{th} microtrack, $i\in\{1, \ldots, N\}$ and Δz stands for the width of each sub-track. The bit response is then

$$h(x) = 0.5\{p(x) - p(x - T_x)\} \quad (18)$$

where T_x denotes the along-track bit period.

This material is reserved for educational use only, not allowed for commercial use.
Forbidden to modify the content, and cite the document when use.

III. Target and Equalizer Design

A. Channel Model

The HAMR channel with equalizer design is shown in Fig.3. The laser is assume to be attached at the center of track in cross-track direction. $a_k \in \{+1,-1\}$ are binary input sequences. a_k with bit period T_s is filtered by using ideal differentiator $(1-D)/2$ to give a transition sequence $b_k \in \{+1,0,-1\}$ where $b_k=\{\pm 1\}$ represents the positive and negative transition and $b_k=\{0\}$ corresponds to no transition. Media noise is assumed to be the position jitter noise Δ_k modeled as a Gaussian random distribution function with zero-mean and variance $\sigma^2_{\Delta k}$, as the percentage of along-track bit period T in the range of $\pm T/2$. The playback signal $r(x)$ is added by the additive white Gaussian noise (AWGN) $n(x)$. In this simulation, SNR is defined as SNR $= 10\log_{10}(1/\sigma^2)$, where σ^2 is the variance of AWGN. The playback signal with AWGN $y(x)$ will be passed to low pass filter (LPF), sampled and then put in equalizer F(D) to equalize the signal in order to facilitate the application of Viterbi detector (VD). Finally, the equalized outputs $z(k)$ are detected by VD.

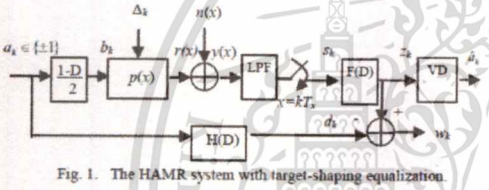


Fig. 1. The HAMR system with target-shaping equalization.

B. Channel Model

In this study, we design the target H(D) and equalizer F(D) by using the minimum-mean squared error (MMSE) method to minimize the mean-squared error (MSE) between desired outputs and equalizer outputs [11], [14]. The target H(D) and its corresponding F(D) can be obtained by minimizing

$$E\left\{w_k^2\right\} = E\left[(z_k - d_k)^2\right] \tag{19}$$

where $E\{\cdot\}$ is the expectation operator, w_k is the difference between output of equalizer, z_k and the desired output, d_k of designed target. The equation (20) can be written in a matrix form as

$$\varepsilon^2 = E\left\{w_k^2\right\} = \mathbf{F}^T\mathbf{R}\mathbf{F} + \mathbf{H}^T\mathbf{A}\mathbf{H} - 2\mathbf{F}^T\mathbf{P}\mathbf{H} \tag{20}$$

where, $\mathbf{H} = [h_0 \;\; h_1 \;\; h_2 \;\ldots\; h_{L-1}]^T$ represents the L-tap GPR target and $\mathbf{F}=[f_{-K}, f_{-K+1} \ldots f_0 \ldots f_K]^T$ represents the $N = 2K+1$-tap equalizer. The matrix $\mathbf{A}$ is an LxL autocorrelation matrix of a_k. $\boldsymbol{R}$ is an MxM autocorrelation matrix of sequence s_k, and $\mathbf{P}$ is an MxL cross-correlation matrix sequence of a_k and s_k. During the minimization process, the specified constraint must be used to avoid the trivial solution of $\mathbf{F} = \mathbf{0}$ and $\mathbf{H} = \mathbf{0}$.

Firstly, by minimizing (21) subject to a monic constraint, the first coefficient of the target is equal to 1 (h_0=1). The matrix form of this constraint is $\mathbf{I}^T\mathbf{H}$=1. The MMSE is [11]-[12]

$$\varepsilon^2 = \mathbf{F}^T\mathbf{R}\mathbf{F} + \mathbf{H}^T\mathbf{A}\mathbf{H} - 2\mathbf{F}^T\mathbf{P}\mathbf{H} - 2\lambda\left(\mathbf{I}^T\mathbf{H}-1\right) \tag{21}$$

Here is the steps of target and equalizer design of h_0=1 constraint. Firstly, we define the number of target tap L and equalizer tap N to create vector $\mathbf{F}$ and $\mathbf{H}$. Secondly, we compute matrix $\mathbf{R}$, $\mathbf{A}$ and $\mathbf{P}$. Thirdly, we create vector $\mathbf{I} = [1, 0, 0, \ldots,0]^T$ which have the size Lx1. Fourthly, we compute the Lagrange multiplier.

$$\lambda = \frac{1}{\mathbf{I}^T\left(\mathbf{A}-\mathbf{P}^T\mathbf{R}^{-1}\mathbf{P}\right)^{-1}\mathbf{I}} \tag{22}$$

Then, we compute the target

$$\mathbf{H} = \lambda\left(\mathbf{A}-\mathbf{P}^T\mathbf{R}^{-1}\mathbf{P}\right)^{-1}\mathbf{I} \tag{23}$$

Finally, we compute the equalizer

$$\mathbf{F} = \mathbf{R}^{-1}\mathbf{P}\mathbf{H} \tag{24}$$

where λ is the Lagrange multiplier and $\mathbf{I}$ is an L-element column vector of which the first element is 1 and the rest is 0. Secondly, we subject to the h_1=1 constraint. For this constraint, we fix the second coefficient to be 1, the first and the rest element can be any values. Here, the vector $\mathbf{J}$ is introduced, where $\mathbf{J}$ is an $Lx1$-element column vector of which the second element is defined to 1 and the other elements are 0. $\mathbf{J} = [0, 1, 0, \ldots. 0]^T$. The solutions are identical to the monic constraint except that $\mathbf{I}$ is replaced by $\mathbf{J}$. Thirdly, the energy $\mathbf{H}^T\mathbf{H}$=1 is fixed to minimize (20) by always maintaining $\mathbf{H}^T\mathbf{H}$ = 1 called the unit energy constraint.

$$\varepsilon^2 = \mathbf{F}^T\mathbf{R}\mathbf{F} + \mathbf{H}^T\mathbf{A}\mathbf{H} - 2\mathbf{F}^T\mathbf{P}\mathbf{H} - 2\lambda\left(\mathbf{H}^T\mathbf{H}-1\right) \tag{25}$$

In this process, the MMSE can be the lowest value by differentiating (25) compared to $\mathbf{F}$, $\mathbf{H}$ and λ, then set all results to be 0, the target and equalizer can be computed from

$$(\mathbf{A} - \mathbf{P}^T\mathbf{R}^{-1}\mathbf{P})\mathbf{H} = \lambda\mathbf{H} \tag{26}$$

It is identical to eigenvalue problem where λ is the MMSE of the matrix $(\mathbf{A}\text{-}\mathbf{P}^T\mathbf{R}^{-1}\mathbf{P})$, $\mathbf{H}$ is the normalized eigenvector, and $\mathbf{F}$ is again given by equation (24). The final constraint is the fixed target constraint according PR target of the form $H(D)=(1+D)^n$. The target function $\mathbf{H}$ is fixed. The equalizer $\mathbf{F}$ which is proper to the fixed target can be computed from (24) by ensuring the MMSE in (20).

IV. Simulation Results

In this work, the medium is assumed to be $Fe_{55-x}Ni_xPt_{45}L1_0$ where $10<x<30\%$ because the linear relationship for M_r and H_c with temperature is resulted in this range, as in [9]-[10]. System parameters are given in Table I. The results show that the unit energy constraint has the lowest minimum MSE as shown in Fig. 2. The 3-tap target with 11-tap equalizer has the MSE equal to 0.062. The h_0=1 constraint gives the MSE of 0.089. For h_1 = 1 constraint, the minimum MSE of this target is 0.086, and the fixed-target constraint using PR2 [1 2 1] has the highest MSE value of 1.631. We can see the frequency responses of the 4 targets in Fig. 3, the frequency response of GPR targets of our system is similar to the frequency response of the longitudinal magnetic recording (LMR). Since the frequency response of PR2 target are all dc-full. That is why

This material is reserved for educational use only, not allowed for commercial use.
Forbidden to modify the content, and cite the document when use.

PR2 target give high MMSE values and therefore they are not suitable for target design.

At the same SNR (SNR =18 dB), the bit error rate (BER) of the h_0=1 constraint is $1x10^{-4}$. BER of the h_1=1 constraint is $8x10^{-4}$. BER of the unit energy constraint is $1.80x10^{-3}$ and BER of the PR2 target constraint is $1.78x10^{-1}$. The BER of the h_0=1 constraint gives the best system performance even though the lowest MMSE is from the unit energy constraint as shown in Fig. 4. The BER performance of VD also depends on the noise correlations and the data patterns. So, the lower MMSE does not necessarily provide the lower BER [12].

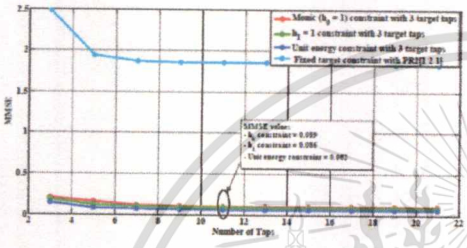


Fig. 2. MMSE of various constraints using 3-tap targets with 11-tap equalizer

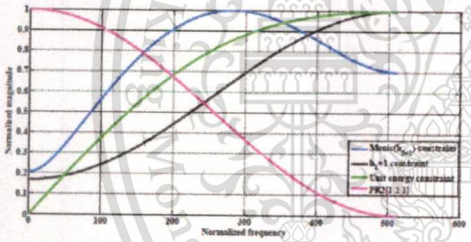


Fig. 3. Frequency responses of GPR targets versus fixed-target (PR2)

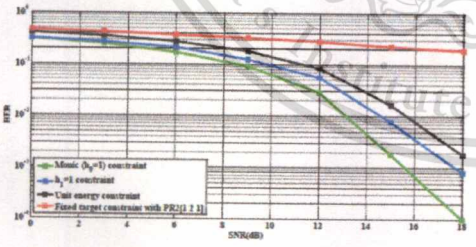


Fig. 4. Bit error rates (BER) of the HAMR system at 5 Tb/in^2

V. Conclusions

In this work, the GPR targets are designed for HAMR systems. From the simulation results, the frequency response of GPR targets of the HAMR systems are similar to the frequency response of LMR and provide the lower MMSE than dc-full PR targets. Although the lowest MMSE of all systems is from the unit energy constraint, the monic constraint gives the best BER. Therefore, the monic constraint outperforms other constraints.

TABLE I SYSTEM PARAMETERS

Parameters	Unit
Track width (TW)	25.4 nm
Number of sub-track (N)	10
Laser position (c_o)	0 nm
Deep gap field (H_0)	$1x10^6$ A/m
Peak temperature (T_{peak})	300 C°
Sigma of temperature profile (σ_t)	16.2 nm
Gap width between pole head and its image (g)	32 nm
Sigma of reader sensitivity function (a_r)	4.23 nm
Head-medium distance or fly height (d)	6 nm
Medium thickness (t)	10 nm
Bit period (T_b)	5 nm
A system specific constant (C)	1
Dependence of coercivity on temperature (H_c)	$-3100T+2.4x10^6$ A/m
Dependence of remanent magnetization on temperature (M_r)	$-700T+1.8x10^6$ A/m
Areal density (AD)	5 Tb/in^2

References

[1] Y. Shiroishi et al., "Future options for HDD storage," *IEEE Trans. Magn.*, vol. 45, no. 10, pp. 3816-3822, Oct. 2009.

[2] E.M. Kurtas et al., "Future read channel technologies and challenges for high density data storage applications, Acoustics, Speech, and Signal Processing," Proceedings of *ICASSP* 2005, pp. 737-740.

[3] M. L. Plumer, J. V. Ek, and W. C. Cain, "New paradigms in magnetic recording," *Physics in Canada*, vol. 67, no. 1, pp. 25-29, Mar. 2011.

[4] T. Rausch, J.A. Bain, D.D. Stancil, and T.E. Schelsinger, "Thermal Williams-Comstock model for predicting transition lengths in heat-assisted magnetic recording system," *IEEE Trans. Magn.*, vol. 40, no.1, pp. 137-147, Jan. 2004.

[5] M.F. Erden, T. Rausch, W.A. Challener, "Cross-track location and transition parameter effects in heat-assisted magnetic recording," *IEEE Trans. Magn.*, vol. 41, no. 6, pp.2189-2194, Jun. 2005.

[6] R. Radhakrishnan et al., "Transition response characteristics of heat-assisted magnetic recording and their performance with MTR Codes," *IEEE Trans. Magn.*, vol. 43, no. 6, pp. 2298-2300, Jun. 2007.

[7] R. Radhakrishnan et al., "Characterization of heat-assisted magnetic recording channels," *DIMACS Series in Discrete Mathematic sand Theoretical Computer Science*, vol. 73, pp. 25-41, 2007.

[8] M.H. Kryder et al., "Heat-assisted magnetic recording," *Invited Paper Proceedings of the IEEE*, vol. 96, no. 11: 1810-1835, Noember. 2008.

[9] R. Wongsathan and P. Supnithi, "Channel response of HAMR with linear temperature-dependent coercivity and remanent magnetization," in *Conf. Rec. 2012 IEEE Int Conf. ECTI-CON*, 2012, pp. 1-4.

[10] J.U. Thiele et al., "Temperature dependent magnetic properties of highly chemically ordered $Fe_{55-x}Ni_xPt_{45}L1_0$ films," *J. Appl. Phys.*, vol. 91, no. 10, pp. 6595-6600, May 2002.

[11] P. Kovintavewat et al., "Generalized partial-response targets for perpendicular recording with jitter noise," *IEEE Trans. Magn.*, vol.38, no.5, pp. 2340-2342, Sep. 2002.

[12] J. Moon and W. Zeng, "Equalization for maximum likelihood detectors," *IEEE Trans. Magn.*, vol.31, no. 2, pp. 1083-1088, Mar 1995.

This material is reserved for educational use only, not allowed for commercial use.
Forbidden to modify the content, and cite the document when use.

APPENDIX B

AUTHOR BIOGRAPHY

King Mongkut's Institute of Technology Ladkrabang

This material is reserved for educational use only, not allowed for commercial use.
Forbidden to modify the content, and cite the document when use.

AUTHOR BIOGRAPHY

Author:	Ms. Panatda Tueku
Date of Birth:	July 31, 1983
Place of Birth:	Surin province
Bachelor Degree:	B. Eng. Electrical Engineering
Subject:	Electrical Engineering
Institute:	Department of Electrical Engineering, Faculty of Electrical Engineering Ubon Ratchathani University (UBU)
Year of Graduation:	2006
Work Experience:	Western Digital (Thailand) Co., Ltd.
Department:	Test Equipment Engineering
Year of Working:	2006-Now

Related Publication:

1. P. Tueku, P. Supnithi, R. Wongsathan, "Target and Equalizer Design for Perpendicular Heat-Assisted Magnetic Recording," *International Conference on Circuits,Systems, and Signal Processing*, Singapore, vol.3, pp. 1032-1038, March 2014.
2. P. Tueku, P. Supnithi, R. Wongsathan, "Target and Equalizer Design for Perpendicular Heat-Assisted Magnetic Recording with Media Jitter Noise," *International Technical Conference on Circuit/Systems Computers and Communications 2014*, Thailand, July 104, 2014.

This material is reserved for educational use only, not allowed for commercial use.
Forbidden to modify the content, and cite the document when use.